

Modeling, Stability Analysis and Control of Renewable Driven Islanded and Grid Connected Microgrids

Prashant Patel

A Thesis Submitted to
Indian Institute of Technology Hyderabad
In Partial Fulfillment of the Requirements for
The Degree of Master of Technology



भारतीय प्रौद्योगिकी संस्थान हैदराबाद
Indian Institute of Technology Hyderabad

Department of Electrical Engineering

June 2011

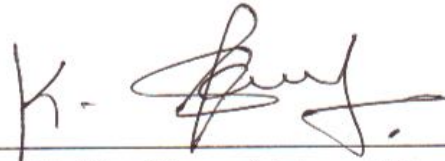
Approval Sheet

This thesis titled "Modeling, Stability Analysis and Control of Renewable Driven Is-landed and Grid Connected Microgrids" by Mr. Prashant Patel is approved for the degree of Master of Technology.



(Dr. P. V. Balasubramanyam) External Examiner

CPRI



(Dr. K. Siva Kumar) Internal Examiner

Dept. of Elec Eng

IITH



(Dr. Vaskar Sarkar) Research Supervisor

Dept. of Elec Eng

IITH



(Dr. R. Prasanth Kumar) Chairman

Dept. of Mech Eng

IITH

Acknowledgements

I would like to express my profound respect for my supervisor Dr. Vaskar Sarkar. He is the person who has sculpted me to my current shape and has shown me the right direction to discover myself. The little work that I have done has been possible only because of his excellent guidance during the two years of my M.Tech work. I can say right from the deep of my heart that the guidance, I have received from him, is unprecedented. I am also grateful to Prof David Koilpillai for the valuable suggestions and inputs that they have provided from time to time.

I am extremely lucky to have lovingly chucks such as Minesh, Rohan, Tejas, Viral, Sandip, Nikunj, Utsav, Uday, Rahul, Thakur, Amit, Shekhar, Balaji, Obul, Sridhar. I would also like to thank my batch mates Alok, Madhav, Sidharth, Ramanuj, Umesh, Gouda, Vanu, Nirala, Arvinth, Balan. I appreciate their patience to tolerate a disturbing person like me. The moral support that they have provided is unforgettable. Being with them is a nice experience that will be in the album of my memory for my entire life. The days I have spent in IIT H and IIT M have been very nurturing and educating for me.

My special gratitude is due to my brother Amit and sister Chetna for their endless loving support in all walks of my life. I am indebted for life to my mom and dad, for believing in me more than myself. To them, I dedicate this thesis. I also would like to thank my lovingly grand mother [nani] for her inspiration, patience and sacrifices. And the last but not the least, To my grand parents, I know, you are blessing me from somewhere.

Prashant Patel

To
The God and My Loving Parents

Abstract

In recent years, the increasing demand of the efficiency and convenience of the power system has driven the development of the microgrid technology. As renewable energy emerges as an alternative way of generating clean energy, the major aim of microgrid is to combine all the benefits of nonconventional/ renewable and low carbon generation technologies to improve the overall efficiency by using combined heat and power systems(CHP). To achieve this goal, proper co-ordination and control of various Distribution Energy Resource(DER) units like photovoltaic systems, fuel cells, micro turbines, variable speed wind turbines, small hydro plants, biomass, geothermal, gas turbines, reciprocating internal combustion engines, etc. are required.

With the above background in place, this work presents modeling and control of DER based microgrid in islanded and grid connected mode, which are supposed to be demanded by the distribution system to harness and provide clean energy from DERs to the critical loads. Microgrid delivers surplus amount of power to the utility grid and it also takes deficit amount of power from the utility grid to maintain the continuity of the supply without any interruption and this is done with the higher quality of power and lesser charge per unit of energy.

The thesis includes design of closed loop dc-dc boost converter with PI controller to boost the dc output voltage of the DERs. PI controller is designed to get the controlled output voltage against the variation of the loads or variation in the input side voltage of the DC-DC converter. Most of the Renewable energy sources have an inverter as a grid interface. The inverter can operate either as a current source or as a voltage source. In ei-

ther case, the basic implementation would be in the form of a voltage source inverter(VSI) and, if necessary, appropriate control loops will be added to make it appear as a controlled current source. The inverter would be fitted with the coupling impedance and, possibly, further passive filter elements to attenuate the switching frequency components of voltage. In the islanded operation, the microgrid has to maintain voltage and frequency constant independently of the main grid because, during islanding operation the microgrid has to supply all the loads presented in a microgrid network. For stable operation of a microgrid, P-f and Q-V droop control and current and voltage loop control have been developed for each microsource. As we know, in the conventional power system P-f and Q-V droops are used to control active and reactive power respectively. The same but slightly variant of conventional P-f and Q-V droop control strategy are adopted in microgrids to regulate real and reactive power respectively. In this thesis, mathematical model and control structure of the islanded and grid connected single unit of DER, multiple units of DER are presented. Further a microgrid, which consists of seven buses and eight lines, has been designed for both islanding and grid connected mode. Finally, the entire microgrid has been simulated during switching from one mode to other mode of operation. Modeling and simulation works are carried out using MATLAB and PSCAD/EMTDC.

Contents

Abstract	i
List of Figures	vii
List of Tables	xiii
Nomenclature	xiv
1 Introduction	1
1.1 Background	1
1.2 Distributed Energy Resources	2
1.3 Concept of Microgrid	4
1.4 Microgrid Structure	5
1.5 Challenges and Disadvantages of Microgrid Development	7
1.6 Objectives	8
1.7 Organization of the Thesis	8
2 Modeling and Design of Closed Loop DC-DC Boost Converter with PI Controller, PWM Techniques and Passive Filter	11
2.1 DC-DC Boost Converter	12
2.1.1 DC-DC boost converter design	13
2.1.2 Boost converter transfer function	15
2.1.3 System transfer function	18
2.1.4 Design of PI controller	19
2.2 Voltage Source Inverter Operation and SPWM	21

2.2.1	Pulse width modulation technique	22
2.3	Design of L-C Filter for Grid-Connected and Islanded Mode Power Converters	25
2.3.1	Design procedure for filter design	26
2.4	Summary	31
3	Overview of Control Strategies for Islanded and Grid-Connected Mode of Operation of Microgrid and Importance of PLL Block	33
3.1	Review of Controller Basics and Its Important in Microgrid	34
3.2	Needs of ABC to dq0 Transformation for Controller Design	36
3.3	Control Task in a Microgrid	38
3.3.1	Types of controller for microgrid	39
3.4	Points to be Pondered upon for Designing of Controller in Islanded or Grid Connected Mode of Microgrid	40
3.4.1	VSI modeling	41
3.4.2	Control of VSC	47
3.4.3	Need for feed forward compensation	49
3.5	Modeling and Controlling of Two Level VSC	51
3.6	Importance of PLL Block and Formulation of Power in dq Domain	53
3.7	Summary	55
4	Modeling and Control of DERs in Grid-Connected and Islanded Mode of Operation of Microgrid	57
4.1	Islanded Distributed Energy Resources [Autonomous Microgrids]	58
4.1.1	Modeling and control of single DER unit in islanded mode	61
4.1.2	Modeling and control of parallel connected DER units in islanded mode	74
4.1.3	Modeling and control of islanded microgrid	84
4.2	Grid-Connected Distributed Energy Resources [Grid-Connected Microgrids]	88
4.2.1	Modeling and control of single DER unit in grid-connected mode	90
4.2.2	Modeling and control of multi DER units in grid-connected mode	94
4.2.3	Modeling and control of grid-connected microgrid	95

4.3	Switching from Islanded to Grid-Connected Mode of the Entire Microgrid and Vice Versa	97
4.4	Summary	101
5	Results and Discussions	103
5.1	PI Controlled Close Loop DC-DC Converter	103
5.2	Results of the Designed LC Filter	105
5.3	Control of Single DER Unit in Islanded Mode	109
5.3.1	Based on the load condition	110
5.3.2	Fault condition	117
5.3.3	Based on the controller reference set point	118
5.4	Control of parallel connected two DER units in islanded mode	120
5.4.1	Based on the reactance values met between the feeding point (i.e. PCC) and the load terminal point	121
5.4.2	Based on droop coefficient values	123
5.5	Islanded Mode of the Entire Grid	125
5.6	Control of Single DER Unit in Grid-Connected Mode	129
5.6.1	Control of active and reactive powers for a given fixed reference value	131
5.6.2	Sharing of active and reactive powers for a different reference values	133
5.6.3	Control of two DER units in grid-connected mode	134
5.6.4	Control of grid-connected microgrid	137
5.7	Switching from Islanded to Grid-Connected Mode and Vice Versa	138
5.8	Summary	146
6	Conclusions and Future Scope of Research	147
6.1	Conclusions:	147
6.2	Future Scope of Research:	148
	Bibliography	151

List of Figures

1.1	Typical grid structure [3]	6
2.1	PWM boost converter basic circuit [9]	12
2.2	Matlab/Simulink circuit of a PWM boost converter without control	12
2.3	Feedback loop control of DC-DC converter	15
2.4	Matlab/Simulink circuit of a PWM boost converter with control	15
2.5	Converter circuit during charging cycle [9]	16
2.6	Converter circuit during discharging cycle [9]	16
2.7	Schematic diagram of a VSI	22
2.8	Sine-triangular pulse width modulator	23
2.9	Sinusoidal pulse width modulation	24
2.10	Equivalent circuit of one leg of grid connected 3-phase VSI	26
2.11	Waveforms of voltage and current across filter inductor	27
2.12	Filter behavior during grid connected and islanded mode	29
2.13	Switching circuits of single leg of the three phase inverter	29
3.1	Basic block diagram of feedback loop control	35
3.2	Block diagram of feed forward loop control	35
3.3	General structure of DPGS	39
3.4	General layout of microgrid structure for islanded and grid connected mode respectively	41
3.5	Switch model of VSI	42
3.6	Averaged model of VSI	43
3.7	Switching waveforms of switches S_a and S'_a	46

3.8	Block diagram to control output current i	48
3.9	Control block diagram of the closed loop half bridge inverter system without and with feed forward control scheme	49
3.10	Averaged equivalent circuit of two level VSC [13]	51
3.11	Control model of two level VSC in dq-reference frame	52
3.12	PLL block diagram [13]	55
4.1	SLD for islanded DER	61
4.2	Schematic diagram for islanded DER with closed loop control scheme	62
4.3	Block diagram of a current control scheme	66
4.4	Equivalent block diagram for the closed loop current control scheme	67
4.5	Block diagram of a voltage control scheme	71
4.6	Equivalent block diagram for the closed loop voltage control scheme	73
4.7	SLD of two islanded DER units connected in parallel and feeding a common load	76
4.8	schematic diagram of a control logic for single DER for paralleling operation in islanded mode	77
4.9	Equivalent circuit of a VSI connected to a bus	78
4.10	Static droop characteristics of P-f and Q-V droops respectively	81
4.11	PCC terminal voltage calculation	83
4.12	Islanded microgrid with a seven bus and eight lines network	85
4.13	Block diagram of the grid connected system	88
4.14	SLD for grid connected DER	90
4.15	Schematic diagram for grid connected DER with closed loop control scheme	91
4.16	Control block diagram of the current reference signal generator	93
4.17	SLD of two DERs connected in grid connected mode	95
4.18	Schematic diagram of multi sources connected to a grid	96
4.19	SLD of a microsource in grid connected/ islanded mode	98
4.20	Seven bus microgrid network with all kinds of controllers	99
4.21	Matlab simulation circuit for seven bus microgrid network with all kinds of controllers	100

4.22	Control logic for single microsource in a microgrid	101
5.1	Output voltage of the boost converter without controller	104
5.2	Output voltage of the boost converter with controller	105
5.3	Inverter output voltages (3-phase) before filter and Zoomed view of inverter output voltages (1-phase) before filter	106
5.4	Inverter output voltages (3-phase) after filter	106
5.5	Bode plot of the designed LC filter for islanded mode	107
5.6	Root-locus plot of the designed LC filter for islanded mode	108
5.7	Bode plot of the designed LC filter for grid connected mode	108
5.8	Root-locus plot of the designed LC filter for grid connected mode	108
5.9	FFT analysis for THD of filter output voltage at no load	109
5.10	Inverter output voltage at no load condition	111
5.11	Inverter output frequency at no load condition	112
5.12	Phase voltages and currents at PCC for load stepping at 0.45 sec	113
5.13	Zoomed view of phase voltages and currents at PCC for load stepping at 0.45 sec	113
5.14	Voltage and current THDs at PCC	114
5.15	Real and reactive powers at PCC / Frequency at PCC for load stepping at 0.45 sec	114
5.16	Phase voltages and currents at PCC without control for nonlinear load	115
5.17	Phase voltages and currents at PCC with control for nonlinear load	115
5.18	Phase voltages and currents at PCC without control while sharing balanced and non linear load	116
5.19	Phase voltages, currents and frequency at PCC with control while sharing balanced and non linear load	117
5.20	Phase voltages and its zoomed view at PCC for LG fault created at 0.3 sec and cleared at 0.6 sec	117
5.21	Phase voltages and its zoomed view at PCC for a changed in V_{sdref} to a peak of 525 V	118
5.22	$[V_{sdref}$ and actual $V_{sd}]$ and $[V_{sqref}$ and actual $V_{sq}]$	119

5.23	Frequency response for a changed V_{sdref}	119
5.24	Real and Reactive power shared by DER-1 and DER-2	121
5.25	Frequency at PCC-1 and PCC-2	121
5.26	Phase voltages at PCC-1, PCC-2 and Load terminals	122
5.27	Zoomed view of phase voltages at PCC-1, PCC-2 and Load terminals . . .	123
5.28	Real and Reactive power shared by DER-1 and DER-2 depends on droop setting	124
5.29	Frequency at PCC-1 and PCC-2	125
5.30	Phase voltages at PCC-1, 2 and load terminals for different droop setting .	125
5.31	Phase voltages at terminals of DG-1 to DG-7 in the islanded microgrid network	127
5.32	Load voltages at Bus-3, Bus-6 and Bus-7 in the islanded microgrid network	128
5.33	Frequency at terminals of DG-1 to DG-7 in the microgrid network	128
5.34	Real power dispatched by all DGs in the microgrid network	129
5.35	FFT analysis for THDs of all DGs in the islanded microgrid network . . .	130
5.36	Control of active and reactive powers for a given fixed reference value . . .	131
5.37	Load voltages, grid injected current and load currents as load Stepped up at 0.15 second and again step down at 0.25 second	132
5.38	Zoomed view of load voltages, grid injected current, load currents as load stepped up at 0.15 second and again step down at 0.25 second	132
5.39	Frequency at PCC as load stepped up at 0.15 second and again step down at 0.25 second	133
5.40	Reference active power switched at 0.2 and 0.4 seconds	134
5.41	Frequency plot for change in reference active power	135
5.42	Voltage and current THDs for single grid connected DER unit	135
5.43	Real power shared by two DERs in grid connected mode	136
5.44	Frequency plot for two DERs in grid connected mode	136
5.45	Real power shared by two DERs for changing in reference active power at 0.35 seconds	137

5.46	Real power shared by all DGs connected in grid connected mode of the entire microgrid	139
5.47	Phase voltages at terminals of all DGs in grid connected mode of the entire microgrid	139
5.48	Frequency at each PCC in grid connected mode of the entire microgrid . .	140
5.49	FFT analysis for THDs of all DGs in the grid connected mode of microgrid network	141
5.50	Phase voltages at PCCs while switching from islanded to grid connected mode of microgrid at 0.2 seconds	142
5.51	Zoomed view of phase voltages at PCCs while switching from islanded to grid connected mode of microgrid at 0.2 seconds	142
5.52	Zoomed view of phase voltages of DG-1 terminals during switching from islanded to grid connected mode at 0.2 seconds	143
5.53	Frequencies of all DGs	143
5.54	Real power dispatched by all DGs during mode changing from islanded to grid connected mode	144
5.55	Phase voltages at PCCs while switching from grid connected to islanded mode of microgrid at 0.1 seconds	144
5.56	Zoomed view of phase voltages of DG-5 terminals during switching of islanded to grid connected mode at 0.1 seconds	145
5.57	Frequencies of all DGs	145
5.58	Real power dispatched by all DGs during mode changing from grid connected to islanded mode	146

List of Tables

2.1	Inverter Pole Voltages with respect to Switch Positions where $i = a, b, c$. . .	21
5.1	System Parameters which are Considered in a Boost Converter Simulation	104
5.2	System Parameters which are Considered in Islanded System	110
5.3	System Parameters which are Considered for Two DERs Connected in Islanded System	120
5.4	System Parameters which are considered for Two DERs Connected in Is- landed System- Based on Droop Coefficient Values	124
5.5	System Parameters which are Considered for the Entire Microgrid in Is- landed Mode	126
5.6	System Parameters which are Considered for Single DER Unit in Grid- Connected Mode	131
5.7	System Parameters which are Considered in Grid-Connected System	138

Nomenclature

List of Symbols

t_{on}	Time interval for switch ON.
D	Duty Ratio.
T	Switching Time Period.
f_s	Switching Frequency.
S	Switch Position (S= 1 when switch is on and S= 0 when switch is off).
P_{max}	Maximum Power Supplied by the Solar panel
Δi_L	Current Ripple.
ΔV	Voltage Ripple.
G_R	PI controller transfer function.
K_R	Gain of the PI Controller for DC-DC Boost Converter.
T_i	Integral Time Constant of the PI Controller for DC-DC Boost Converter.
m_a	Amplitude modulation index for SPWM.
m_f	Frequency modulation index for SPWM.
Δi_{p-p}	Peak to peak ripple current in the inductor.
f_{res}	Resonance Frequency.

i_g	Grid injected current.
K_s	Park Transformation matrix.
ρ	Speed of the rotation of dq-reference frame.
V_{tabc}	Inverter terminal voltages in ABC domain.
V_{sabc}	PCC terminal voltages in ABC domain.
i_{abc}	Current through the inductor of an LC filter in ABC domain.
i_{cabc}	Current through the capacitor of an LC filter in ABC domain.
i_{Labc}	Load Current in ABC domain.
m_a, m_b, m_c	Reference modulating waveforms in ABC domain.
m_d, m_q	Reference modulating waveforms in dq-domain.
V_{sdq}	PCC terminal voltages in dq-domain.
i_{dq}	Current through the inductor of an LC filter in dq-domain.
i_{Ldq}	Load current in dq-domain.
i_{dqref}	Reference current through the inductor of an LC filter in dq-domain.
V_{sdqref}	Reference PCC terminal voltages in dq-domain.
ϕ	Phase angle between the output voltage of a VSI and PCC voltage.
θ	Impedance angle.
m	P-f droop co-efficient.
n	Q-V droop co-efficient.

List of Acronyms

DER	Distributed Energy Resources.
DG	Distributed Generation.
CHP	Combined Heat and Power.
RES	Renewable Energy System.
CB	Circuit Breaker.
KVL	Kirchhoff's Voltage Law.
DPGS	Distributed Power Generation System.
VSI	Voltage Source Inverter.
PWM	Pulse Width Modulation.
SPWM	Sinusoidal Pulse Width Modulation.
IGBT	Insulated Gate Bi-polar Transistor.
MOSFET	Metal-Oxide Semiconductor Field Effect Transistor.
THD	Total Harmonic Distortion.
PLL	Phase Locked Loop.
PEI	Power Electronics Interface.
CC	Central Controller.
MC	Microsource Controller.
VSC	Voltage Source Converter.
PCC	Point of Common Coupling.
SMES	Superconducting Magnetic Energy Storage.

PV	Photovoltaic System.
IMC	Islanded Mode Controller.
GMC	Grid-connected Mode Controller.
L-G	Line to Ground.
SLD	Single Line Diagram.
MATLAB	MATrix LABoratory.
FFT	Fast Fourier Transform.
PI	Proportional-Integral.

Chapter 1

Introduction

1.1 Background

Since the beginning of establishment of the power system, there has been a continuous increase in the requirement of electric power. After the advent of electronic gadgets and devices, the nonlinearity in the system has been increasing continuously. The nonlinear loads degrade the quality of power, hence the quality of power needs to be maintained according to the standards. Moreover, Some problems such as more losses in transmission and distribution of power and instability of the system also need to be addressed. These problems have led to a new trend of generating and distributing power locally at distribution voltage level by using non-conventional/ renewable energy sources.

In the utility grid, the occurrence of power system downtime, i.e., the duration for which the utility grid is inoperable due to undesire power quality problems such as voltage sags, swells, interruptions, black-outs, so on, has become a great concern. One of the solutions for these problems is to construct a new conceptual electrical power system, which may integrate both conventional and non conventional energy sources. Up to now several concepts have been proposed and studied such as “FRIENDS”, “PREMIUM POWER PARK”, “MICROGRID” and so on, but among these approaches “MICROGRID” is the most exhilarating because it challenges the entire architecture that have been established for electricity generation, transmission and distribution over the past

100 years.

During recent years, conventional power generations, such as thermal, hydro and nuclear, are facing the problems of gradual depletion of fossil fuel resources, poor energy efficiency and environmental pollution. Moreover, the need of reducing CO_2 emissions in the electricity generation, restructuring of power industries and technological development in the micro generation has lead to the growing interest in the use of microgeneration, i.e., electrical power generation in small scale by using non-conventional/ renewable energy sources like natural gas, biogas, wind power, solar photovoltaic cells, fuel cells, CHP systems, micro turbines and sterling engines and their integration into the utility distribution network [1]-[2]. This type of power generation is termed as distributed generation (DG) and the energy sources are termed as distributed energy resources (DERs) [3].

MICROGRID is a cluster of loads and microsources operating as a single controllable system that provides both power and heat to its local area. As most of the DER units do not generate AC voltages of required magnitude and frequency, Power Electronic Interfaces (PEIs) are required to connect these renewable energy resources to the grid [4]. Therefore, by using PEIs, we are able to operate these different kinds of distributed energy resources (DERs) in a small scale grid, which is treated as a controlled entity within the power system, known as microgrid. It may be said that, the microgrid is a new paradigm of power system operation. This aspect of the microgrid clears that the microgrid is a new architecture for the electricity grid for harvesting the advantages of DERs such as green power, lower cost, higher reliability, reduced black-out problem, interruption of power supply and improving efficiency by CHP system.

1.2 Distributed Energy Resources

The need for electricity is never ending. Along with the growth in demand for electrical energy, sustainable development, environmental issues, and power quality and reliability have become concerns. Electric utilities are becoming more and more stressed since ex-

isting transmission and distribution systems are facing their operating constraints with growing load. Greenhouse gas emission has resulted in a call for cleaner and renewable power sources. Development in technology has been making the whole society more and more electricity dependent and creating more and more critical loads. Under such circumstance, distributed generation (DG) with alternative sources has caught everybody's attention as a promising solution to the above problems. According to L. Philipson [5], distributed generation defers from dispersed generation. The distributed generation entails using many small generators of 2-50 MW output, situated at numerous strategic points throughout cities and towns, so that each provides power to a small number of consumers nearby, while dispersed generation refers to use of even smaller generating units, of less than 500 KW output and often sized to serve individual homes or businesses. Later publications tend to combine the two categories into one, i.e., distributed generation, to refer to power generation at customer sites to serve part or all of customer load or as backup power or at substations to reduce peak load demand and defer substation capacity reinforcements [2]. In this proposal, the combined concept is used [3], [5].

- It is not centrally planned by the power utility, nor centrally dispatched.
- It is normally smaller than 50 MW.
- The power sources or distributed generators are usually connected to the distribution system, which is typically having a voltage level within the range from 230/415 V to 145 KV.

Distributed generation is not a new concept since traditional diesel generator as backup power source for critical load has being used for decades. However, due to its low efficiency, high cost, and noise and exhaust, diesel generator would be objectionable in many applications; for that reason, it has never become a true distributed generation source on today's basis. Hence, environmental friendly renewable energy sources, (such as photovoltaic devices and wind electric generators), clean and efficient fossil-fuel technologies, (such as micro gas turbines), and hydrogen electric devices - fuel cells, have provided great

opportunities for the development in distributed generation. Gas offered micro-turbines in the 25-100 KW range can be mass produced at low cost which use air bearing and recuperation to achieve a reasonable efficiency of 40% for only electrical output and efficiency of 90% for electrical and heat co-generation [6]. Fuel cells have the virtue of zero emission, high efficiency and reliability, and therefore, have the potential to truly revolutionize of power generation. The hydrogen can be either directly supplied or reformed from natural gas or liquid fuels such as alcohols or gasoline. Individual units range in size from 3-250 KW or even larger MW size [2]. The fastest growing renewable energy source is wind power. On a world-wide basis, available wind energy exceeds the presently installed capacity of conventional energy sources by a factor of four.

DER based microgrid could potentially offer following conspicuous benefits: shorter lead times for construction, increased flexibility to respond to market forces, improved reliability of electricity, improved power grid security, reduced transport losses, improved power quality, diverse fuel availability. Owing to these benefits, today DER systems are recognized by governments, environmental organizations and commercial organizations as a technology with the potential to supply a significant part of the world's energy needs in a sustainable and renewable manner. Moreover, due to the extensive improvement in inverter technologies, DER generation is now being preferred and deployed worldwide for augmentation of local generation at distribution voltage level. Though DER can be effectively used in a microgrid, yet they go through the disadvantages of high installation cost and low energy efficiency [6].

1.3 Concept of Microgrid

Today our conventional distribution network is unidirectional/ passive in nature, but it becomes bidirectional/ active with the integration of DG. Microgrid is essentially an active distribution network because it is the conglomeration of DG systems and different loads at distribution voltage level. The generators or microsources employed in a microgrid are usually renewable/ nonconventional DERs integrated together to generate power at

distribution voltage. The key differences between a microgrid and a conventional power plant are as follows [3].

- Microsources are of much smaller capacity with respect to the large generators in conventional power plants.
- Power generated at distribution voltage can be directly fed to the utility distribution network.
- Microsources are normally installed close to the customers' premises so that the electrical/ heat loads can be efficiently supplied with satisfactory voltage and frequency profile, and with negligible line losses.

From operational point of view, the micro sources must be equipped with power electronic interfaces (PEIs) and controls to provide the required flexibility to ensure operation as a single aggregated system and to maintain the specified power quality and energy output. In all, microgrids do offer the following benefits [4]:

- reduce the cost of energy and manage price volatility;
- improve customer and system reliability;
- increase the power systems' security;
- promote the deployment and integration of green technologies;
- make more efficient the power delivery system;
- provide different levels and quality of service to customer;
- monitor and control more effectively.

1.4 Microgrid Structure

The typical microgrid structure is shown in Fig.1.1. There are three radial feeders (A, B and C) in the Fig.1 to supply the electrical and heat loads. It is also having two

CHP microsources, two non-CHP microsources as well as storage devices. Microsources and storage devices are connected to feeders A and C through microsource controllers (MCs). Some loads on feeders A and C are assumed to be priority loads (i.e. requiring uninterrupted power supply), while others are non-priority loads. Feeder B, however, contains only non-priority electrical loads. The microgrid is connected to the main utility grid (denoted as 'main grid') through the PCC (point of common coupling) circuit breaker CB4 as per standard interface regulations.

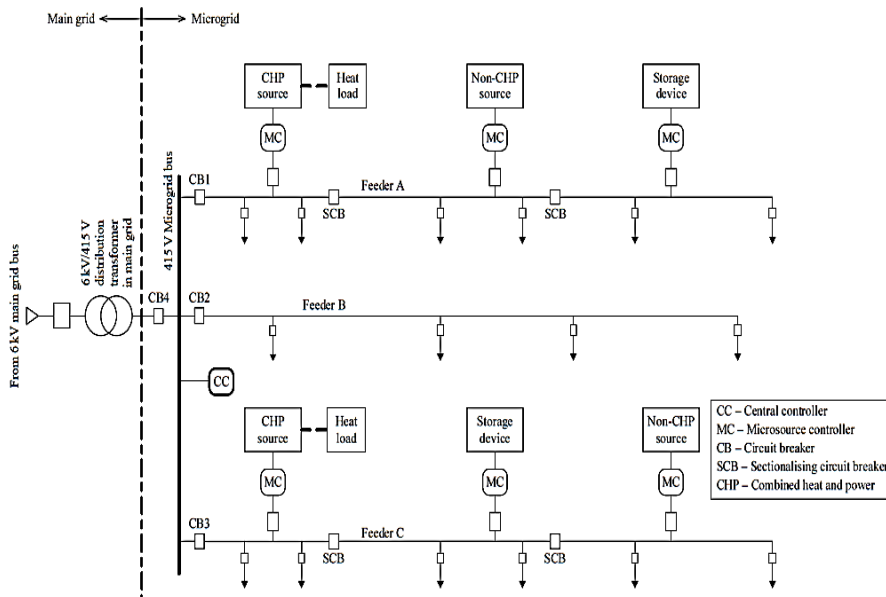


Figure 1.1: Typical grid structure [3]

CB4 is operated to connect and disconnect the entire microgrid from the main grid as per the selected mode of operation. Feeders A, B and C can however be connected and disconnected by operating breakers CB1, CB2 and CB3, respectively. The microsources on feeders A and C are placed quite apart from the microgrid bus to ensure reduction in line losses, good voltage profile and optimal use of waste heat. Although the control of power flow and voltage profile along radial feeders is quite complicated when several microsources are connected to a common radial feeder and not to a common generator bus, this configuration is necessary to avail the plug-and-play feature of the microsources.

The microgrid is operated in two modes:

1. Grid-connected mode
2. Stand alone mode

In grid-connected mode, the microgrid remains connected to the main grid either totally or partially, and imports or exports power from or to the main grid. In case of any disturbance in the main grid, the microgrid switches over to stand-alone mode while still feeding power to the priority loads. This can be achieved by either (i) disconnecting the entire microgrid by opening CB4 or (ii) disconnecting feeders A and C by opening CB1 and CB3. For option (i), the microgrid will operate as an autonomous system with all the microsources feeding all the loads in feeders A, B and C, whereas for option (ii), feeders A and C will supply only the priority loads while feeder B will be left to ride through the disturbance.

1.5 Challenges and Disadvantages of Microgrid Development

Microgrids face following challenges and drawbacks [7]-[8]:

1. high costs of distributed energy resources;
2. technical difficulties;
3. administrative and legal barriers;
4. absence of standards;
5. voltage, frequency and power quality are three main parameters that must be considered and controlled to an acceptable limits;
6. control and co-ordination of microsources;
7. microgrid protection;
8. re-synchronization with utility grid is difficult.

1.6 Objectives

Based on the need for knowledge of the microgrid system, the present work has the following objectives:

- to understand the complete model of microgrid, a detailed study has to be carried out on microgrid structure, its modeling and control.
- to describes the importance of dc-dc boost converter and design of closed loop DC-DC boost converter.
- to develop the mathematical model of microgrid in grid connected and islanded modes and design controller for stable operation of microgrid in both the modes.
- to design droop controller along with voltage and current controller for islanded mode of single DER unit, multi DER units and the entire microgrid.
- to design controller for real and reactive power flow in consort with VSC current controller for grid connected mode of single DER unit, multi DER units and the entire microgrid.
- to study the control of entire microgrid during both islanded as well as grid connected mode.
- to describe the problems faced while synchronizing of microgrid with the utility grid.
- to evaluate the performance of microgrid under different conditions using time domain simulations.

1.7 Organization of the Thesis

The thesis is organized as follows

Chapter 2, describes the procedure of designing closed loop DC-DC Boost converter with PI controller and passive filter components for islanded and grid connected inverter.

In Chapter 3, discusses the mathematical modeling and analysis of microgrid for designing of grid connected and islanded mode controller with feed forward and ratio control techniques in conjunction with feedback loop control. This chapter also discusses the importance of PLL block and needs of ABC to dq0 transformation.

In Chapter 4, the mathematical modeling and decoupled control of single DER unit / multi DER units and entire microgrid in both grid connected and islanded modes are discussed. This chapter also focuses on the operation of microgrid during switching from one mode to other mode of operation.

In Chapter 5, the detail study and simulation results of dc-dc boost converter, single DER unit, multi DER units and entire microgrid operating in islanded and grid connected modes are presented.

In Chapter 6, conclusions are drawn and future scope of the work is discussed.

Chapter 2

Modeling and Design of Closed Loop DC-DC Boost Converter with PI Controller, PWM Techniques and Passive Filter

In this project inverter has been designed such that it generates 230 Vrms phase voltage at modulation index of 0.8 as it would be difficult to track crossing point between modulating waveform and carrier waveform by DSP if modulation index of above 0.9. Taking this into consideration, the input voltage of inverter is maintained at $814 V_{dc}$. As Most of the DERs do not generate DC voltage at this level, we need to boost up it up to the required voltage level. Also we have to maintain this DC voltage at constant level against any variation in source voltage and load. This task can be fulfilled by designing a closed loop DC-DC converter with PI controller.

In this Chapter, initially the modeling of closed loop DC-DC converter has been carried out for designing of PI controller. Then, three phase current controlled VSI and modulation technique to generate switching pulses have been explained. At the end of this chapter design of passive LC filter has been explained satisfactory.

2.1 DC-DC Boost Converter

The circuit of the PWM boost dc-dc converter is shown in Fig.2.1. Its output voltage V_0 is always higher than the input voltage V_1 for steady-state operation of the converter. It ‘boosts’ the dc input voltage to the desired output voltage by varying the duty ratio (D) of the switch appropriately. The converter consists of an inductor L , a power MOSFET, a diode D , a filter capacitor C , and a load resistor R_L . The switch S gets turned on and off at the switching frequency $f_s = 1/T$ with the ON duty ratio $D = t_{on}/T$, where t_{on} is the time interval when the switch S is ON. The boost converter can operate in either continuous or discontinuous conduction mode [9]-[11]. It depends on the waveform of the inductor current. The Matlab simulation circuit of a DC-DC converter without controller is shown in Fig.2.2.

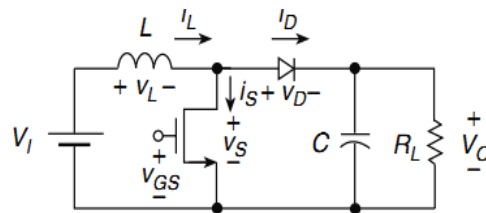


Figure 2.1: PWM boost converter basic circuit [9]

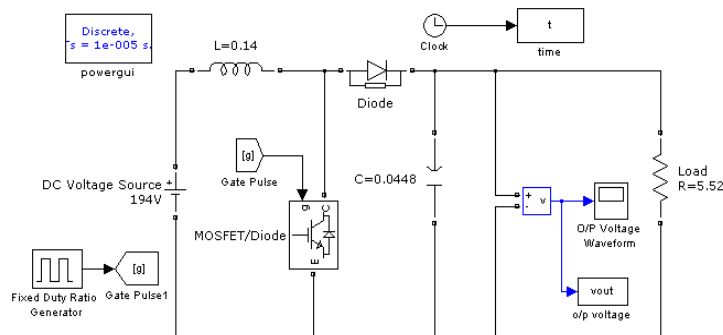


Figure 2.2: Matlab/Simulink circuit of a PWM boost converter without control

2.1.1 DC-DC boost converter design

Design specification:

Here, DC-DC boost converter has been designed for solar pv systems. The design specifications given at the Standard Test Condition are the following:

1. Output voltage of dc-dc converter = 814 V
2. Output voltage ripple = 0.25 V
3. Ripple current = 0.1 A
4. Switching frequency = 10 KHz

The inductor and capacitor values in the converter are decided according to the current and voltage ripple respectively. The value of the load resistance is determined according to the desired output voltage and the maximum power supplied by the solar panel at Standard Test Condition. For the given specifications, the calculation of the inductance and capacitance and load resistance is shown in the following few lines.

Under Standard Test Condition, maximum power supplied by the solar panel array is 120 KW and it occurs at the array output voltage of 194 V (i.e. $P_{max} = 120$ KW).

$$P_{max} = 120 \text{ KW}$$

$$V_1 = 194 \text{ V}$$

$$V_0 = 814 \text{ V}$$

$$P_{max} = \frac{V_0^2}{R_L}$$

$$\Rightarrow R_L = 5.52 \Omega$$

Now, the duty ratio for the boost converter is given by [9],

$$D = 1 - \frac{V_1}{V_0} = 0.76$$

However, by using Boost converter basic equations [9] (2.1) and (2.2), we get the inductor and capacitor values for boost converter,

$$\Delta i_L = \frac{V_0}{4f_s L}$$

Therefore,

$$L = \frac{V_0}{4f_s \Delta i_L} \quad (2.1)$$

$$\Delta V = \frac{V_0 D}{RCf_s}$$

So we get,

$$C = \frac{V_0 D}{RCf_s} \quad (2.2)$$

From equations (2.1) and (2.2) we get,

$$L = 0.14 \text{ H}$$

$$C = 0.0448 \text{ F}$$

The designed closed loop dc-dc boost converter is shown in Fig.2.3 and the Matlab simulation circuit of a closed loop boost converter with PI controller is shown in Fig.2.4

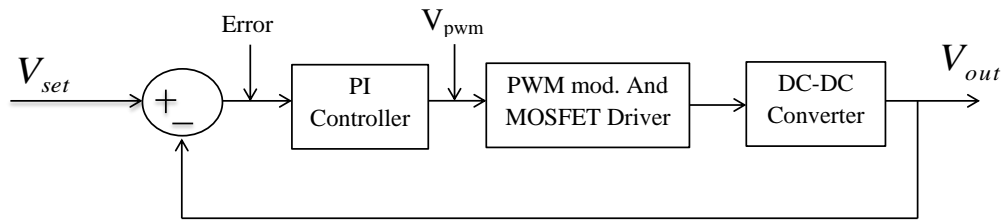


Figure 2.3: Feedback loop control of DC-DC converter

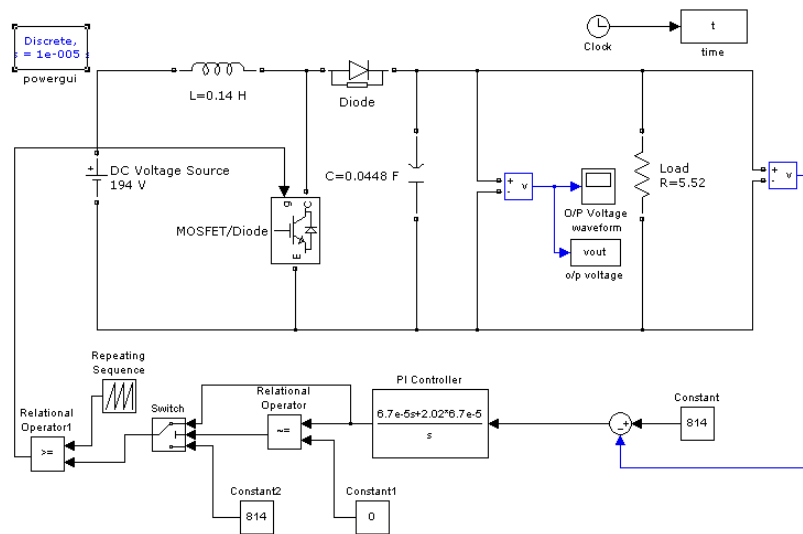


Figure 2.4: Matlab/Simulink circuit of a PWM boost converter with control

2.1.2 Boost converter transfer function

The boost converter has two cycles of operation in one switching period.

1. Charging cycle
2. Discharging cycle

1) Charging cycle :

When switch S is ON,

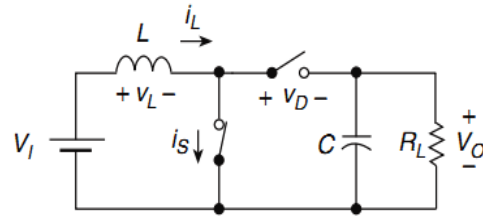


Figure 2.5: Converter circuit during charging cycle [9]

Applying KVL to the circuit, we have,

$$V_L = V_1 = L \frac{di_L}{dt}$$

\Rightarrow

$$\frac{di_L}{dt} = \frac{V_1}{L} \quad (2.3)$$

The capacitor current is given by,

$$\frac{dV_0}{dt} = -\frac{1}{C} \left(\frac{V_0}{R_L} \right), \quad 0 < t < t_{on}, S_1 : ON \quad (2.4)$$

2) Discharging cycle :

When switch S is OFF,

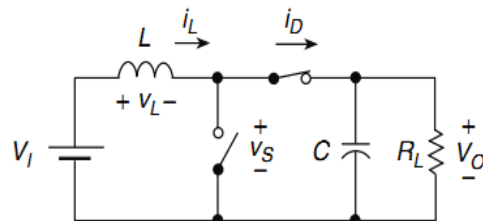


Figure 2.6: Converter circuit during discharging cycle [9]

Applying KVL to the circuit, we have,

$$V_1 - V_0 = L \frac{di_L}{dt}, \quad T_{on} < t < T, S_1 : OFF$$

\Rightarrow

$$\frac{di_L}{dt} = \frac{1}{L}(V_1 - V_0) \quad (2.5)$$

The capacitor current is given by,

$$\frac{dV_0}{dt} = \frac{1}{C}(i_L - \frac{V_0}{R_L}) \quad (2.6)$$

Averaging the derivatives over a switching period (T_s), we have,

$$\frac{di_L}{dt} = \frac{V_1 - V_0(1 - D)}{L} \quad (2.7)$$

$$\frac{dV_0}{dt} = \frac{i_L(1 - D)}{C} - \frac{V_0}{R_L C} \quad (2.8)$$

Considering the small perturbation, using equation (2.7) and (2.8) and ignoring $\Delta V_0 \Delta D$ we have,

$$\frac{d\Delta i_L}{dt} = \frac{\Delta V_1 + V_0 \Delta D - \Delta V_0 + \Delta V_0 D}{L} \quad (2.9)$$

The corresponding form for equation (2.8) is:

$$\frac{d\Delta V_0}{dt} = \frac{\Delta i_L - D \Delta i_L - \Delta i_L}{C} - \frac{\Delta V_0}{RC} \quad (2.10)$$

\Rightarrow

$$\frac{d^2 \Delta V_0}{dt^2} = \frac{1}{C} \left[\frac{d\Delta i_L}{dt} - D \frac{d\Delta i_L}{dt} - \Delta D \frac{d\Delta i_L}{dt} \right] - \frac{1}{RC} \frac{d\Delta V_0}{dt}$$

Further simplification is done by using equation

\Rightarrow

$$\frac{d^2 \Delta V_0}{dt^2} = \frac{1}{C} \left[-\frac{V_1 \Delta D}{L} + \frac{2V_0 \Delta D}{L} - \frac{\Delta D D 2V_0}{L} + \frac{D \Delta V_0}{L} - \frac{D^2 \Delta V_0}{L} - \frac{\Delta V_0}{L} + \frac{D \Delta V_0}{L} + \frac{\Delta V_1}{L} - \frac{D \Delta V_1}{L} \right] - \frac{1}{R} \Delta V_0 \quad (2.11)$$

Taking laplace transform of the equation (2.11) we have,

\Rightarrow

$$V_0(s) = \frac{V_1(s) \left[\frac{1}{LC} - \frac{D}{LC} \right]}{s^2 + \frac{s}{RC} - \left[-\frac{1}{LC} + \frac{2D}{LC} - \frac{D^2}{LC} \right]} + \frac{D(s) \left[\frac{2V_0}{LC} - \frac{2V_0 D}{LC} - \frac{V_1}{LC} \right]}{s^2 + \frac{s}{RC} - \left[-\frac{1}{LC} + \frac{2D}{LC} - \frac{D^2}{LC} \right]} \quad (2.12)$$

Equation (2.12) represents the dependence of output voltage of the dc-dc boost converter on the input voltage of the converter and the duty ratio of the control signal fed into the switching device.

2.1.3 System transfer function

The system here consists of the solar panel array and the dc-dc boost converter. The solar panel can be modeled in two ways [12]:

1. A constant voltage source: The solar panel array is considered as a constant voltage source when we attempt to control the output voltage of the converter by varying the duty ratio of the control signal. In this case, the input voltage of the converter is considered to be varying very slowly and hence assumed a constant source. Here, the variation of the output voltage with the duty ratio of the control signal is studied to develop a suitable controller for this system.
2. A current source with a capacitor in parallel: The solar panel array is considered as a current source with a parallel capacitor when we are trying to control the input voltage of the converter (i.e. the output voltage of the solar panel).

The solar panel is considered as a constant voltage source (or the output voltage of the solar panel changes so slowly that it can be considered as a dc- source) then $V_1(s) = 0$ [since $\Delta V_0 = 0$]. Then equation (2.12) becomes,

$$V_0(s) = \frac{D(s) \left[\frac{2V_0}{LC} - \frac{2V_0 D}{LC} - \frac{V_1}{LC} \right]}{s^2 + \frac{s}{RC} - \left[-\frac{1}{LC} + \frac{2D}{LC} - \frac{D^2}{LC} \right]} \quad (2.13)$$

The equation (2.13) represents the transfer function of the system when the controller (to be designed in later section) attempts to control the dc-dc boost converter output voltage.

Substituting the values of L, C and R_L , we get the following transfer function,

$$\begin{aligned} G_s &= \frac{V_0(s)}{D(s)} \\ &= \frac{31364.79}{(s + 2.02)(s + 2.02)} \end{aligned} \quad (2.14)$$

Here, we get the transfer function of the boost converter. The output of the transfer function gives us duty ratio which generates the switching pulses to get controlled output voltage (i.e. 814 V).

2.1.4 Design of PI controller

The PI controller consists of a constant added to an integrator with a gain stage.

The basic PI controller transfer function appears like

$$G_R = K_R \frac{(s + 1/T_i)}{s}$$

Where,

K_R = Gain of the controller

T_i = Integration time constant

The PI controller parameters (K_R, T_i) depend upon the system we consider for the design. The Fig.2.4 represents the closed loop system along with the PI controller when the output of the dc-dc boost converter is traced by the controller.

The open loop transfer function is given by,

$$G_s \cdot G_R = \frac{31364.79}{(s + 2.02)(s + 2.02)} \frac{K_R(s + 1/T_i)}{s} \quad (2.15)$$

According to Pole-Zero cancelation [11] we remove RHS pole, $1/T_i = 2.02$ Then, the characteristic equation is given by the closed loop system is,

$$s^2 + 2.02s + K_R(31364.79) = 0$$

So we have, $2\delta\omega_n = 2.02$

$$\Rightarrow \omega_n = 1.45 \quad [\delta = 0.7]$$

And for K_R ,

$$\omega_n^2 = (31364.79)K_R$$

\Rightarrow

$$K_R = 6.7 \times 10^{-5}$$

PI controller equation is become,

$$G_R = \frac{6.7 \times 10^{-5}(s + 2.02)}{s}$$

In this thesis work we have assumed that the DC input voltage of an inverter is constant irrespective of variation in source voltage and load, so closed loop DC-DC boost converter with PI controller fulfill this assumptions.

The above system, consisting of a constant voltage source, dc-dc boost converter and a PI controller (as designed), is implemented in Matlab Simulink and the results are discussed in Chapter 5.

2.2 Voltage Source Inverter Operation and SPWM

An important function of the Voltage Source Inverter (VSI) for distributed generation application is to control the balance between ac and dc power. Single phase VSIs cover low-range power applications and three phase VSIs cover the medium- to high-power applications. The main purpose of these topologies is to provide a three-phase voltage source, where the amplitude, phase and frequency of the output voltages should always be controllable. A three phase, three leg voltage source inverter with input DC source and three phase AC output LC filters is shown in Fig.2.7. Using a VSI, the DC is converted to AC of required voltage and frequency [10],[13]. A three phase, three legs voltage source inverter with input DC source and three phase AC output LC filters is shown in Fig.2.7 and the eight valid switch states are given in Table 2.1.

Table 2.1: Inverter Pole Voltages with respect to Switch Positions where $i = a, b, c$

S_i	S'_i	V_{in}
0	1	$-V_{dc}/2$
1	0	$+V_{dc}/2$

The switches of any leg of the inverter cannot be switched on simultaneously because this would result in a short circuit across the dc link voltage supply. In order to generate a given voltage waveform, the inverter moves from one state to another. Thus the resulting ac output line voltages consist of discrete values of voltages that are $-V_i/2, 0, V_i/2$ for the topology shown in Table 2.1. The selection of the states in order to generate the given

waveform is done by the modulating technique that should ensure the use of only the valid states. The LC filter eliminates harmonics and provides a near sinusoidal output voltage. In Fig.2.7 $V_{dc}/2$ is input dc source voltage and L_a, L_b, L_c and C_a, C_b, C_c are filter inductances and capacitances, respectively. The impedance Z_{Load} represents the load impedance. Voltages V_{la}, V_{lb}, V_{lc} are load voltages and i_{Labc}, i_{oabc} are three phase filter inductor currents and load (output) currents respectively. Switches S_a, S_b, S_c are top switches and switches S'_a, S'_b, S'_c are bottom switches.

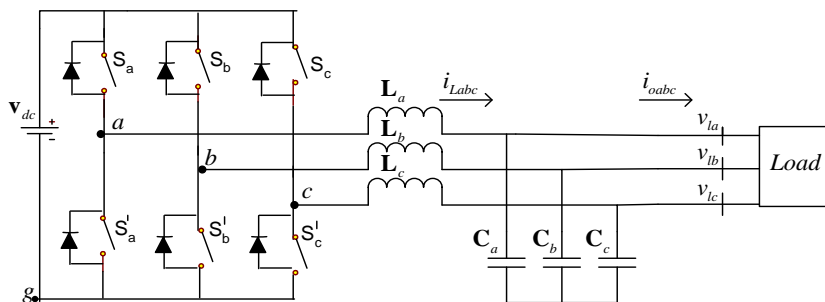


Figure 2.7: Schematic diagram of a VSI

In practice, these switches are implemented using IGBTs or MOSFETs. The gate signals to these switches are obtained using Sinusoidal Pulse Width Modulation (SPWM) technique. The SPWM technique is explained in the next section.

2.2.1 Pulse width modulation technique

Pulse width modulation control is the most widely used method of controlling the modulation depth of inverters, some popular PWM techniques are Sine-PWM (SPWM), Sine + 3rd harmonic PWM and space vector PWM (SV-PWM). Among these here we have discussed SPWM technique and in this technique three reference sinusoidal signals which are phase shifted by 120° from each other are compared with a high frequency carrier signal. The sine-triangle pulse width modulation technique is shown in Fig.2.8. When the reference voltage signal is compared with the carrier signal (triangular wave is used generally) as shown in Fig.2.9 then if reference signal is greater than carrier signal S_a

is switched on ($S_a = 1$), otherwise S'_a is on ($S'_a = 1$). Similarly the gate signals for the switches in the remaining two legs are generated by comparing reference voltage signals with carrier signal. The switches are triggered in a complementary fashion, i.e. no two switches in a particular leg are switched at a time [9],[10]. Based on this logic pulse width modulator is designed in the thesis as shown in below figure. The amplitude, phase and frequency of the reference signals are set to control the output voltages of 3-phase VSI. Fig.2.8 shows the generation of PWM waveform by using SPWM technique.

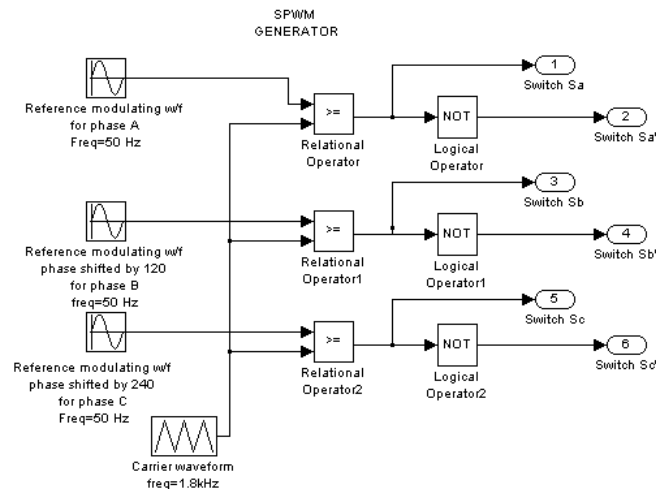


Figure 2.8: Sine-triangular pulse width modulator

If ($S_a = 0$ or 1) then ($S'_a = 1$ or 0)

The peak value of per phase fundamental voltage obtained using SPWM technique is given by,

$$V_o = m_a V_{dc}/2 \quad (2.16)$$

where, m_a is amplitude modulation index, which is the ratio of peak value of reference signal to peak value of carrier signal. Let V_s be the peak value of reference sinusoidal signal and V_c be the peak value of carrier signal. Mathematically, amplitude modulation index is given as,

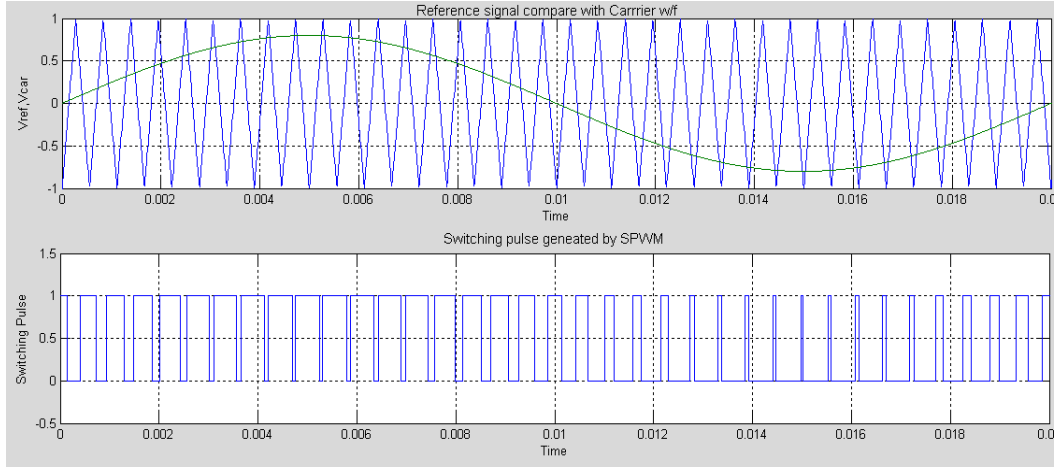


Figure 2.9: Sinusoidal pulse width modulation

$$m_a = \frac{V_s}{V_c} \quad (2.17)$$

The harmonics in voltage generated will be centered on frequency modulation index (m_f) and its multiples. Let f_s be the frequency of reference sinusoidal signal and f_c be the frequency of carrier signal. Mathematically, frequency modulation index is given as,

$$m_f = \frac{f_c}{f_s} \quad (2.18)$$

To help in the iterative process of controller design and optimization, average models of the system replace the switching models. Average models tend to have simulation times that are orders of magnitude smaller than those of the switching models. To further help in the design of the control system, the models are derived in both stationary (ABC) and rotating (dqo) coordinate frames. The modeling of VSI in ABC frame is presented in the next Chapter.

2.3 Design of L-C Filter for Grid-Connected and Is-landed Mode Power Converters

Most renewable sources of energy like wind, solar, fuel cell, and so on, are interfaced to the existing power supply by a power converter because they are not going to generate voltage and frequency of desired magnitude. But use of power converters will also introduce undesirable harmonics that can affect nearby loads at the point of common coupling to the grid. And as per standard the injected current into the grid should not have a THD larger than 5%. Hence all such converters have a filter to eliminate these harmonics and to improve power quality. So power filter uses to meet imposed utility distortion limits, to improve power quality and also to avoid parallel resonance. Passive harmonic filters are often used to meet reduce voltage harmonics and current distortion in distributed generation systems.

The present work is on design of such filters for high power (10's to 100's of KW) pulse width modulated voltage source inverter for grid-connected as well as islanded converter applications. In a grid connected mode, the harmonic current injected into the grid is the main issue while in an islanded mode the DG unit is the source of power and voltage harmonics which are the main concern. According to IEEE 519 standard harmonic orders greater than 35 must not exceed 0.3% of rated current. The conventional method to interface these converters is through a simple first order low-pass filter, which is bulky, inefficient and cannot meet regulatory requirements [14]. So it is better to use 2nd order low pass LC filter instead of 1st order L filter.

When dealing with filter circuits, it is always important to note that the response of the filter depends on the filter component values and independent of the load. There are certain simplifying assumptions that are made to analyze the frequency characteristics of the grid connected as well as islanded low pass filter. The assumptions are made to keep the initial design simple.

- All filter elements are considered ideal, i.e. no winding resistance, inter-turn/inter winding capacitance in case of inductor, and no equivalent series resistance, parasitic inductance in case of capacitor.
- Grid is considered as an ideal voltage source, i.e. zero impedance, and supplying constant voltage/current at fundamental (50Hz) frequency. This is a valid assumption since any impedance at the grid can be lumped with the output impedance of the filter.
- The filter design procedure is appropriate for grid connected PWM voltage-source inverters. Current source inverters are not considered.
- The design procedure assumes only grid connected mode of operation. Stand alone converter applications are only briefly discussed.

2.3.1 Design procedure for filter design

A single leg of a three-phase inverter can be represented as shown in Fig.2.10. The inverter voltage and current are represented as V_i , i_i and the grid voltage and current are represented as V_g and i_g .

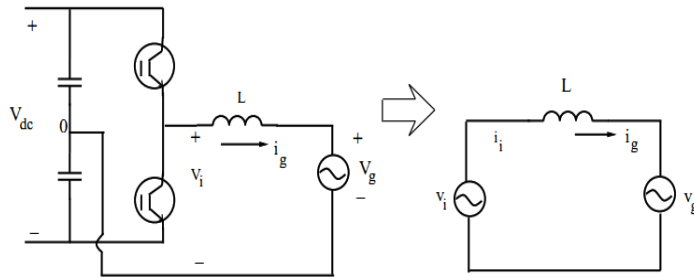


Figure 2.10: Equivalent circuit of one leg of grid connected 3-phase VSI

We can define the dc bus voltage V_{dc} in terms of pole voltage V_i . The pole voltage can be defined based on the base voltage $V_g = V_{base}$. The assumptions are that the grid voltage can have a maximum variation of 10%, and the pole voltage will be reduced by 5% because of dead band switching requirement. We are also taking into account the

voltage drop due to a series filter, which usually will not exceed 10% of the inverter pole voltage.

Considering the Single lag of the three phase inverter,

$$\frac{V_{dc}}{2} = V_i = V_{base} \times \sqrt{2} \times 1.1 \times 1.05 \times 1.1 \quad (2.19)$$

For the three phase topology shown in Fig.2.10 the pole voltage V_i depends on the modulation method. In case of sine-triangle modulation, the peak pole voltage amplitude (in case of linear modulation) is

$$V_i = \frac{m_a V_{dc}}{2} \quad (2.20)$$

Where m_a is modulation index. So the maximum Dc bus voltage will be when $m_a = 1$.

Voltage and Current ripple:

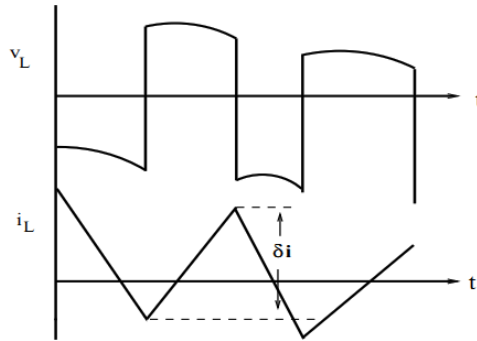


Figure 2.11: Waveforms of voltage and current across filter inductor

From the Fig.2.11 if Δi_{p-p} is the peak to peak ripple current in the inductor, then

$$\Delta i_{rms} = \frac{\Delta i_{p-p}}{2\sqrt{3}} \quad (2.21)$$

The grid voltage is assumed vary from -20% to +10%, i.e.

$$0.8V_g \leq V_g \leq 1.1V_g$$

The inverter pole voltage is a combination of fundamental voltage and harmonic voltages at various higher frequencies. By assuming this the most dominant harmonic voltage is at switching frequency, we can write the rms value of the inverter pole voltage as,

$$V_{i(rms)}^2 = V_{i(50)}^2 + V_{i(fsw)}^2 \quad (2.22)$$

Where $V_{i(50)}$ is the rms value of the fundamental voltage at 50 Hz and $V_{i(fsw)}$ is the rms value of the switching frequency harmonic voltage. From Fig.2.11, it is clear that the total rms value of the inverter pole voltage is $V_{i(rms)} = \frac{V_{dc}}{2}$ (waveform is square). The rms value of the fundamental depends on the modulation index.

In grid connected mode the design of an L filter is based on the current ripple at switching frequency that is present in the PWM output.

If we consider one single switching cycle of the inverter, from Fig.2.13

During T_{on} ,

$$V_{i(50)}^2 = \left[\frac{1}{\sqrt{2}} \frac{V_{dc}}{2} m_a \right]^2 \quad (2.23)$$

$$L \frac{\Delta i_{p-p}}{T_{on}} = \frac{V_{dc}}{2} - V_g \quad (2.24)$$

During T_{off} ,

$$L \frac{\Delta i_{p-p}}{T_{off}} = -\frac{V_{dc}}{2} - V_g \quad (2.25)$$

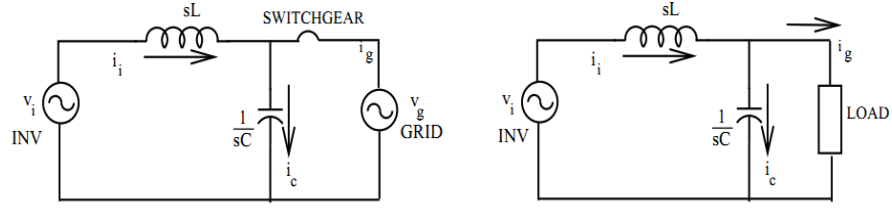


Figure 2.12: Filter behavior during grid connected and islanded mode

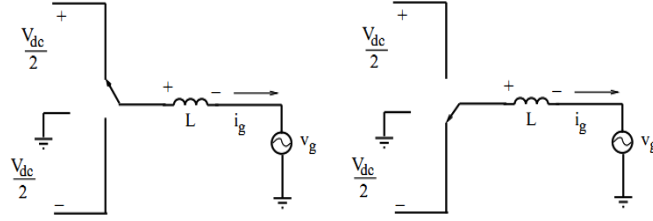


Figure 2.13: Switching circuits of single leg of the three phase inverter

Where, $v_g = V_m \sin \omega t$ and $T_{on} + T_{off} = T_{sw}$,

Since the modulation method is sine-triangle modulation, the duty ratio D is [9],

$$D = 0.5 + \frac{V_m \sin \omega t}{V_{dc}} = 0.5 + \frac{V_g}{V_{dc}} \quad (2.26)$$

So from equations (2.24) and (2.25) we get,

$$T_{on} = L \frac{\Delta i_{p-p}}{V_{dc}(1-D)} \quad (2.27)$$

$$T_{off} = L \frac{\Delta i_{p-p}}{V_{dc}D} \quad (2.28)$$

Adding the above two equations, we get

$$L_{actual} = \frac{V_{dc}D(1-D)}{f_{sw} \times 2\sqrt{3} \times \Delta i_{rms}} \quad (2.29)$$

Here, D is the duty cycle of the switch such that the average voltage at fundamental frequency is sinusoidal.

In stand-alone or islanded mode design procedure of L filter would be same but designing of 2^{nd} order LC filter would be much more complicated since the placement of the resonant frequency becomes an important factor which affects the closed loop response. The allowable current ripple is once again the criteria for designing L. The capacitor C is constrained by two factors.

- The resonant frequency of the filter elements
- The bandwidth of the closed loop system

The capacitance of the LC filter is decided by the resonant frequency. The design decision on selecting the resonant frequency depends on the bandwidth of the closed loop system. Selection of capacitor based on Resonance frequency,

$$f_{res} = \frac{1}{2\Pi\sqrt{L_{actual}C_{actual}}} \quad (2.30)$$

Therefore,

$$C_{actual} = \frac{1}{(2\Pi)^2 f_{res}^2 L_{actual}} \quad (2.31)$$

The transfer function of grid current i_g to inverter voltage V_i is same for L and LC filters when parasitic grid impedances are neglected (Fig.2.10). Therefore, the size of inductor does not change from L to LC filter [14]. Consider an LC filter connected between an inverter and external load. Then the transimpedance transfer function for islanded mode will be,

$$\frac{i_g}{V_i} = \frac{1}{s^2LCR + sL + R} \quad (2.32)$$

Now, for grid connected mode the DER is connected with a grid having assumption that the grid has constant voltage, constant frequency and zero impedance. As utility grid has zero impedance capacitor does not have any effect on output response. So, the transimpedance transfer function for grid connected mode will be

$$\frac{i_g}{V_i} = \frac{1}{sL} \quad (2.33)$$

Additionally, a grid connected LC filter can behave as an LCL filter because of the parasitic impedances of the grid. But this arrangement is not reliable since the parasitic impedance of the grid is not under the control of the converter designer. Designed L-C filter parameters and graphs are discussed in Chapter 5.

2.4 Summary

In this chapter, we looked at the basic theory of the boost converter which can help us to analyze the transfer function of the converter. Derivation of the closed loop transfer function is explained step-wise. Further, the basic introduction of the VSI operation and pulse width modulation technique are explained. Finally, the filter design of VSI for grid connected as well as stand-alone (islanded) application has been discussed.

Chapter 3

Overview of Control Strategies for Islanded and Grid-Connected Mode of Operation of Microgrid and Importance of PLL Block

From Chapter 2, where SPWM is discussed, it is known that by setting magnitude, phase and frequency of reference signal, the output voltage magnitude and frequency can be controlled. The task of setting the proper value of magnitude, phase and frequency according to the system requirement is done by a controller. So, the prime challenge in microgrid is to design suitable controller for proper co-ordination and control of DERs and harvesting maximum energy from DERs. This leads to grid stability, synchronization with utility grid, proper load sharing among DERs, real-reactive power transfer between microgrid and utility grid, maintaining voltage and frequency within allowable range at each bus etc. In other words controller is the heart of the microgrid.

In this chapter first the basics and needs of controller have been explained along with the control tasks. Then needs of ABC to dq0 transformation has been discussed in detail. Later, VSI switched and averaged model have been developed to explain the control task of two level VSC in microgrid. Finally, at the end of this chapter PLL block and formation

of real and reactive powers in dq domain have been covered briefly.

3.1 Review of Controller Basics and Its Important in Microgrid

Necessity:

By designing proper controller, any quantity of interest of a system is maintained within specified limits or altered in accordance with a desired manner.

Basics of controller:

There are several types of controllers like P, PI, PID, Intelligent controller, Smart controller, Robust controller, Adaptive controller, Stochastic controller, Genetic controller, Optimal controller, Fuzzy controller and so on [15]. Design and type of the controller depends on - type of control action, type of system, type of response, time of response, limits of steady state error, type of disturbance and so on. Though, there are several methods for controller design, in this thesis, feedback control, feed forward control, cross coupling control and ratio control have been discussed.

Control action starts immediately for a change in set point of a controller. For a change in load disturbance there is a delay introduced by feedback loop, due to VSI and LC filter. If the load disturbances are sensed and the sensed signal is given to the controller, the control action start after a delay in time and not instantaneously, due to the reason mentioned above. However, change in set point of controller will result in instantaneous control action because it will not suffer from delay introduced by feedback loop. Therefore it is clear that as feedback structure alone is not much sufficient to neutralize the effect of disturbances feed forward control needs to be included in conjunction with feedback control. For frequent change in load disturbance, feedback regulation is an ineffective process for taking control action. This is the disadvantage of feedback control structure. Therefore to compensate it we may incorporate feed forward control with feedback control such that the combined effect would improve the dynamic response of the system.

Feedback and feed forward control :

The basic block diagrams of feedback and feed forward control for microgrid system are shown in Fig.3.1 and Fig.3.2 respectively.

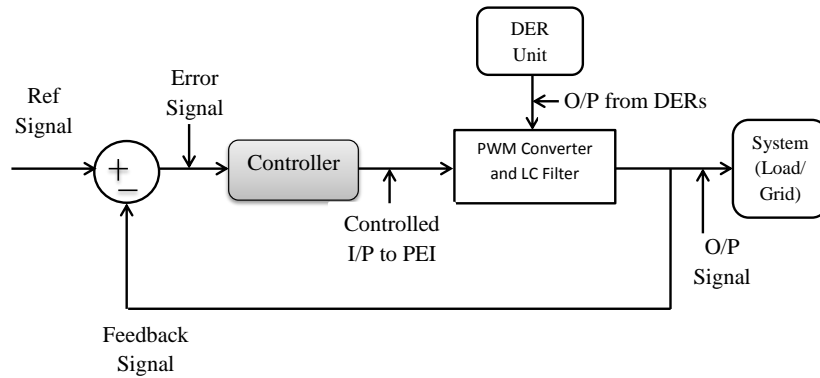


Figure 3.1: Basic block diagram of feedback loop control

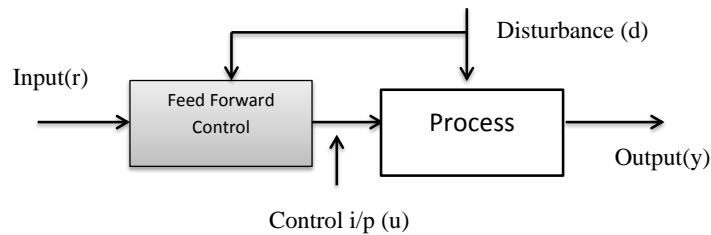


Figure 3.2: Block diagram of feed forward loop control

Feed forward control measures the load disturbance and takes predictive action even before it affects the output. Therefore, the control input to PEI (u) will change according to the change in the disturbance (Fig.3.1). For taking accurate action we have to know the correct model of process/ plant because in feed forward the feedback path is not available to check the output. Thus, the disadvantage of feed forward control is that the control is heavily dependent on model accuracy, while in feedback control it is not required to know accurately the process model because output is corrected through feedback action. So, by using both feedback and feed forward control simultaneously, we are utilizing the best of both controls. Feed forward control is used to mitigate the impacts of,

- load dynamics on system stability and performance and,
- inherent inter couplings and nonlinearities of the control system.

Stability characteristics depend only on the feedback loop control because feed forward control is an open loop system. Therefore, no stability issues concern with the feed forward control. Here control energy is mostly supplied from the feed forward system compare to the feedback system, while error in feed forward control is corrected by feedback control. In the feed forward control we need to know the parameters of the system where as in the feedback control we do not need to know the parameters and hence the feed forward control is not much popular.

3.2 Needs of ABC to dq0 Transformation for Controller Design

Because of microgrid is a complex structure, in which several subsystems like energy sources, power electronics converters, filters, loads, energy storage systems are interacted with each others. Modeling and analysis of the whole system assist to get insight view of a microgrid, which can be used to control it properly. There are several domains, such as ABC domain, dq0 domain, arbitrary reference frame domain, $\alpha - \beta$ ref frame domain and so on, present for doing modeling of a system. It is too difficult to extract some information from one domain, so to get this hidden information, transformation from present domain to another domain is required. Generally a system which needs to be controlled is in dynamic nature and dynamic system is characterized by differential equations, so differential equations play an important roles in a controller designing task. In this work, first all differential equations have been wrote in abc domain then transformed them from abc domain to dq domain for the ease of calculation and reducing complexity of the controller design.

The Park transformation as per equation (3.1) is used to transform from ABC domain to

dq domain [16],

$$f_{dq0} = K_s f_{abc} \quad (3.1)$$

where,

$$f_{dq0} = \left[f_d \ f_q \ f_0 \right]^T, f_{abc} = \left. \begin{array}{c} \left[f_a \right]^T \\ f_b \\ f_c \end{array} \right\}$$

and the Park transformation matrix K_s is given by,

$$K_s = (2/3) \left. \begin{array}{c} \left[\begin{array}{ccc} \sin(\omega t) & \sin(\omega t - 2\Pi/3) & \sin(\omega t + 2\Pi/3) \\ \cos(\omega t) & \cos(\omega t - 2\Pi/3) & \cos(\omega t + 2\Pi/3) \\ 1/2 & 1/2 & 1/2 \end{array} \right] \end{array} \right\} \quad (3.2)$$

Where, ω = rotational speed (rad/s) of the rotating frame.

The following are the reasons of transforming from ABC to dq domain:

1. For getting zero steady state error loop gain magnitude should be infinitive at the frequency of command signal while in the dq frame control, zero steady state error is readily achieved by including integral terms in the compensators since the control variables are DC quantities.
2. The sinusoidal command tracking should be achieved if controller is designed in such a way that the BW of the closed loop system adequately larger than the frequency of the command signal. Alternatively the compensators can include complex conjugate pairs of poles at the AC system frequency and other frequencies of interest to increase the loop gain.
3. In ABC domain Lag Compensator is needed to include large magnitude at low frequency.
4. Relatively higher order compensator is required for AC compare to DC for the same

system and in same conditions.

5. The only one disadvantage of dq frame control is that it requires a synchronization mechanism that is usually achieved through the PLL. The PLL block we will explain later in this chapter.

3.3 Control Task in a Microgrid

As microgrid is an active distribution network, flexible and intelligent control system need to be incorporated, in order to harness clean energy from renewable energy sources. One important part of a distribution system is to design a control task for DPGS (Distributed Power Generation Systems-known as a Microgrid) as it is in autonomous mode or in grid connected mode. The general structure for DPGS is shown in Fig.3.3.

The control task can be divided into two major parts:

1. Source (Input) side controller design
 - The main function of these controllers is to take control action such that maximum power has been extracted from the microsources and their sub function is to provide protection of the input side of the converter.
2. Grid (Load) side controller design
 - This design aspect depends on number of tasks that the designed controller needs to be performed. The main tasks are:
 - control of voltage and frequency within specified limit in an autonomous mode;
 - control of P and Q in grid connected mode;
 - control of DC link voltage;
 - control of quality of the injected power;
 - control of synchronization from islanded to grid connected mode and vice versa.

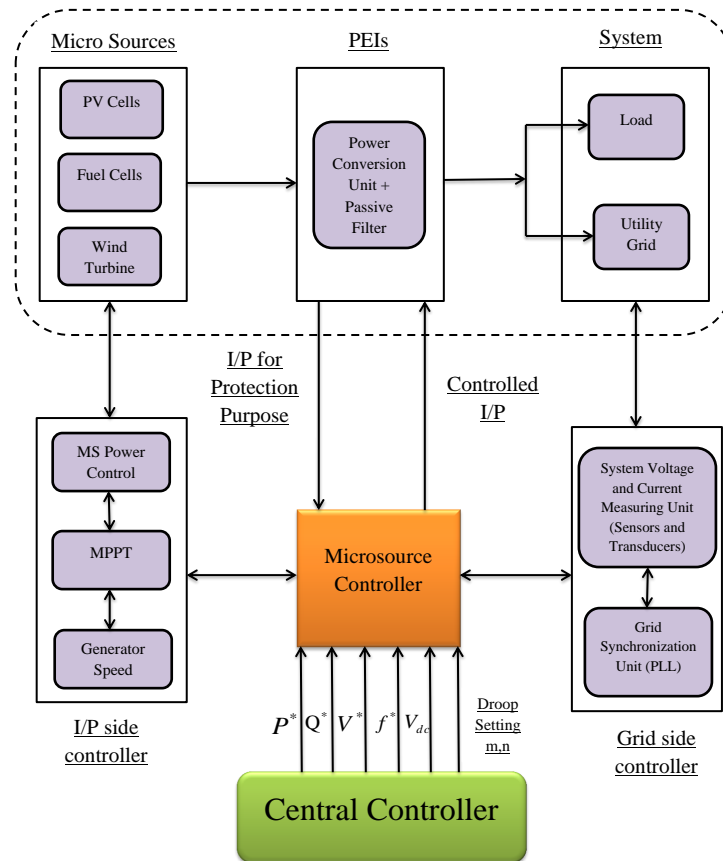


Figure 3.3: General structure of DPGS

3.3.1 Types of controller for microgrid

In a microgrid there is separate local controller for each microsource known as Micro Controller (MC) and there is one master controller which controls all the MCs known as Central Controller (CC) [3].

Micro Controller (MC):

It uses local information to control the microsource during all events. Because of MC each inverter is able to respond to load changes in a predetermined manner without communication of data from other sources, which enables plug and play capabilities. Plug and play implies that a microsource can be added to the microgrid without changes to the control and protection of units that are already part of the system. It facilitates placing generator near the heat loads thereby allowing more effective use of waste heat without

complex heat distribution. It controls the operations based on measurement of voltages and currents. The primary inputs to this controller are steady state set points for output power and local bus voltage.

The local microcontroller helps in harvesting many desirable features from DERs such as, expendability, modularity, maintainability, redundancy and reliability.

Central Controller (CC) :

It uses global information to control all MCs such that whole microgrid operates as a controllable entity. It gives reference commands (V^* , P^* , Q^* , Droop coefficients m , n , etc.) to all MCs so that all the DERs in grid can be operated optimally and efficiently. CC also provides supervisory control on all MCs by sending and receiving the information from MCs.

3.4 Points to be Pondered upon for Designing of Controller in Islanded or Grid Connected Mode of Microgrid

In an autonomous mode the microsourses are controlled to supply all the power needed by the local loads while maintaining the voltage and frequency within the acceptable limits. The terminal voltage and frequency of microsourses, which are going to be connected in parallel or with the same bus, are maintained at constant level in spite of change in load condition, nonlinear loads, unbalanced loads, faults, etc. If it would not be maintained within permissible limits there will be a chance of flowing loop current (circulating current), which may exceed the ratings of microsourses and it would damage the PEIs.

In a grid connected mode the microsourses act as constant power sources which are controlled to inject the demanded power into the grid. Hence, to develop these control

tasks we need to control the PEIs through controller actions. The general layout of microgrid structure is shown in below Fig.3.4 for autonomous mode and for grid connected mode.

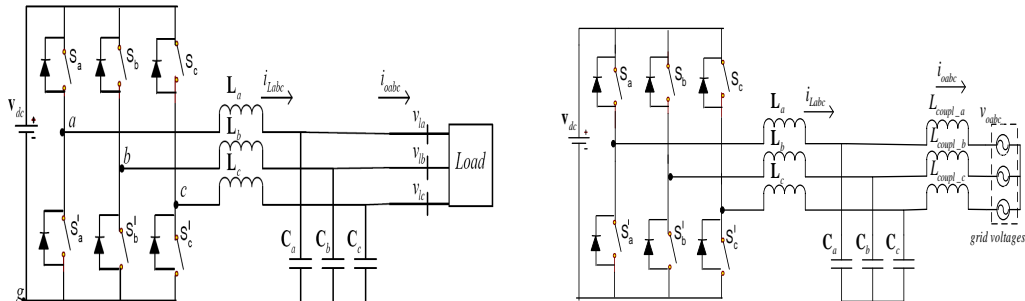


Figure 3.4: General layout of microgrid structure for islanded and grid connected mode respectively

The modeling of the whole system is required to design controller for both modes. Modeling represents physical behavior of the system by mathematical means, i.e. analysis of the circuit by mathematical means. Analysis can be done in time domain, frequency domain or in pole-zero domain. The systematic design of a controller for the entire microgrid can be carried out based on the system dynamic model. Analysis helps to get an insight view of the entire system. The effect of the control variables on the output variables can be studied using modeling and analysis of the system.

3.4.1 VSI modeling

For designing control strategies of Full Bridge Inverter, the characteristics of the converter as observed from its terminals need to be identified and to obtain these characteristics modeling of VSC ought to be done. The modeling of VSC can be done by using switched model of VSC or averaged model of VSC [17]-[20]. VSI Modeling is needed for deriving the relationship between the control variables and the output variables. With the help of this, output voltage and frequency are able to be controlled as per requirements.

1) Switched model of VSC

As shown in Fig.3.5, if only one leg of a 3-phase VSI is considered, then it is like a

half bridge inverter and once the control strategies for a half bridge converter have been developed, it is similar for 3- ϕ full bridge converter and easy to implement it.

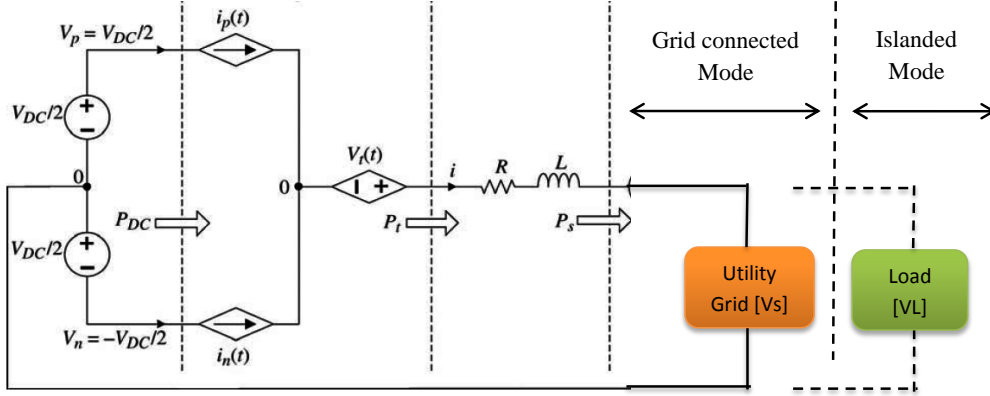


Figure 3.5: Switch model of VSI

The switched model accurately describes the steady-state and dynamic behavior of the converter. The instantaneous values of the current and voltage variables can be computed by means of the switched model. When $S_a = 1$, the upper switch is closed and the lower one is open, therefore, $V_t = V_p = V_{DC}/2$, $i_p = i$ and $i_n = 0$. Alternatively, when $S'_a = 1$, the lower switch is closed but the upper one is open, consequently, $V_t = V_n = -V_{DC}/2$, $i_p = 0$ and $i_n = i$. This holds for both $i > 0$ and $i < 0$, as illustrated in Fig.3.5.

Here,

$$S_a(t) + S_{a'}(t) \equiv 1 \quad (3.3)$$

Now inverter terminal voltage is given by,

$$V_t(t) = (V_{DC}/2)S_a(t) - (V_{DC}/2)S_{a'}(t) \quad (3.4)$$

And inverter leg current is given by,

$$i_p(t) = i \times S_a(t) \quad (3.5)$$

$$i_n(t) = i \times S_a(t) \quad (3.6)$$

Equations (3.3) to (3.6) describe the relationship between the half bridge converter terminal voltages/ currents and the switching functions. Here, the computed variables include high-frequency components, for example, due to the switching process, as well as slow transients. However, the relationships between the modulating signal, which is the main control variable, and the current/ voltage variables are not easily understood from the switched model. Moreover, for dynamic analysis and control design purposes, knowledge about the high-frequency details of variables is often not necessary, as the compensators and filters in a closed-loop control system typically exhibit low-pass characteristics and do not react to high-frequency components. For these reasons, we are often interested in the dynamics of the average values of variables, rather than in the dynamics of the instantaneous values. An averaged model also enables us to describe the converter dynamics as a function of the modulating signal.

2) Averaged model of VSC

The Fig.3.6, as shown below indicate averaged equivalent circuit of a half bridge converter.

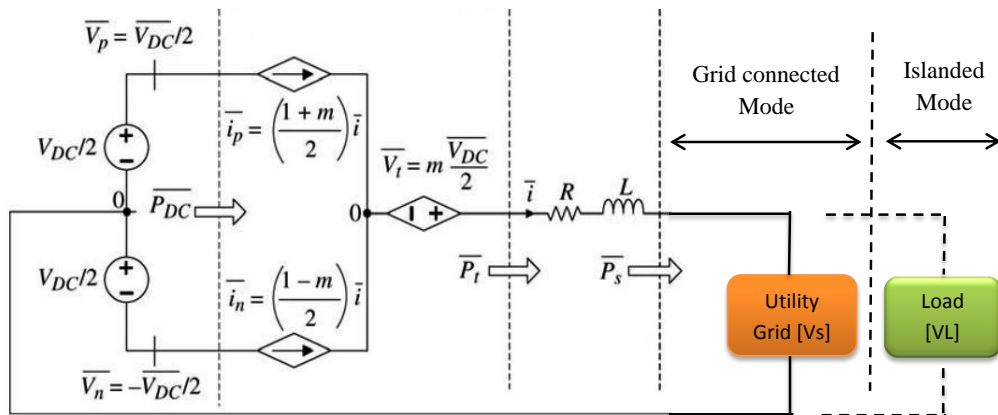


Figure 3.6: Averaged model of VSI

From Fig.3.6 we can write, the first order differential equation as shown below,

$$L \frac{di(t)}{dt} + Ri(t) = V_t(t) - V_s \quad (3.7)$$

Here, $V_t(t)$ is a periodic function with period T_s it can be described by the following fourier series:

$$V_t(t) = 1/T_s \int_0^{T_s} V_t(\tau) d\tau + \sum_{h=1}^{\infty} [a_h \cos(h\omega_s t) + b_h \sin(h\omega_s t)] \quad (3.8)$$

Substitute eqn (3.8) in eqn(3.7), we get,

$$L \frac{di}{dt} + Ri = (1/T_s \int_0^{T_s} V_t(\tau) d\tau - V_s) + \sum_{h=1}^{\infty} [a_h \cos(h\omega_s t) + b_h \sin(h\omega_s t)] \quad (3.9)$$

The above equation (3.9) describes the behavior of low pass filter, whose output is i . The input to the filter consists of two components, the constant (DC) component,

$$L \frac{d\bar{i}}{dt} + R\bar{i} = 1/T_s \int_0^{T_s} V_t(\tau) d\tau - V_s \quad (3.10)$$

and the periodic component,

$$L \frac{d\tilde{i}}{dt} + R\tilde{i} = \sum_{h=1}^{\infty} [a_h \cos(h\omega_s t) + b_h \sin(h\omega_s t)] \quad (3.11)$$

Equation (3.9) is linear, therefore, based on the superposition principle, the response of the filter to the composite input can be regarded as the summation of its responses to individual input components. Therefore,

$$i(t) = \bar{i}(t) + \tilde{i}(t) \quad (3.12)$$

Where, $\bar{i}(t)$ and $\tilde{i}(t)$ are, respectively, the responses of the filter to the DC (low frequency) component and the periodic (high-frequency) component of the filter input. Here, $\tilde{i}(t)$ is referred as the ripple. According to (3.11), if ω_s is adequately larger than R/L , then the periodic component of the input has a negligible contribution to the entire output, the ripple is small, and we can assume that $i(t) \approx \bar{i}(t)$. Thus, the dynamics of the converter system are primarily described by (3.10). This concept is known as averaging in nonlinear systems theory based on moving average principle as shown in equation (3.13) [13].

$$\bar{x}(t) = 1/T_s \int_{t-T_s}^t x(\tau) d\tau \quad (3.13)$$

The periodic switched waveforms are generated by a PWM process. Thus, it can be concluded from Fig.2.9 [Chapter 2] that if the modulating waveform is not constant but varies in time, the switched waveforms S_a and S'_a will not retain their precisely periodic forms. Moreover, the average of the switched waveforms varies from one switching cycle to another. The definition of the average, based on (3.13), allows one to also include such switched waveforms in the averaging process. A prerequisite for validity of equation (3.13) is that the frequency of the carrier waveform should be sufficiently, for example, 10 times, larger than that of the modulating waveform.

Applying the averaging operator, as shown in equation (3.13), to $S_a(t)$ and $S'_a(t)$, we can deduce

$$\overline{S_a}(t) = d \quad (3.14)$$

$$\overline{S'_a}(t) = 1 - d \quad (3.15)$$

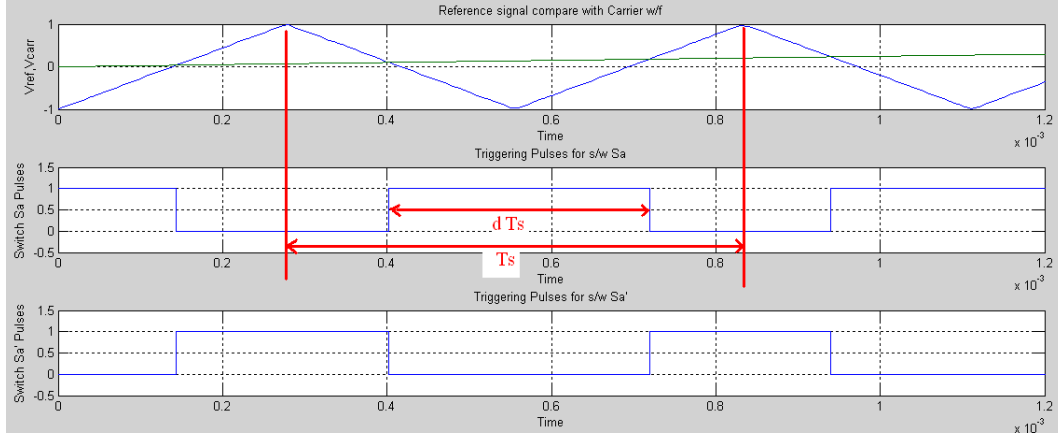


Figure 3.7: Switching waveforms of switches S_a and S'_a

If the carrier frequency is adequately higher than that of the modulating signal, \bar{i} and \bar{V}_{DC} can be assumed as constant values over one switching cycle [9], [11], [13]. Substitute equations (3.14) and (3.15) into equations (3.3) to (3.6) and take average of both sides, we get,

$$\bar{V}_t = \frac{V_{DC}}{2}(2d - 1) \quad (3.16)$$

$$\bar{i}_p = d \times i \quad (3.17)$$

$$\bar{i}_n = (1 - d) \times i \quad (3.18)$$

The duty ratio d can assume any value between 0 and 1. If the PWM strategy is adopted, $m = 2d - 1$ describes the relationship between the magnitude of the modulating signal and the duty ratio. Substituting for $d = (m + 1)/2$,

$$\bar{V}_t = m \frac{V_{DC}}{2} \quad (3.19)$$

$$\bar{i}_p = \frac{(1 + m)}{2} \times i \quad (3.20)$$

$$\bar{i}_n = \frac{(1 - m)}{2} \times i \quad (3.21)$$

The advantage of the change of variable $d = (m + 1)/2$ becomes evident in equation (3.19), if m is changed from -1 to 1, the averaged AC-side terminal voltage V_i changes linearly from $-V_{DC}/2$ to $V_{DC}/2$, with $m = 0$ corresponding to the zero averaged voltage. Fig.3.6 illustrates the averaged equivalent circuit of the half-bridge converter.

3.4.2 Control of VSC

In Section 3.4.1, the basic model of VSC has been developed and the relationship between the modulating signal and the terminal voltage of an inverter has been derived. The terminal voltage of a VSI can be controlled by controlling the modulating signal through some external control. The beauty of a VSC is that its terminal voltage can be changed just by varying the magnitude of modulating signal as per equation (3.19), to control its output voltage magnitude. Here m is determined by a closed loop control scheme whose function is to regulate current (i).

Controlling of VSC depends on types of VSC systems, there are mainly three types of VSC system [13], [21]-[23].

1. Controlled frequency VSC system

In this type, the AC system frequency is regulated by the control scheme of the VSC system, where the reference for the frequency may be obtained from a supervisory control system.

2. Grid imposed frequency VSC system

In this group, the VSC system is interfaced with a relatively large AC system like a stiff utility grid. Therefore the operating frequency is dictated by the AC system and is fairly constant.

3. Variable frequency VSC system

In a variable frequency VSC system, the VSC is interfaced with an electric machine, and the operating frequency is a state variable of the overall VSC system, depends on the system operating point and is not directly regulated.

AC side control of VSC

Based on the converter averaged equivalent circuit, the dynamics of the ac side current i is described by ,

$$L \frac{di}{dt} = -(R + r_{on})i + V_t - V_s \quad (3.22)$$

where,

$$V_t = \frac{V_{DC}}{2}m \quad (3.23)$$

Here i is the state variable, V_t is the control input and V_s is the disturbance input.

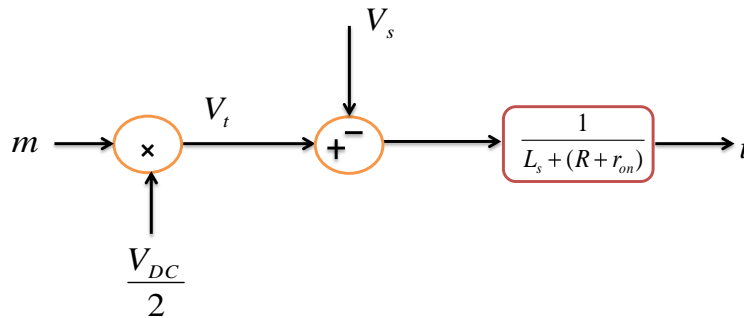


Figure 3.8: Block diagram to control output current i

Here in the open loop system as shown in Fig.3.8, the current (i) is the output and the control objective is to regulate (i) at a pre specified reference value ,this can be achieved via the closed loop system in which the actual output (i) is compared with reference (i_{ref}) and error signal (e) is generated. Then the compensator $K(s)$ processes (e) and provides the control signal (u). Then (u) is divided by $V_{DC}/2$ to compensate for the converter voltage gain as shown in equation (3.23). If the DC side voltage is constant, the numerical value of $V_{DC}/2$ is known in advance and the gain compensation becomes trivial. However,

if the DC- side voltage is subject to variations, V_{DC} must be measured, for example, by a Hall-effect voltage transducer, to enable the gain compensation that can be regarded as a feed-forward compensation.

The output of the controller must be limited prior to being delivered to the converter pulse-width modulation (PWM) signal generator, to ensure that $|m| \leq 1$. Depending on the type of the reference signal and the desired performance, different types of compensator may be used for the control. However, for this thesis work controllers are used in dq domain, i.e., all the quantities which are to be processed and to be controlled are steady in nature so PI controller is sufficient for the control. The integral term of PI controller guarantees that (i) tracks (i_{ref}) with zero steady state error, in spite of the disturbance V_s .

3.4.3 Need for feed forward compensation

a) To reduce startup transient and disturbance rejection capability

The undesirable start-up transient can be avoided if the feedback control scheme is augmented with a feed-forward compensation scheme, as shown in Fig.3.9. [Left side of Fig.3.9 indicates feedback loop control and right side of Fig.3.9 indicates feedback loop in conjunction with feed forward control]

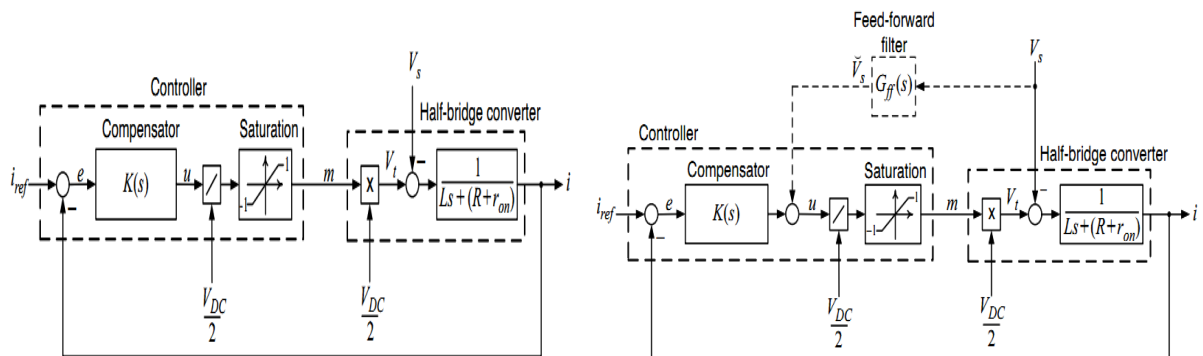


Figure 3.9: Control block diagram of the closed loop half bridge inverter system without and with feed forward control scheme

The feed-forward scheme augments the compensator output with a measure of V_s . This measure, denoted by \widehat{V}_s , can be obtained from a voltage transducer whose (dynamic) gain is $G_{ff}(s)$, where $G_{ff}(0) = 1$. Therefore, at the start-up instant when the compensator output is zero, the AC-side terminal voltage to be generated starts from a value equal to V_s , and the AC-side current remains at zero. Therefore, $V_t = V_s$, the voltage across the series RL interface reactor equals zero, and thus no current excursion is experienced.

b) To decouple dynamic coupling between converter system and AC system

The benefit of the feed-forward compensation is not restricted to improving the converter start-up transients. The feed-forward compensation can also decouple dynamics of the converter system from those of the AC system with which the converter system is interfaced.

Without the feed-forward compensation, that is, $G_{ff}(s) \equiv 0$, the compensator design must take into account dynamics of the AC system. The dynamics may be uncertain, time varying, nonlinear and of a high order. Therefore, the compensator design would be laborious and may not be straightforward. Moreover, the impact of the AC system transients on the control cannot be readily mitigated. However, if the feed-forward compensation is employed, a prior knowledge of the AC system dynamics is not essential for the controller design. The reason is that the dynamics of the half-bridge converter system become effectively decoupled from those of the AC system if $G_{ff}(s) \approx 1$ in the range of frequencies over which the AC system modes have considerable energy. The feed-forward compensation in mitigating dynamic interactions between the AC system and the converter system. However, when the feed-forward compensation is disabled, the dynamics of the AC system interact through the feedback loop with those of the compensator and the converter.

3.5 Modeling and Controlling of Two Level VSC

Modeling and controlling of two level VSC is similar to the single phase half bridge inverter. The non-ideality of a converter like on state resistance of a switch may be considered as a series resistance r_{on} connected in series with an inductor of a filter.

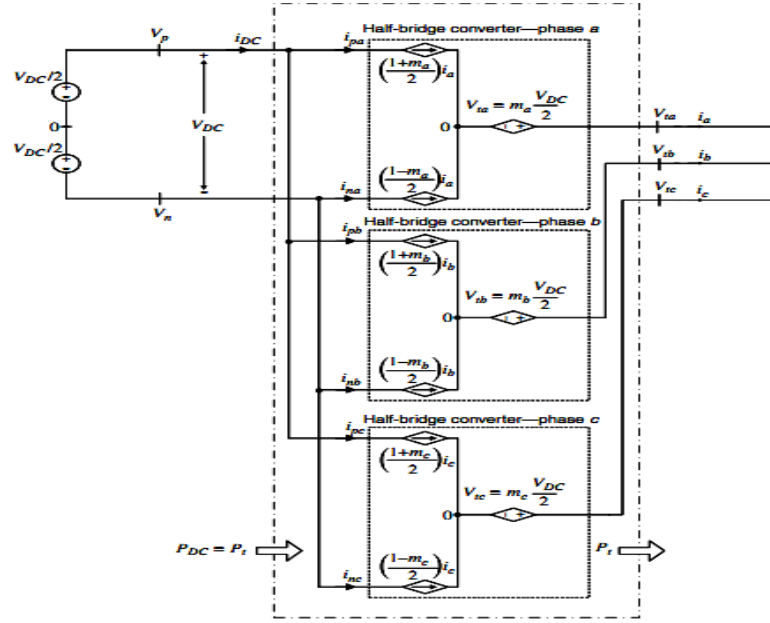


Figure 3.10: Averaged equivalent circuit of two level VSC [13]

Fig.3.10 illustrates the averaged equivalent circuit of an ideal two level VSC [13] and the AC side terminal voltages are,

$$V_{tabc}(t) = \frac{V_{DC}}{2} m_{abc}(t) \quad (3.24)$$

In dq-frame, the signals assume DC under steady-state conditions. This, in turn, permits utilization of compensators with simpler structures and lower dynamic orders. Moreover, zero steady-state tracking error can be achieved by including integral terms in the compensators. Therefore we may say a dq-frame representation of a three-phase system is also more suitable for analysis and control design tasks. Now the space phasor $f(t)$ can be converted into dq frame by using following equation,

$$\vec{f}(t) = (f_d + jf_q)e^{j\rho(t)} \quad (3.25)$$

where, ρ = speed of the rotation of dq-frame.

Substituting for $m(t) = (m_d + jm_q)e^{j\rho(t)}$ and $V_t(t) = (V_{td} + jV_{tq})e^{j\rho(t)}$ for dq- frame representation of two level VSC.

$$(V_{td} + jV_{tq})e^{j\rho(t)} = \frac{V_{DC}}{2}(m_d + jm_q)e^{j\rho(t)} \quad (3.26)$$

$$V_{td}(t) = \frac{V_{DC}}{2}m_d(t) \quad (3.27)$$

$$V_{tq}(t) = \frac{V_{DC}}{2}m_q(t) \quad (3.28)$$

Equations (3.27) and (3.28) suggest that the d- and q- axis components of the VSC AC side terminal voltage are linearly proportional to the corresponding components of the modulating signal, and the proportionality constant is $V_{DC}/2$. It also imply that the two-level VSC can be described by two linear, time-varying subsystems in dq-frame. The transfer function of each subsystem is a time-varying gain, $V_{DC}/2$.

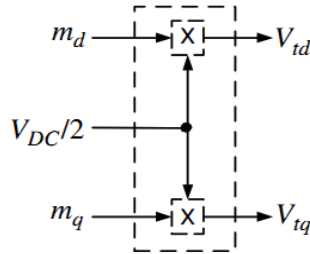


Figure 3.11: Control model of two level VSC in dq-reference frame

3.6 Importance of PLL Block and Formulation of Power in dq Domain

PLL block and its important :

The function of PLL block is to regulate ρ_0 at $(\omega_0(t) + \theta_0)$ to convert alternating quantities into DC terms [24]. This will be understood by following example. Assume that the AC system voltage in the VSC system is expressed as,

$$V_{sa}(t) = \widehat{V}_s \cos[\omega_0 t + \theta_0] \quad (3.29)$$

$$V_{sb}(t) = \widehat{V}_s \cos[\omega_0 t + \theta_0 - \frac{2\pi}{3}] \quad (3.30)$$

$$V_{sc}(t) = \widehat{V}_s \cos[\omega_0 t + \theta_0 - \frac{4\pi}{3}] \quad (3.31)$$

Where, \widehat{V}_s is the peak value of the line to neutral voltage, ω_0 is the AC system frequency and θ_0 is the sources initial phase angle. So, the phasor equivalent of V_{sabc} is,

$$\vec{V}_s(t) = \widehat{V}_s e^{j(\omega_0 t + \theta_0)} \quad (3.32)$$

Put value of above equations in equation (3.7), we get,

$$L \frac{d\vec{i}}{dt} = -(R + r_{on}) \vec{i} + \vec{V}_t - \widehat{V}_s e^{j(\omega_0 t + \theta_0)} \quad (3.33)$$

Transform above equation from abc to dq domain, we will get,

$$L \frac{d(i_d)}{dt} = L\omega(t)i_q - (R + r_{on})i_d + V_{td} - \widehat{V}_s \cos[\omega_0 t + \theta_0 - \rho] \quad (3.34)$$

$$L \frac{d(i_q)}{dt} = -L\omega(t)i_d - (R + r_{on})i_q + V_{tq} - \widehat{V}_s \sin[\omega_0 t + \theta_0 - \rho] \quad (3.35)$$

Where,

$$\frac{d\rho}{dt} = \omega(t) \quad (3.36)$$

Here i_d , i_q and ρ are the state variables and v_{td} , v_{tq} and ω are the control inputs. These equations are nonlinear due to presence of the terms ωi_d , ωi_q , $\cos(\omega_0 t + \theta_0 - \rho)$ and $\sin(\omega_0 t + \theta_0 - \rho)$. Choose ρ such that above equations becomes steady in nature with respect to time instead of alternating in nature. So, select $\rho = \omega_0 t + \theta_0$. Therefore above equations become,

$$L \frac{d(i_d)}{dt} = L\omega_0 i_q - (R + r_{on})i_d + V_{td} - \widehat{V}_s \quad (3.37)$$

$$L \frac{d(i_q)}{dt} = -L\omega_0 i_d - (R + r_{on})i_q + V_{tq} \quad (3.38)$$

Which describe a second order linear system that is excited by the constant input \widehat{V}_s . Thus, if v_{td} and v_{tq} are DC variables, i_d and i_q are also DC variables in the steady state. The mechanism to ensure $\rho(t) = \omega_0 t + \theta_0$ is referred to as the PLL. The PLL block diagram is shown in Fig.3.12 [13].

Formulation of power in dq-reference frame:

The instantaneous real power in three phase system is given by, [16]

$$P(t) = Re\left\{\frac{3}{2} \vec{v}(t) \vec{i}^*(t)\right\} \quad (3.39)$$

And the instantaneous reactive power in three phase system is ,

$$Q(t) = Im\left\{\frac{3}{2} \vec{v}(t) \vec{i}^*(t)\right\} \quad (3.40)$$

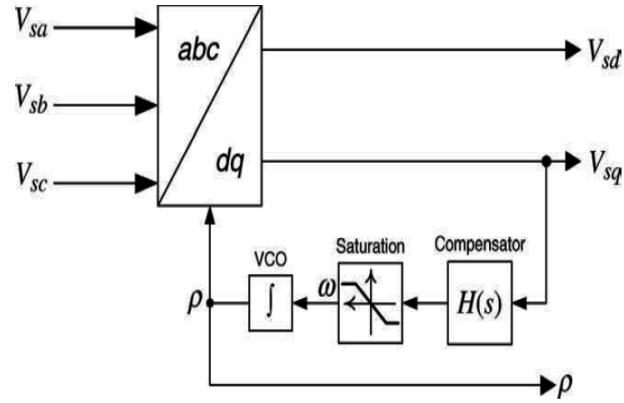


Figure 3.12: PLL block diagram [13]

Now, $V(t) = (V_d + jV_q)e^{j\rho t}$ and $i(t) = (i_d + ji_q)e^{j\rho t}$

Put these values in above instantaneous real and reactive power equations, the instantaneous real and reactive powers in dq-domain are given by,

$$P(t) = \frac{3}{2}[v_d(t)i_d(t) + v_q(t)i_q(t)] \quad (3.41)$$

$$Q(t) = \frac{3}{2}[-v_d(t)i_q(t) + v_q(t)i_d(t)] \quad (3.42)$$

3.7 Summary

In this chapter, at start the basic introduction of the controller is explained. Then pros of controller design in dq domain instead of ABC domain are discussed. Next, switched and averaged model of VSI has been developed to explain the control task of an inverter as per the system requirements. Further, PLL block and its importance have been discussed briefly. Finally, formation of instantaneous real and reactive powers have been touched up.

Chapter 4

Modeling and Control of DERs in Grid-Connected and Islanded Mode of Operation of Microgrid

The generators or microsources employed in a microgrid are usually renewable/non-conventional Distributed Energy Resources (DERs) integrated together to generate power at distribution voltage. Many of these new distributed power sources, such as wind turbine generators and fuel cells, do not generate power at AC 50 Hz. From operational point of view, the microsources must be equipped with power electronic interfaces (PEIs) and controls to provide the required flexibility to ensure operation as a single aggregated system and to maintain the specified power quality and energy output. PEIs not only generate utility grade AC power, but also facilitate their overall integration in microgrids. The output of different DER units is converted to DC voltage using power converters. The output DC voltage is then converted to AC of required voltage and frequency using a Voltage Source Inverter (VSI). Hence, it is assumed from here after that by some means the output of DER units is converted to DC voltage and the analysis starts by assuming an availability of DC voltage source.

Growth of power generation using DER units has led to distribution systems with a mixture of rotating machine generators and inverter interfaced generators [5]. To increase

the system reliability, DER units should be capable of operating in islanded as well as in grid connected mode. It is desirable to design DER units in such a way, that they can able to operate in the islanded or grid connected mode with the same hardware structure and modest (or ideally no) modifications in the control. This chapter also presents a control strategy that attempts to fulfill the aforementioned objective and also to present a convenient method for the controller design.

In this Chapter firstly the control of single DER unit, multiple DER units and the entire microgrid in islanded mode of operation has been discussed. In islanded mode, the control tasks are mainly based on inner current loop control and outer voltage loop control. Subsequently, the control of single DER unit, multiple DER units and the entire microgrid in grid connected mode has been developed. Here, the control strategies mainly consist of, control for real and reactive power flow along with current control scheme. In the case of multiple DERs, it is desirable to use droop control along with voltage and current control scheme. At end of this chapter, the control procedure and behavior for the entire microgrid, which consists of seven buses and eight lines, connected in islanded as well as in grid connected mode has been covered.

4.1 Islanded Distributed Energy Resources [Autonomous Microgrids]

In this architecture the microgrid operate in isolated mode, having to self-suffice energy demand and power quality and reliability needs of local customers. This mode of operation is envisioned for systems located in geographical remote areas where access to backbone grid is difficult or too expensive. The design and planning process of an autonomous microgrid is more complex than the grid-connected counterpart because the sustainability dimensions of isolated operation. The main drivers of autonomous operation are the availability of local energy resources, energy independence and reliability.

In a distribution system, when a Utility grid is disconnected for any reason, the dis-

tributed generation still supplies the required power to any section of local loads. Phenomenon is called “Islanding Phenomena” [25], [26]. When an islanding occurs, the voltages and frequencies in the islanded area cannot be controlled by the grid system. Therefor during islanding operation, voltages and frequencies have to be maintained, otherwise, this may lead to damage of electrical equipments and pose a danger to the working personnel [6].

Islanding once again can be classified into two types namely:

i) Unintentional Islanding

ii) Intentional Islanding

(i) Unintentional islanding: As the name suggests, it is an undesirable islanding caused in a power grid. It occurs when a part of the distribution system becomes electrically isolated from the whole power grid and is still being energized by the distributed generators. The reason for such occurrence of islanding is due to several reasons such as inverter misinterpreting, the voltage and frequency harmonics of utility grid, ground fault on the feeder from grid and so on. During a steady state, the real and reactive power produced by the distributed generators and the utility grid should match with the consumption. Any mismatch in real power gives rise to frequency deviation. Also the distributed generators in the islanded microgrid can be damaged if the island is reconnected to the utility grid as the distributed systems usually tend to operate at a different frequency in the islanded mode and could be out of synchronism with the utility grid. This may also give rise to high starter currents which in turn may once again result in tripping of the utility system.

(ii) Intentional islanding: Intentional islanding can be explained as a purposeful islanding of a microgrid from the remaining power grid system. When there is a power outage, many distributed generators may go out of synchronism with one another and therefore it is required to have specific islands at points where there is a slight mismatch between load and generation. Circuit breaking operations are executed to develop is-

landed systems. It also occurs when the quality of the utility grid power is degraded.

The inverter developed in this thesis is a grid tie inverter. It is used in distributed generation systems to convert the direct current (DC) from the distributed generators into an alternating current (AC) and supply it to the load and utility grid. From a business point of view, the residences and buildings that own a grid tied electrical system are allowed to sell the energy developed by their system to the utility grid.

When a grid is islanded, the inverter must have the ability to increase the power supply from the distribution system in negligible amount of time to sustain the sudden increase in the load demand. Care should be taken such that, when the utility grid breaks off from the load, the power from the distributed generation should be supplied to the load without any major hindrances to the voltage and frequency parameters of the grid system. And, when the utility grid is connected to the load, the distribution system should allow the load to reconnect itself to the grid in an equally error-free manner. This islanded distributed system is simulated using MATLAB SIMULINK.

Control task:

When a single DER unit is connected in islanded mode, the main control objective is to regulate voltage and frequency within permissible limits at PCC. Some researchers have mentioned that this control task can be done in ABC domain by inner current loop and outer voltage loop control. The thesis work concentrates on current and voltage control schemes adopted in dq domain instead of ABC domain with the incorporation of feed forward and ratio control along with feed back loop control. It is observed that this scheme gives better performance than work discussed by other researchers. The simulation results are briefly explained in Chapter 5. In the next section, for controlling of multi DER units in islanded mode, droop control in conjunction with VSC voltage and current control schemes have been used. By collaborating all these control schemes, a seven bus microgrid system operating in islanded mode has been

designed. Simulation results have been carried out on MATLAB SIMULINK and the results are discussed in Chapter 5.

4.1.1 Modeling and control of single DER unit in islanded mode

A single line diagram for islanded DER is shown in Fig.4.1 and its schematic diagram with closed loop control scheme is shown in Fig.4.2

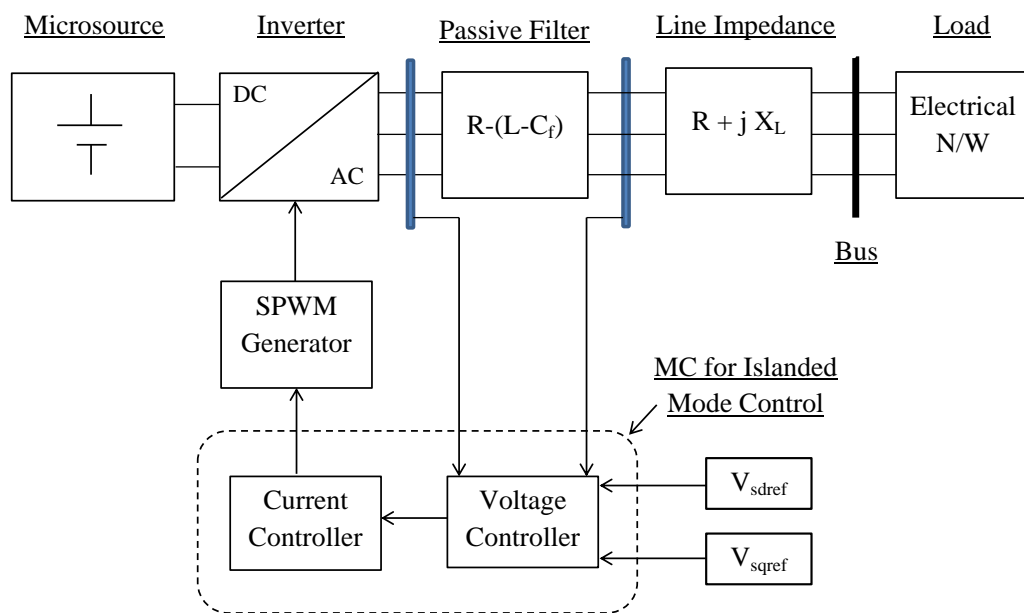


Figure 4.1: SLD for islanded DER

Fig.4.1 shows single DER unit is connected to load through a current controlled voltage source converter (VSC) and three phase LC filter. An aggregate of the network loads as viewed from the DER unit terminals is labeled as the “effective load” and is referred to as “load”. The components L and C_f represent the inductance and capacitance of the filter. R Models the ohmic loss of the filter inductor and also includes the effect of the on-state resistance of the VSI switches.

Fig.4.2 illustrates that the control is performed in a rotating dq0 reference frame whose d-axis makes an angle ρ with respect to the stationary a-axis. ρ is obtained from a PLL

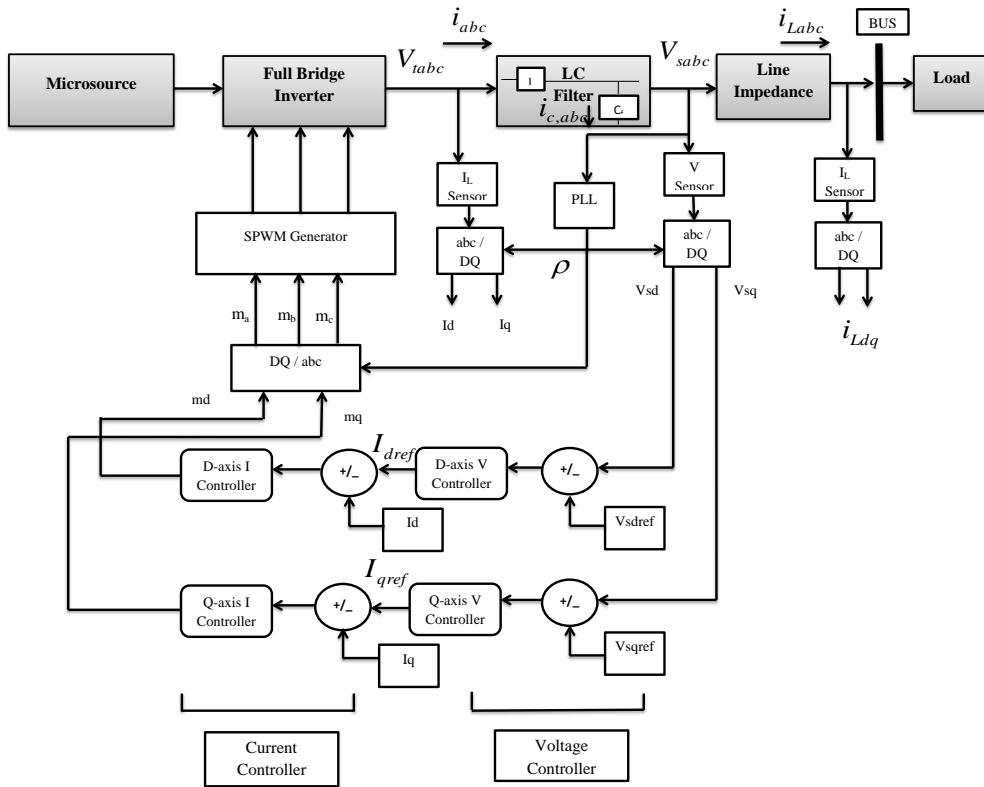


Figure 4.2: Schematic diagram for islanded DER with closed loop control scheme

which constitutes an essential part of a modern electronically-coupled DER unit as discussed in Chapter 2. The PLL also provides ω , i.e., the frequency of V_{sabc} [PCC voltage]. In the grid connected mode of operation, V_{sabc} is dictated by the grid, in this case ρ and ω represent, respectively, the phase-angle of the PCC voltage and power system frequency.

There are two types of control schemes, which are widely adopted in microgrids [13], [27].

1. Voltage control scheme

- The voltage-mode control is simple and has a low number of control loops.
- However, the main shortcoming of the voltage-mode control is that there is no closed control loop on the VSC line current.
- Consequently, the VSC is not protected against over currents, and the current

may undergo large excursions if the power commands are rapidly changed or faults take place in the AC system.

Therefore, to overcome this problem current control scheme is also used in conjunction with voltage control scheme.

2. Current control scheme

- The VSC line current is tightly regulated by a current control loop.
- The real power (P) and reactive power (Q) are controlled by the phase angle and the amplitude of the VSC line current w.r.t. PCC voltage.
- Robustness against variations in the parameters of the VSC system and the AC system.
- Good dynamic performance and higher control precision.

In the first part of this section, design of current controller in dq reference frame has been discussed. In the next part, design of voltage control scheme in dq domain has been discussed for islanded DER unit.

a) Task : Design of an inner current loop controller, i.e., determination of parameter values for a current controller, based on dq-reference frame current mode control.

The purpose of designing the current controller for a microsource is to regulate the current delivered by the microsource according to its rating. Here, reference value of current which is based on the rating of the DERs is compared with the actual current delivered by the DERs and the error produced is based on this comparison. This error is fed to the current controller to change the value of current and nullify the error by taking necessary corrective or preventive action. With this idea, the entire system needs to be modeled for determining the proper parameter values of a current controller.

For the sake of designing of a current controller, consider the differential equations (3.34) and (3.35) from Chapter 3,

$$L \frac{d(i_d)}{dt} = L\omega(t)i_q - (R + r_{on})i_d + V_{td} - \widehat{V}_s \cos[\omega_0 t + \theta_0 - \rho] \quad (4.1)$$

$$L \frac{d(i_q)}{dt} = -L\omega(t)i_d - (R + r_{on})i_q + V_{tq} - \widehat{V}_s \sin[\omega_0 t + \theta_0 - \rho] \quad (4.2)$$

Now, the phasor equivalent of AC system voltages in the VSC system is expressed as,

$$\vec{V}_s(t) = \widehat{V}_s e^{(j\omega_0 t + \theta_0)} \quad (4.3)$$

This phasor is converted from ABC to dq domain and its d-axis and q-axis components are separated out as shown below,

$$V_{sd} = \widehat{V}_s \cos(\omega_0 t + \theta_0 - \rho) \quad (4.4)$$

$$V_{sq} = \widehat{V}_s \sin(\omega_0 t + \theta_0 - \rho) \quad (4.5)$$

Assuming steady state operating condition and by substituting equations (4.4) and (4.5) into equations (4.1) and (4.2), the following equations can be derived.

$$L \frac{d(i_d)}{dt} = L\omega_0 i_q - (R + r_{on})i_d + V_{td} - V_{sd} \quad (4.6)$$

$$L \frac{d(i_q)}{dt} = -L\omega_0 i_d - (R + r_{on})i_q + V_{tq} - V_{sq} \quad (4.7)$$

As, it has been seen in previous chapter, the following equations represent the dq model

of two level VSC.

$$V_{td}(t) = \frac{V_{DC}}{2}m_d(t) \quad (4.8)$$

$$V_{tq}(t) = \frac{V_{DC}}{2}m_q(t) \quad (4.9)$$

Substitute equations (4.8) and (4.9) in equations (4.6) and (4.7),

$$L\frac{d(i_d)}{dt} = L\omega_0 i_q - (R + r_{on})i_d + \frac{V_{DC}}{2}m_d(t) - V_{sd} \quad (4.10)$$

$$L\frac{d(i_q)}{dt} = -L\omega_0 i_d - (R + r_{on})i_q + \frac{V_{DC}}{2}m_q(t) - V_{sq} \quad (4.11)$$

Here, i_d and i_q are state variables, v_{td} and v_{tq} are control inputs and v_{sd} and v_{sq} are disturbance inputs. Due to presence of $L\omega_0$ terms in equations (4.10) and (4.11), dynamics of i_d and i_q are coupled, so we need to decouple this dynamics by selecting proper value of m_d and m_q . To decouple the dynamics, take m_d and m_q as,

$$m_d = \frac{2}{V_{DC}}(u_d - L\omega_0 i_q + V_{sd}) \quad (4.12)$$

$$m_q = \frac{2}{V_{DC}}(u_q - L\omega_0 i_d + V_{sq}) \quad (4.13)$$

Where, u_d and u_q are two new control inputs, which are generated by d- and q-axis current controller respectively. Substitute equations (4.12) and (4.13) into equations (4.10) and (4.11),

$$L\frac{d(i_d)}{dt} = -(R + r_{on})i_d + u_d \quad (4.14)$$

$$L\frac{d(i_q)}{dt} = -(R + r_{on})i_q + u_q \quad (4.15)$$

Above equations describe two decoupled, first order, linear systems. It is clear from these equations that i_d and i_q are controlled by u_d and u_q respectively. Fig.4.3 shows a block representation of the d and q-axis current controllers of the VSC system connected in islanded mode, in which u_d and u_q are the outputs of the two corresponding compensators.

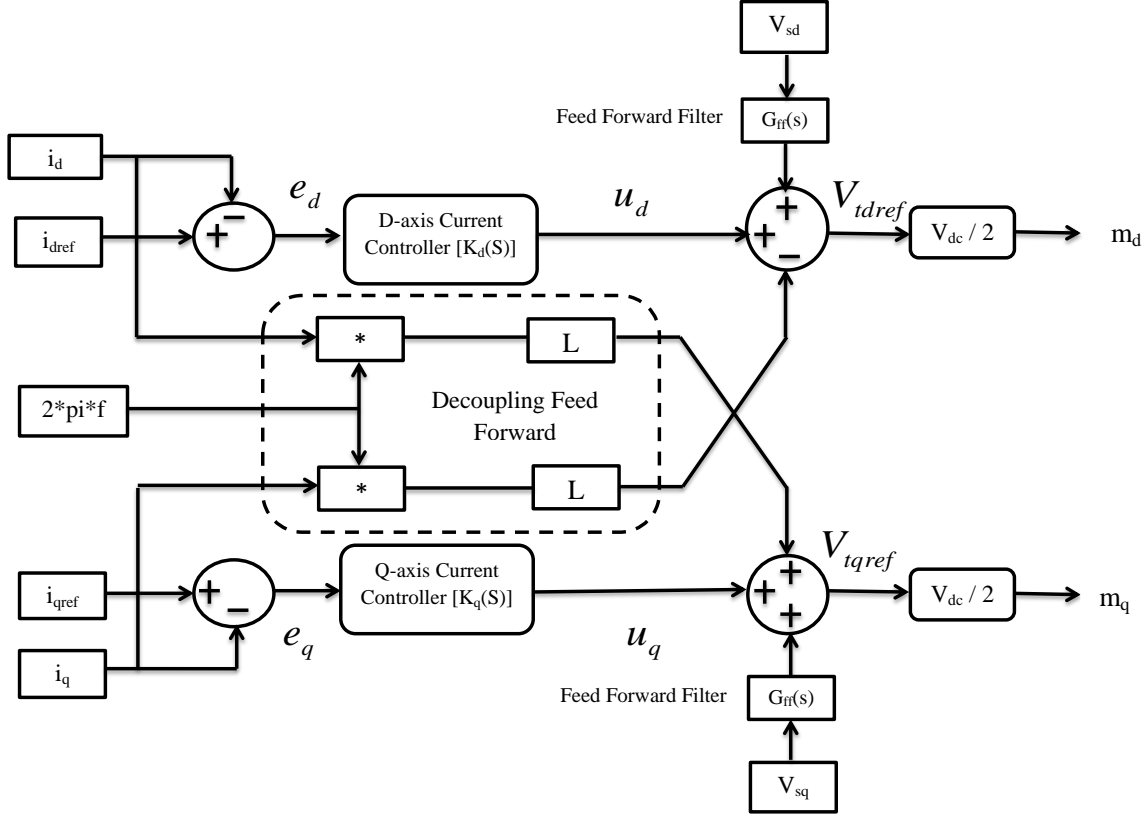


Figure 4.3: Block diagram of a current control scheme

The d- and q-axis compensators, $k_d(s)$ and $k_q(s)$, process the error signals $e_d = i_{dref} - i_d$ and $e_q = i_{qref} - i_q$ and deliver the outputs u_d and u_q , respectively. Then, u_d and u_q are augmented by feed-forward signals $V_{sd} - L\omega i_q$ and $V_{sq} + L\omega i_d$, and the signals V_{tdref} and V_{tqref} are generated. V_{tdref} and V_{tqref} are equivalent to d- and q-axis components of the VSC averaged AC-side terminal voltage; by the subscript ref we distinguish them from their counterparts in the actual AC-side terminal voltage, that is, V_{td} and V_{tq} . The feed-forward compensation is (i) to decouple dynamics of i_d and i_q , (ii) to enhance the disturbance

rejection capability of the closed-loop system, (iii) to ensure a bumpless system start-up, and (iv) to decouple dynamics of i_d and i_q from those of the grid. For the feed-forward compensation, ω , that is, the rotational speed of the dq-frame, is obtained from the PLL. Fig.4.3 also shows that to generate m_d and m_q , V_{tdref} and V_{tqref} are divided by $\frac{V_{DC}}{2}$. This operation can be considered as a feed-forward compensation, and has to compensate for the VSC conversion gain $\frac{V_{DC}}{2}$ and to ensure that V_{td} and V_{tq} (in the actual converter AC-side terminal voltage) are an accurate reproduction of, respectively, V_{tdref} and V_{tqref} .

Fig.4.4, shows the simplified block diagram of the current controlled VSC system. It indicates both d- and q-axis current control loops are identical. Therefore, the corresponding compensators can also be identical. Here, simple Proportional-Integral (PI) controller has been used as $k_d(s)$ and $k_q(s)$. Therefore,

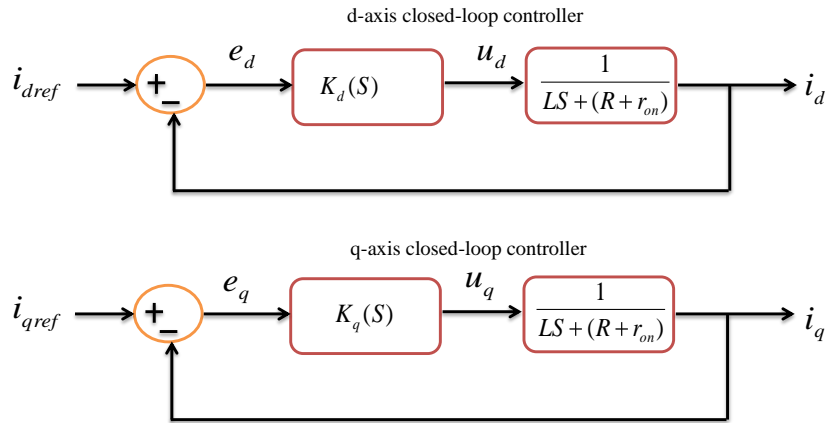


Figure 4.4: Equivalent block diagram for the closed loop current control scheme

$$k_d(s) = \frac{k_p s + k_i}{s} \quad (4.16)$$

where, k_p and k_i are proportional and integral gains respectively. For finding the proper value of k_p and k_i write open loop gain $p(s)$ of a current control loop. So, we get,

$$p(s) = \left(\frac{k_p}{Ls}\right) \frac{s + k_i/k_p}{s + (R + r_{on})/L} \quad (4.17)$$

From above equation it is clear that, the plant has a pole at $(R + r_{on})/L$, which is very close to origin and so it is responsible for sluggish behavior of a system. Hence, we may cancel it with controller zero by using pole-zero cancelation technique. Now after pole-zero cancelation, the open loop transfer function of a current control loop becomes,

$$p(s) = \frac{k_p}{Ls}$$

where,

$$\frac{k_i}{k_p} = (R + r_{on})/L$$

Further, the closed loop transfer functions becomes,

$$\frac{I_d(s)}{I_{dref}(s)} = G_i(s) = \frac{1}{\tau_i s + 1} \quad (4.18)$$

where,

$$\tau_i = L/k_p \Rightarrow k_p = L/\tau_i \quad (4.19)$$

$$k_i = (R + r_{on})/\tau_i \quad (4.20)$$

Here, τ_i is the time constant of the resultant closed loop system and it should be small for a fast current control response but adequately large such that $1/\tau_i$, that is, the bandwidth of the closed loop control system is considerably smaller. Therefore, τ_i is typically selected in the range of 0.5 to 5 ms.

Results : By doing current control analysis in dq reference frame, the controller parameters k_p and k_i have been found as per equations (4.19) and (4.20).

b) Task : Design of an outer voltage loop controller, i.e., determination of parameter values for a voltage controller, based on dq-reference frame voltage mode control.

The control objective for the design of a voltage controller in islanded mode is to regulate the amplitude of the voltage and frequency at PCC. Hence, we compare reference value of voltage which is based on the desired value of PCC voltage with the actual voltage delivered by the DERs at PCC and the error produced is based on this comparison. This error is fed to the voltage controller to change the value of voltage at PCC and nullify the error by taking necessary corrective or preventive action. The entire system needs to be modeled with this logic for determining the proper parameter values of a voltage controller.

Now from Fig.4.2, the differential equation in terms of capacitor current, inductor current and load current can be written easily.

$$C_f \frac{d\vec{V}_s}{dt} = \vec{i} - \vec{i}_L \quad (4.21)$$

Converting the above equation into dq domain by using the equation $\vec{f} = (f_d + jf_q)e^{j\rho(t)}$,

$$C_f \frac{d[(V_{sd} + jV_{sq})e^{j\rho}]}{dt} = (i_d + ji_q)e^{j\rho} - (i_{Ld} + ji_{Lq})e^{j\rho} \quad (4.22)$$

Separate out the d-axis and q-axis components of the above equation,

$$C_f \frac{dV_{sd}}{dt} = C_f(\omega V_{sq}) + i_d - i_{Ld} \quad (4.23)$$

$$C_f \frac{dV_{sq}}{dt} = -C_f(\omega V_{sd}) + i_q - i_{Lq} \quad (4.24)$$

where, $\frac{d\rho}{dt} = \omega(t)$,

From equations (4.23) and (4.24), it is clear that V_{sd} and V_{sq} can be controlled by i_{dref} and i_{qref} , Moreover, these equations also reveals that V_{sd} and V_{sq} are coupled and it also includes the effect of i_{Ld} and i_{Lq} . So the coupling between V_{sd} and V_{sq} is eliminated by a decoupling feed forward compensation and is similar to the one utilized to decouple i_d and i_q in a current control scheme. Therefore the compensated system performs under all load conditions almost the same way as the system without the load compensating feed forward would perform under a no load condition.

Fig.4.5 shows a block representation of the d- and q-axis voltage controllers of the VSC system connected in islanded mode in which u_d and u_q are the outputs of the two corresponding compensators. The d-axis and q-axis compensators, $k(s)$, process the error signals $e_d = V_{sdref} - V_{sd}$ and $e_q = V_{sqref} - V_{sq}$ and deliver the outputs u_d and u_q , respectively. Then, u_d and u_q are augmented by feed-forward signals $i_{Ld} - C_f(\omega V_{sq})$ and $i_{Lq} + C_f(\omega V_{sd})$, and the signals i_{sdref} and i_{sqref} are generated, which are fed to the current controller as a reference signal.

Form Fig.4.5, it can be written,

$$i_{dref} = u_d - C_f(\omega V_{sq}) + i_{Ld} \quad (4.25)$$

$$i_{qref} = u_q + C_f(\omega V_{sd}) + i_{Lq} \quad (4.26)$$

Where, u_d and u_q are two dummy control inputs. Now, from equation (4.17),

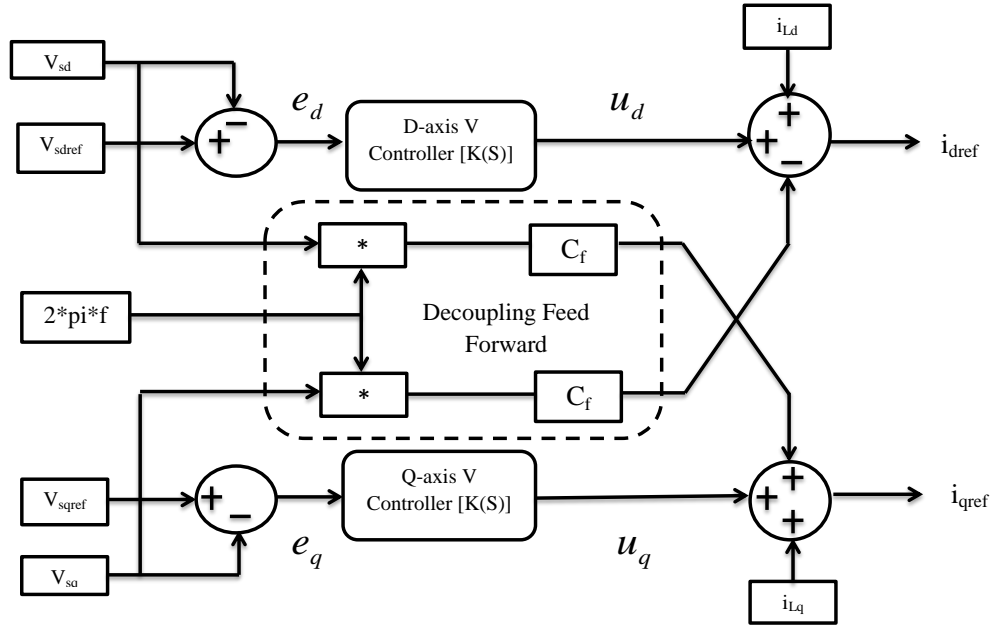


Figure 4.5: Block diagram of a voltage control scheme

$$i_d(s) = G_i(s)I_{dref}(s) \quad (4.27)$$

$$i_q(s) = G_i(s)I_{qref}(s) \quad (4.28)$$

Substitute equations (4.25) and (4.26) into (4.27) and (4.28),

$$I_d(s) = G_i(s)U_d(s) - C_f G_i(s)\omega(s)V_{sq}(s) + G_i(s)I_{Ld}(s) \quad (4.29)$$

$$I_q(s) = G_i(s)U_q(s) + C_f G_i(s)\omega(s)V_{sd}(s) + G_i(s)I_{Lq}(s) \quad (4.30)$$

Substitute equations (4.29) and (4.30) into Laplace transform of equations (4.23) and (4.24),

$$C_f s V_{sd}(s) = G_i(s) U_d(s) + C_f [1 - G_i(s)] \omega(s) V_{sq}(s) - [1 - G_i(s)] I_{Ld}(s) \quad (4.31)$$

$$C_f s V_{sq}(s) = G_i(s) U_q(s) + C_f [1 - G_i(s)] \omega(s) V_{sd}(s) - [1 - G_i(s)] I_{Lq}(s) \quad (4.32)$$

It is then noted that the transfer function $G_i(s) = \frac{1}{\tau_i s + 1}$, has a unity DC gain and therefore, $1 - G_i(s) = \frac{s\tau_i}{1 + \tau_i s}$ has a zero DC gain. Hence, if τ_i is adequately small, then equations (4.31) and (4.32) can be approximated as,

$$\frac{V_{sd}(s)}{U_d(s)} \approx G_i(s) \frac{1}{C_f(s)} \quad (4.33)$$

$$\frac{V_{sq}(s)}{U_q(s)} \approx G_i(s) \frac{1}{C_f(s)} \quad (4.34)$$

Equations (4.33) and (4.34) indicate that $V_{sd}(s)$ and $V_{sq}(s)$ can be independently controlled by, $u_d(s)$ and $u_q(s)$, respectively. This alternatively means that the control scheme of Fig.4.5 divides the overall voltage control plant, effectively, into two independent Single-Input-Single-Output (SISO) plants of Fig.4.6

From Fig.4.6, it can be noted that each loop includes an integral term, i.e., a pole at $s = 0$, and a real pole at $s = -p = -1/\tau_i$. For such a plant, a PI compensator, k_s , can ensure a stable fast response and zero steady state error. The following procedure is used for designing a PI compensator [6]. Let, the PI compensator be,

$$k(s) = k \frac{s + z}{s} \quad (4.35)$$

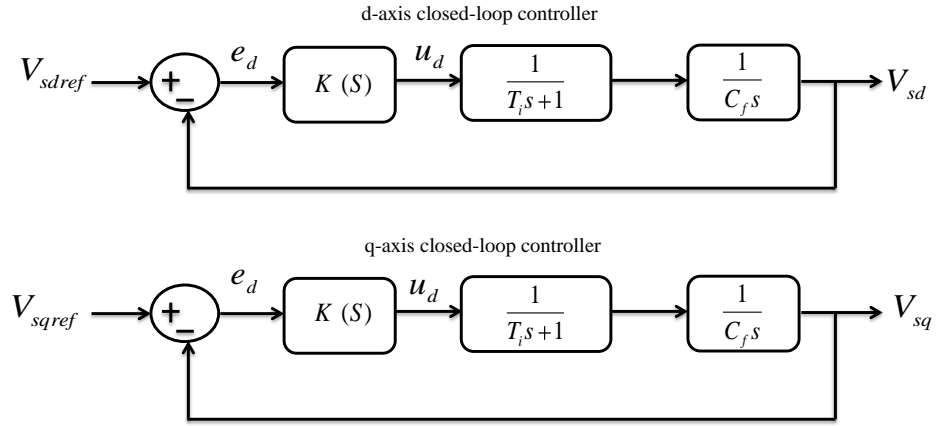


Figure 4.6: Equivalent block diagram for the closed loop voltage control scheme

Here, the open loop gain is,

$$l(s) = \frac{k}{\tau_i C_f} \left(\frac{s+z}{s+\tau_i^{-1}} \right) \frac{1}{s^2} \quad (4.36)$$

At very low frequencies, the open-loop phase $\angle l(j\omega)$ is approximately equal to -180° . If $z < p$, then $\angle l(j\omega)$ first increases until reaches its maximum, δ_m , at $\omega = \omega_m$. For $\omega > \omega_m$, $\angle l(j\omega)$ drops and approaches -180° at very high frequencies. Therefore, to achieve the maximum phase-margin, one should pick the gain crossover frequency as $\omega_c = \omega_m$ and δ_m becomes the phase-margin. Knowing δ_m , z can be calculated from,

$$\delta_m = \sin^{-1} \left(\frac{1 - \tau_i z}{1 + \tau_i z} \right) \quad (4.37)$$

The gain cross over frequency is determined based on,

$$\omega_m = \sqrt{(z\tau_i^{-1})} \quad (4.38)$$

The compensator gain, k , is obtained from the solution to $|l(j\omega_c)|$, that is,

$$k = C_f \times \omega_c \quad (4.39)$$

Based on the above mentioned design procedure, the resultant closed-loop voltage control system is of the third order. It can be shown that the closed-loop system always has a real pole at $s = -\omega_c$, while the two other complex conjugate poles are located on a circle whose radius is ω_c . The exact locations of the two poles depend on the phase margin which is typically chosen in the range of 30° to 75° . For the particular choice of $\delta_m = 53^\circ$, the two poles are at $s = -\omega_c$ and thus the closed-loop system has a triple poles at $s = -\omega_c$.

Results: After doing the voltage control analysis in dq reference frame the controller parameter values have been found as per equations (4.37) to (4.39).

As seen in Section 4.1.1.a and 4.1.1.b, by using voltage and current control mode, single DER unit can be perfectly controlled in islanded mode. The results are briefly explained in Chapter 5.

4.1.2 Modeling and control of parallel connected DER units in islanded mode

As discussed in Section 4.1.1, when a single DER unit is connected in islanded mode, the terminal voltage and frequency are kept constant by using voltage and current control scheme. But when more than one DERs are connected in parallel we ought to maintain their terminal voltage at same level. Otherwise, looping current will flow between microsources, which are going to be connected in parallel or at the same bus. This looping current may damage the PEIs. Now, if we use droop control along with the voltage and current control scheme the performance and load sharing capabilities of the DERs become better than without droop control. Apart from this, because of droop control all DER units operate at the same frequency [28]-[32].

The basic control objective in a microgrid is to achieve accurate power sharing, while maintaining the close regulation of voltage and frequency. Parallel operation of small

VSI's give modularity to the system and provide extra reliability, redundancy and the power level of the plant can be upgraded without the need of complete reconfiguration. Increase in number of VSI's increases the stiffness of the system and makes it more stable against external disturbances. Hence, the parallel operation of inverters in RES system offers several advantages in addition to low maintenance cost of low power unit compared to that of high power unit [28].

A single line diagram of two islanded DER units connected in parallel and feeding a common load is shown in Fig.4.7. Fig.4.8 shows the schematic diagram of a control logic for single DER, connected in parallel for islanded mode.

In the first part of this section the control strategy for two islanded DER units connected in parallel and feeding a common load has been developed. Then, the control strategies for multisources connected in parallel in islanded mode has been discussed. As shown in Fig.4.8 there are three types of controller used in multi sources feeding a common load, i) droop controller, ii) voltage controller, and iii) current controller. Moreover, the effect on system performance has been observed after aggregation of the droop control with the voltage and current control. The effect of different droop setting is also noticed and discussed briefly in Chapter 5 with the simulation results.

a) Task : Design of a voltage and current controller in dq-reference frame by using voltage and current control scheme, respectively

As the controlling has been done separately for each microsource for getting advantages of plug and play operation. The design procedures for voltage and current controller are same as discussed in the previous section.

b) Task : Design of a droop controller by using dq-reference frame

The primary condition for paralleling of DERs is that they would share the load ac-

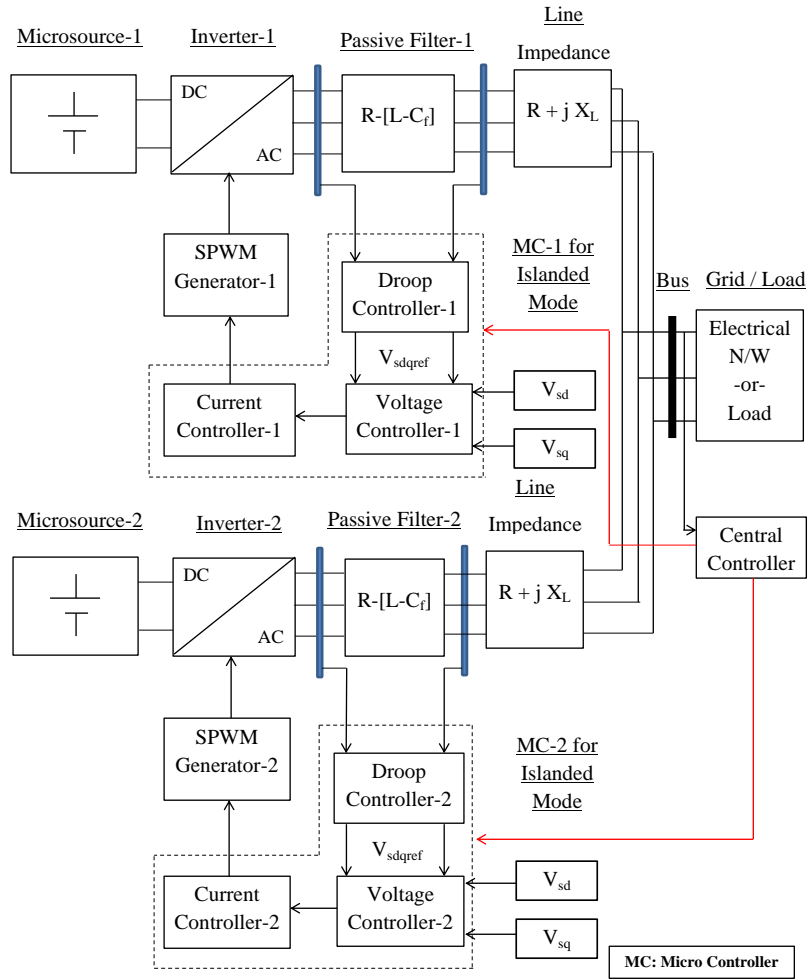


Figure 4.7: SLD of two islanded DER units connected in parallel and feeding a common load

According to their capacities, i. e., paralleling of modules requires interconnection between them to achieve balanced load sharing. One of the methods of ensuring proper load sharing among parallel connected inverters is to use a master-slave configuration. This gives proper load sharing despite the presence of line impedances, but it is difficult to physically implement communication links between all DERs, which may be located at some remote places. So, to achieve true modularity each module must be able to operate independently. This task can be full-filled by droop control scheme. The droop method is also named as wireless or autonomous control because it operates without control intercommunications. The conventional droop method is based on the principle that the

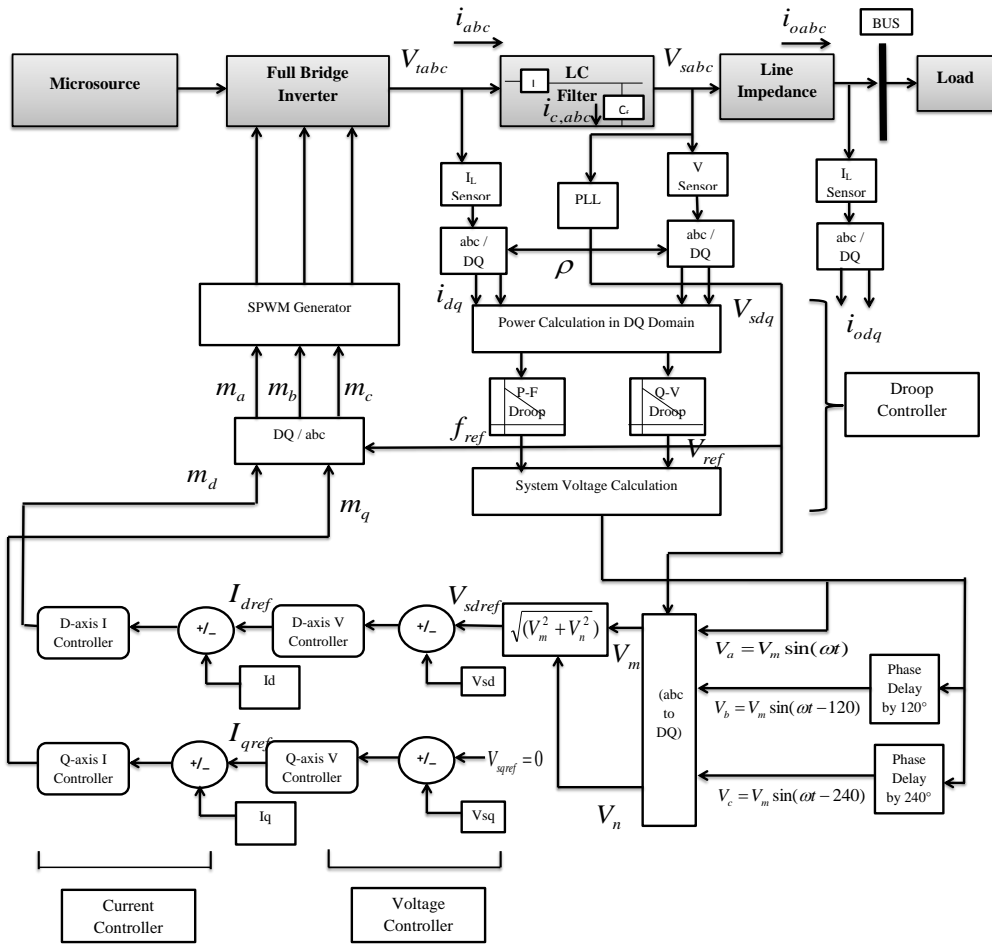


Figure 4.8: schematic diagram of a control logic for single DER for paralleling operation in islanded mode

phase and the amplitude of the inverter can be used to control active and reactive power flows respectively. Hence, it will ensure that changes in load are taken up by the inverter in a predetermined manner without communication.

Stable operation of a power system needs good control of the real power (P) and the reactive power (Q) flow. Fig.4.9 shows the equivalent circuits of a VSI connected to a common bus (PCC). It is used for showing real and reactive powers flow between a VSI and a bus [33],[34].

where,

$Z=R+jX$: Output impedance of the inverter,

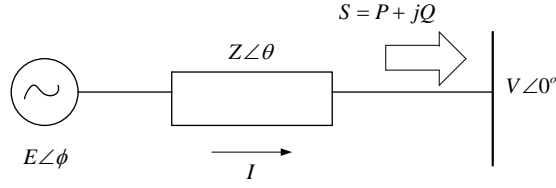


Figure 4.9: Equivalent circuit of a VSI connected to a bus

X : Output reactance of the inverter,

ϕ : Phase angle between the output voltage of a VSI and voltage of a common bus,

E and V : The amplitude of the output voltage of VSI and load voltage respectively.

Here, the output of DG and bus (PCC) are connected by feeder impedance $|Z|\angle\theta$ as shown in Fig.4.9. Let, the phasor voltage of DG is $|E|\angle\phi$ and bus voltage (PCC) is $|V|\angle 0$

$$I = \frac{|E|\angle\phi - |V|\angle 0}{|Z|\angle\theta} \quad (4.40)$$

$$I = \frac{|E|}{|Z|}\angle(\phi - \theta) - \frac{|V|}{|Z|}\angle(-\theta) \quad (4.41)$$

Hence, the complex power flows from the DG to the bus (PCC) is given by,

$$S = EI^* \quad (4.42)$$

$$S = \frac{|E|^2}{|Z|}\angle\theta - \frac{|E||V|}{|Z|}\angle(\theta + \phi) \quad (4.43)$$

Thus, the real and reactive power at the sending end, i.e., at DG are,

$$P = \frac{|E|^2}{|Z|}\cos\theta - \frac{|E||V|}{|Z|}\cos(\theta + \phi) \quad (4.44)$$

$$Q = \frac{|E|^2}{|Z|} \sin \theta - \frac{|E||V|}{|Z|} \sin(\theta + \phi) \quad (4.45)$$

Now, consider the output impedance of an inverter is mainly inductive due to the large filter inductor value between the DG and the common bus (PCC). So, the ratio of R/X is very small. Therefore, assuming $R \approx 0$, the above equations become,

$$P = \frac{|E||V|}{|Z|} \sin \phi \quad (4.46)$$

$$Q = \frac{|E|^2 - |E||V| \cos \phi}{|Z|} \quad (4.47)$$

If ϕ is very small $\Rightarrow \cos \phi \approx 1$, therefore,

$$Q = \frac{|E|}{|Z|} (|E| - |V|) \quad (4.48)$$

$$Q = \frac{|E|}{|Z|} (\text{Voltage Drop}) \quad (4.49)$$

Above equations (4.46) and (4.48) reveal that, P and Q in an ac system are decoupled to a good extent. P predominantly depends on the power angle and Q predominantly depends on the voltage magnitude. Therefore, to control active and reactive power properly, it is essential to have a good control on the power angle and the voltage level by means of the inverter.

As it is known that if load changes, there would be a change in real and reactive power requirement of the system. Thus the focal task is to sense the change in real and reactive power requirement of the system and gives the appropriate command to controller for taking essential control action to match with the new requirement of the system. Hence, one of the solution to sense the changes in real and reactive powers requirement is to use

P-f and Q-V droops. The moral idea of the droop control is to operate all the DER units, which are connected in parallel, at same frequency and at same terminal voltage. Thus the prior advantages of paralleling of microsources, such as to enhance power capability, efficiency, system reliability and to reduce output current ripple and so on, can be harvested from DERs.

There are mainly two types of droop:

1. Real Power (P) Vs. Frequency (f) droop
2. Reactive power (Q) Vs. Voltage (V) droop

1) Real Power (P) Vs. Frequency (f) droop

The real power requirement is reduced if load decreases and vice-versa, so, the control task is to get the information about changes in load. One of the simplest and accurate way is to use P-f droop for the same. According to this droop control if there is an increase in load demand the frequency should fall down and vice-versa and it is also clear from P-f droop as shown in Fig.4.10. The logic behind the P-f droop is to operate all DERs, which are going to be connected in parallel, at same frequency level. Hence, there would not be a frequency mismatch between DERs. As shown in Fig.4.10 the real power Vs. frequency droop is designed such that when the real power requirement is zero, the frequency of a DER is maintained at its rated value. The droop value is set such that when the real power requirement increases from its zero to maximum value, the frequency falls from its rated value of ω^* to a value of $(\omega^* \pm 0.5)$, which is allowable according to the standards in distribution system.

In conventional power system each generator has been placed with P-f droop control to permit each generator, to take up changes in total load in a pre-determined manner by its frequency droop characteristics. Frequency is essentially utilized as a communication link between the generator to control them. In this section, the same philosophy is used to

ensure proper distribution of total power between parallel connected inverters in islanded system. Similarly, a droop in the voltage with reactive power is used to ensure reactive power sharing among DERs.

The P-f droop characteristic is shown in Fig.4.10 and it is also defined mathematically as given in equation (4.50) [35],

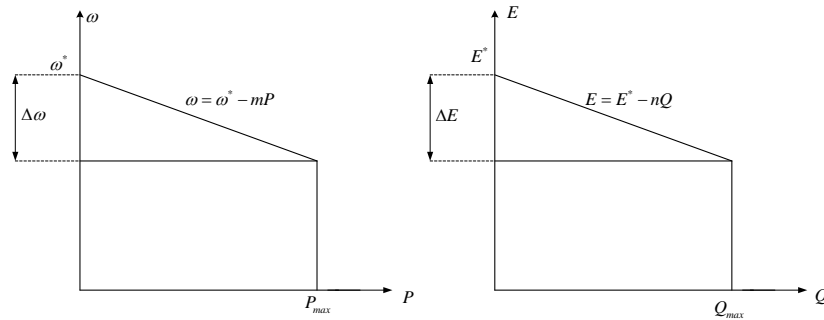


Figure 4.10: Static droop characteristics of P-f and Q-V droops respectively

$$\omega = \omega^* - mP \quad (4.50)$$

Where,

ω^* is the rated frequency of a VSI under no load condition and,

m is a droop coefficient for P-f droop.

2) Reactive power (Q) Vs. Voltage (V) droop

Voltage regulation is necessary for local reliability and stability. Without local voltage control, system with high penetration of microsources can experience voltage and/ or reactive power oscillations. Voltage control requires care to insure that there are not large circulating reactive currents between sources. The issues are identical to those encountered in the control of large synchronous generators. In the power grid the impedance between generators is usually large enough to greatly reducing the possibility of circulat-

ing currents. In a microgrid, which is typically radial, the problem of large circulating reactive currents is immense. With small errors in voltage set points the circulating currents can exceed the ratings of the microsources. To prevent from such a situation reactive power Vs. voltage droop control is used. The function of the basic Q-V droop control is shown in Fig.4.10. As shown in Fig.4.10., the reactive power Vs. voltage droop is designed such that when the reactive power requirement is zero, the terminal voltage of a DER is maintained at its rated voltage value. The droop value is set such that when reactive power requirement increases from its zero to maximum value, the terminal voltage falls from its rated value E^* to a value of $0.94E^*$, which is allowable according to 6% voltage regulation as per standard in distribution system.

The Q-V droop characteristic is shown in Fig.4.10 and it is also defined mathematically by equation (4.51),

$$E = E^* - nQ \quad (4.51)$$

Where,

E^* is the rated amplitude of the output voltage of a VSI under no load condition, and n is a droop coefficient for Q-V droop.

Reference voltage calculation from P-f and Q-V droop

If two or more DER units actively participate in grid stabilization and voltage regulation, then frequency-droop and voltage-droop control strategies are used. The control strategies decide the components of real and reactive powers to be shared by DERs based on the droop characteristics and load level, such that the voltage and frequency of the microgrid may deviate from their rated values within acceptable limits.

As shown in Fig.4.8 the DER unit is connected with a common bus through a PEI (power electronics interface) and a passive LC filter. The output voltage across the filter capacitor and the current through the filter inductor are measured through voltage and current

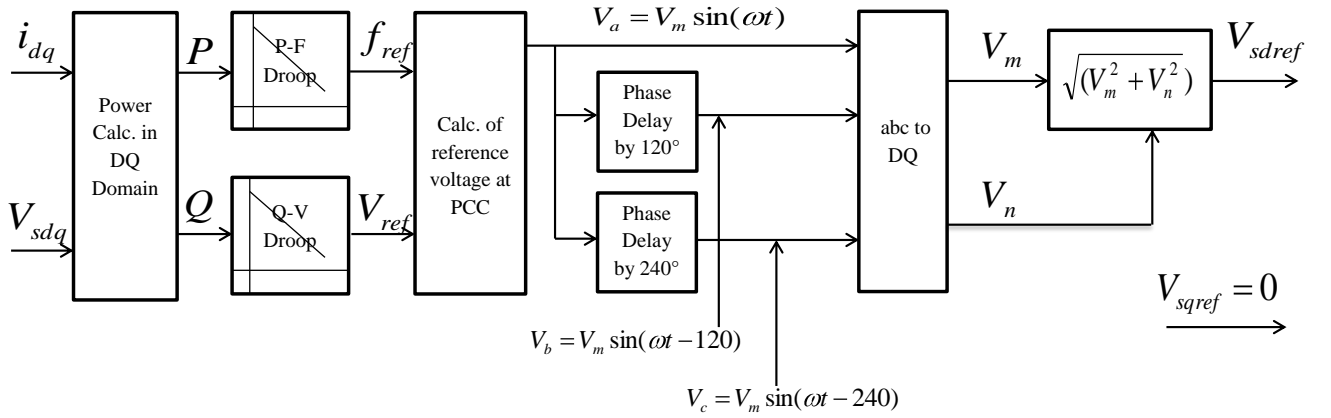


Figure 4.11: PCC terminal voltage calculation

sensors respectively. From Fig.4.11 it is clear that the sensed voltages and currents are converted into dqo reference frame by using equation, $\vec{f}(t) = (f_d + jf_q)e^{j\rho(t)}$. These voltages and currents of dq reference frame are fed to the power calculation block as shown in Fig.4.11. The Power calculation block calculates instantaneous real power (P) and reactive power (Q) [based on equations (4.46) and (4.48)], in dq reference frame, delivered by the DER unit at a common bus. From Fig.4.11 it is clear that by using P-f and Q-V static droop characteristic it is possible to get the reference value of frequency and voltage that need to be maintained at the common bus. If the bus voltage and frequency are not maintained at these values, then power delivered by the source may exceed its capacity in the case of large power requirement by the system. In other words, when the voltage and frequency are not maintained at required level, the power delivered by the source exceeds its capacity, if the requirement of the loads are too large. By using this reference voltage and reference frequency, a-phase reference modulating waveform is generated. By delaying this waveform by 120° and 240° respectively, b-phase and c-phase reference modulating waveforms are developed. $[V_m \sin \omega(t), V_m \sin(\omega(t) - 120), V_m \sin(\omega(t) - 240)]$. After getting three reference modulating waveforms, we are converting them from abc to dq domain as shown in Fig.4.11. So, we are getting d and q axis modulating reference waveforms V_m and V_n respectively.

Now, it is clear that in the islanded mode, the control of DER unit involves regulation of PCC line to neutral voltage magnitude. Suppose, the PCC line to neutral voltage magnitude value is V_{sdref} and it is need to be maintained according to the system requisite. As shown in Fig.4.11, we are generating V_{sdref} by using equation(4.52) and taking V_{sqref} settles down to zero in steady state. The advantage of taking $V_{sqref}=0$, is clear from the output voltage magnitude equation, $|\hat{V}_s| = \sqrt{(V_{sd}^2 + V_{sq}^2)}$. Therefore, the regulation of the PCC voltage magnitude boils down to that of V_{sd} as $V_{sqref}=0$. So, the magnitude of the PCC voltage is solely controlled by V_{sdref} . It means the PCC voltage magnitude can be controlled by single control input V_{sdref} .

$$V_{sdref} = \sqrt{V_m^2 + V_n^2} \quad (4.52)$$

Now, these V_{sdref} and V_{sqref} values are fed to the voltage controller as references, and they are compared with actual V_{sd} and V_{sq} values. This comparison generates error signals. These error signals are given to the voltage controller as discussed in Section(4.1.1.b) and it will generate reference I_{sdref} and I_{sqref} values for the current controller. These values are compared with actual current through the inductor of filter, i.e., I_{sd} and I_{sq} values. These comparison also generates error signals and these errors are rectified by current controller by generating d and q axis modulating waveforms as shown in Fig.4.8. Now, these d and q axis modulating waveforms are converted into three modulating waveforms of abc domain by dq0 to abc transformation. As shown in Fig.4.8, these three modulating waveforms m_a , m_b and m_c are used as reference signals for PWM techniques to generate desired PCC voltage magnitude.

4.1.3 Modeling and control of islanded microgrid

Based on the control strategies developed in Sections 4.1.1 and 4.1.2, in this section, islanded microgrid has been designed. It consists of a seven bus and eight lines system, among which there are five generator buses and two load buses as shown in Fig.4.12.

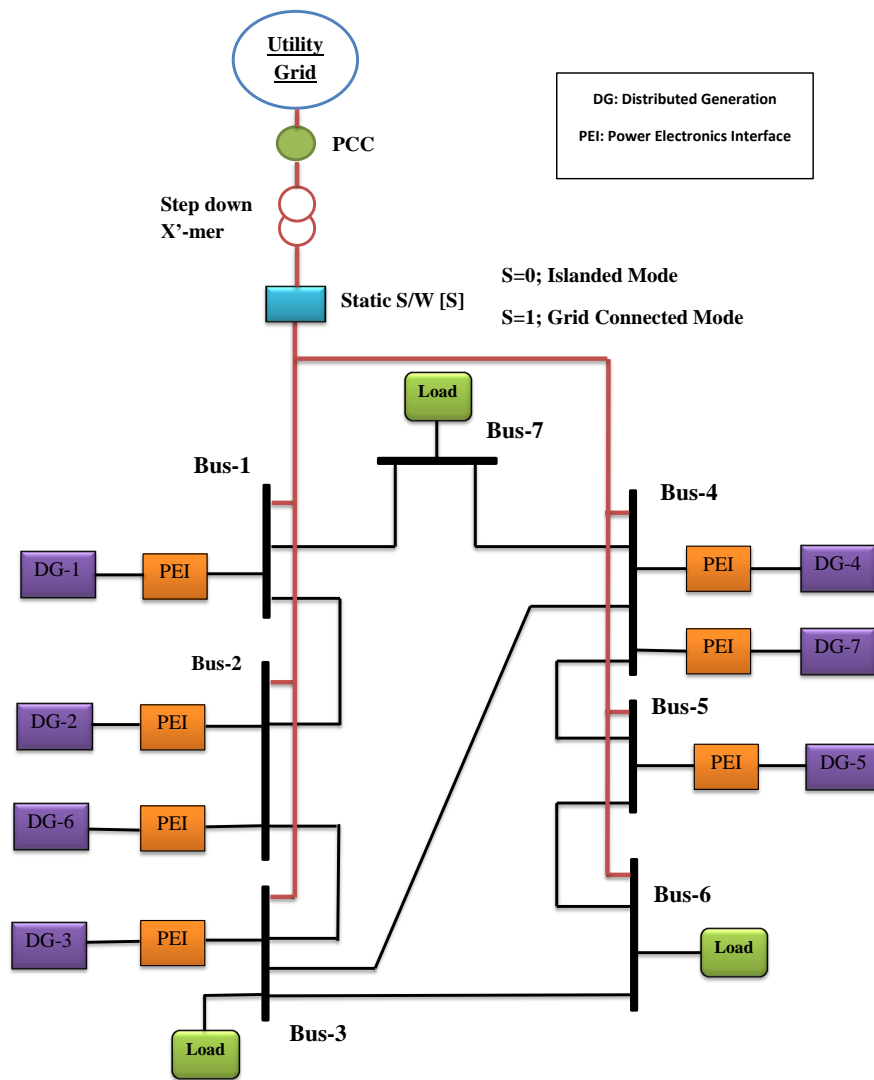


Figure 4.12: Islanded microgrid with a seven bus and eight lines network

It is clear from above discussion that during islanded operation of a grid, the terminal voltage and frequency at each bus has to be controlled within acceptable limits. As shown in Fig.12 the microsource-1 is connected to bus-1, microsources-2 and 6 are connected to bus-2, microsource-3 is connected to bus-3, microsources-4 and 7 are connected to bus-4, microsource-5 is connected to bus-5, and, bus 6 and 7 are the load buses. It is also visible from Fig.4.12 that, the entire microgrid is connected with the utility grid through a step down transformer at PCC.

Primary control tasks in islanded microgrid

As discussed previously, during islanded operation the whole grid is disconnected from the utility grid. In islanded operation there should be a balance between generation and load, otherwise the system may lose its stability. In other words, the power generated by DGs should be sufficient to meet the load requirement and also the losses occurring in the system. If the generation P_{gen} is lesser than summation of load power P_{load} and losses P_{loss} ($P_{gen} < P_{load} + P_{loss}$), some non critical loads have to be switched off. As a result, the critical loads are going to survive during islanded operation. To do this work, segregation of loads has to be carried out for the design of islanded microgrid. So, loads are distributed according to their criticality. But, if the generation P_{gen} is greater than summation of load power P_{load} and losses P_{loss} ($P_{gen} > P_{load} + P_{loss}$), the surplus amount of power generated in a microgrid can be used for charging of storage devices, such as batteries, SMES (Superconducting Magnetic Energy Storage) and so on; the stored power can be used during deficit of power.

The second main challenge is that, the terminal voltage and frequency at each bus has to be within tolerable limits. This control task can be full-filled by an inner current and outer voltage loop control. By using these control strategies with the incursion of the feed forward and the ratio control in dq domain, higher degree of accuracy has been obtained. The simulation results are obtained for the same and discussed in Chapter 5 [36].

In islanded mode the total loads are shared by all the microsources. Each microsource shares the load, depending on their droop setting and the reactance value which is seen between a source and the load bus. The microsource which has a large reactance between its terminal to feeding end point should share less power compare to the others and it is also true that the microsource which has a small value of droop co-efficient should share more power compares to the others. Because of droop controller the load sharing becomes uniform, i.e., it is not possible to have some sources in overloading condition and the rest on under loading condition. As a result of droop setting, each source shares the load

according to its capacity [droop setting]. The droop setting has been done by central controller according to the power required by the load and the generation capacity of the microsources. The above statement is verified from the simulation results as discussed in Chapter 5.

Because of the separate microsource controller (MC) for each micro source, plug and play operation is possible and we can separately maintain the terminal voltage of each source as per our requirements. The central controller gives commands to each microsource controller i.e., the central controller gives the V_{ref} and f_{ref} values to the microsource controller of each microsource. Hence, according to these references each microsource maintains its terminal voltages and frequency at this value in islanded mode. If we change V_{sdref} (i.e. reference value for terminal voltage) the controller should take necessary action and change the value of terminal voltage from the present value to a new reference value within a fraction of a second; This can be achieved by modeling the controller accurately. All the results are briefly explained in Chapter 5.

After the proper design of controller for islanded mode, the stability of the grid has to be maintained, in spite of occurrence of the faults, sudden change in large loads, unbalance loads and so on. So, by proper co-ordination and control of each microsource through its controller which is controlled by a central controller, a great stability, load sharing can be achieved successfully. This is also observed in results discussed in Chapter 5.

The control strategy presented in islanded mode takes advantage of suitable feed-forward compensation techniques to mitigate the impact of load dynamics, inherent inter-couplings and nonlinearities of the control system.

4.2 Grid-Connected Distributed Energy Resources [Grid-Connected Microgrids]

Many of the forms of new and renewable energy are not natural 50 Hz source and the question arises of how to incorporate them into a standard electricity grid. Most of this technology (PV panels, high-speed microturbines and fuel cells) has an inverter as a grid interface. Inverter-interfaced generators are not yet that mature and the modeling of inverters for network stability studies requires much more work, if grid stability is to be ensured with high penetrations of distributed generation (DG). A DG unit affects the system stability by generating or consuming active and reactive power [14]. Therefore, power control performance of the DG unit determines its impact on the utility grid it connects to. If the power control performance is good, the DG unit can be used as means to enhance the system stability and improve power quality; otherwise it could undermine the system stability. In grid-connected mode, the system looks like as shown in Fig.4.13. This section presents a power control method for a grid-connected voltage source inverter which achieves good P, Q decoupling and fast power response.

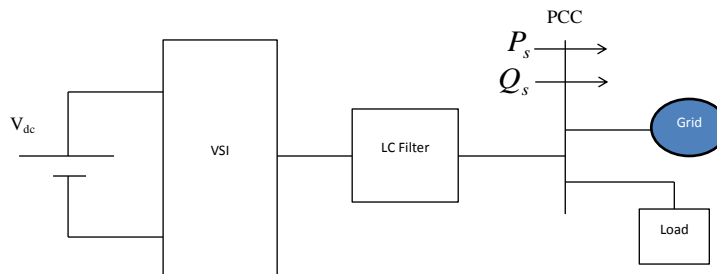


Figure 4.13: Block diagram of the grid connected system

In situations where a strong network connection is available, that is, a connection point with an already tightly regulated voltage and frequency, it is common to export power into that connection through setting a current reference for the inverter. That reference can represent any combination of real and reactive power. The exported power will not significantly influence the voltage or frequency at the point of connection. It is

also assumed that V_{sabc} is balanced, sinusoidal and of a relatively constant frequency. The VSC system exchanges real and reactive power components $P_s(t)$ and $Q_s(t)$ with the AC system, at the point of common coupling (PCC). Hence, the control task is to maintain real and reactive power control in grid connected mode.

Control task:

The VSC DC side is connected in parallel with a DC voltage source and the objective is to control the instantaneous real and reactive powers that the VSC system exchanges with the AC system. Firstly, when single DER unit is connected in grid-connected mode, the main control objective is to regulate real and reactive powers sharing between source and utility grid while maintaining voltage and frequency within permissible limits at PCC. Some researchers have mentioned that this control task can be done in ABC domain by using voltage control scheme, as real power can be controlled by controlling phase angle δ and the reactive power can be controlled by varying the amplitude of the PCC voltage. In this method, real and reactive power should be decoupled only when there is a small difference in the phase and amplitude between the inverter terminal voltage and PCC voltage otherwise, it is difficult to control real and reactive power independently as they are mutually coupled with each other. The project work concentrates on control of real and reactive powers shared by each microsource to the utility grid based on the current control schemes adopted in dq domain instead of ABC domain with the incorporation of feed forward and ratio control along with feed back loop control. It is observed that this schemes gives better performance than the work discussed by other researchers. The simulation results are briefly explained in Chapter 5. In the next section, controlling of a multisource in grid connected mode has been explained. Finally, at the end of this section, a seven bus microgrid system operating in grid-connected mode has been designed. Simulations have been carried out on MATLAB SIMULINK and the

results are discussed in Chapter 5.

4.2.1 Modeling and control of single DER unit in grid-connected mode

A single line diagram for grid-connected DER is shown in Fig.4.14 and its schematic diagram with closed loop control scheme is shown in Fig.4.15.

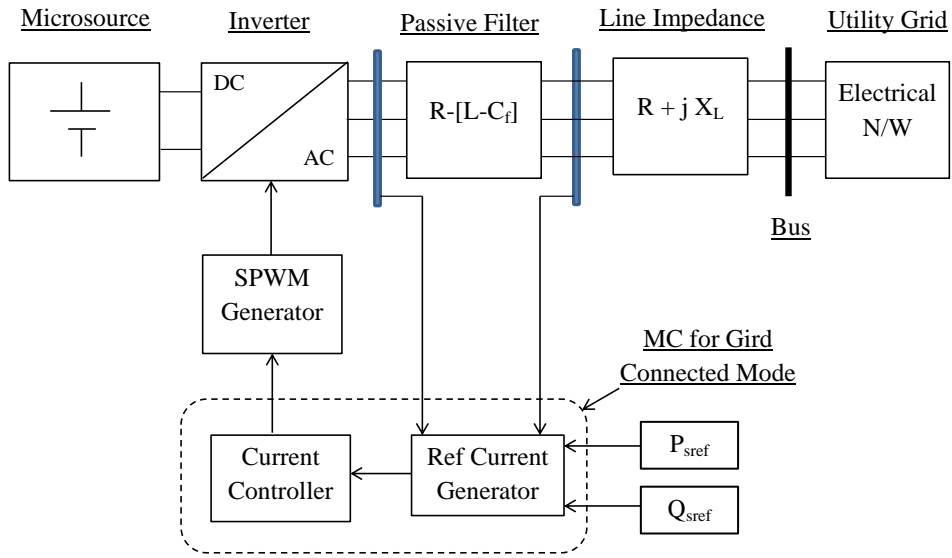


Figure 4.14: SLD for grid connected DER

Fig.4.14 shows single DER unit is connected to utility grid through a current controlled voltage source converter (VSC) and three phase LC filter. The components L and C_f represent the inductance and capacitance of the filter. R Models the ohmic loss of filter inductor and also includes the effect of the on-state resistance of the VSI switches. Fig.4.15 illustrates that the control is performed in a rotating dq0 reference frame and in the grid connected mode of operation, V_{sabc} is dictated by the grid. In this case, ρ and ω represent the phase-angle of the PCC voltage and power system frequency, respectively.

In the first part of this section, design of controller for real and reactive power flow [37], has been explained. In the later part, current control scheme in dq domain has been

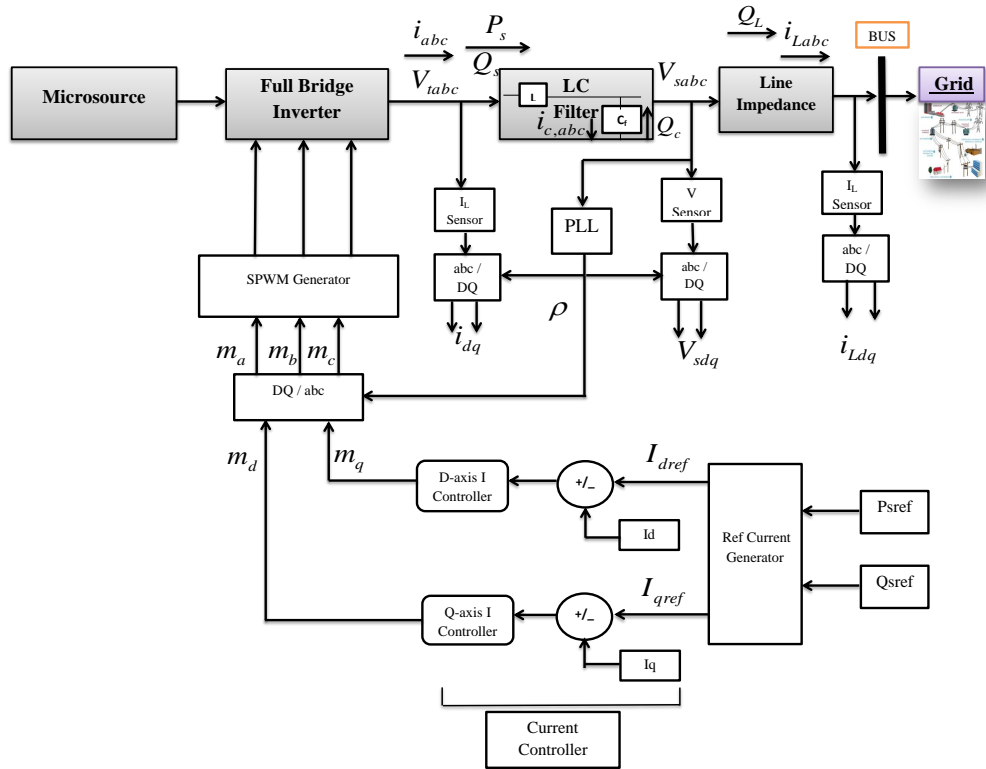


Figure 4.15: Schematic diagram for grid connected DER with closed loop control scheme

discussed for single DER in grid connected mode.

a) Task : Design of controller for real and reactive power flow, based on dq-reference frame.

There are two methods for real and reactive power control, the first method is voltage mode control and the second one is current mode control. Here we have adopted current mode control approach due to the following reasons against voltage mode control. In a voltage controlled VSC system the real and reactive power are controlled respectively by the phase angle and the amplitude of the VSC AC side terminal voltage relative to the PCC voltage. If the amplitude and phase angle of V_{tabc} are close to those of V_{sabc} , the real and reactive powers are almost decoupled and two independent compensators can be employed for their control. Although the voltage-mode control is simple, the current mode control has been adopted due to the reasons that have already been discussed in

the Section 4.1.1.a.

Controller for real and reactive power flow

From Chapter 3, where formulation of real and reactive powers are discussed, it is known that the real and reactive powers in dq domain are given by the following equations.

$$P(s) = \frac{3}{2}[v_{sd}i_d + v_{sq}i_q] \quad (4.53)$$

$$Q(s) = \frac{3}{2}[-v_{sd}i_q + v_{sq}i_d] \quad (4.54)$$

As discussed earlier, if the PCC voltage is balanced, then in steady state, V_{sq} equals to zero and V_{sd} becomes equal to the amplitude of the PCC line-to-neutral voltage. Now, substituting $V_{sq} = 0$ in above equations,

$$P(s) = \frac{3}{2}v_{sd}i_d \quad (4.55)$$

$$Q(s) = -\frac{3}{2}v_{sd}i_q \quad (4.56)$$

The PCC voltage, $|\hat{V}_s| = \sqrt{(V_{sd}^2 + V_{sq}^2)}$, becomes,

$$|\hat{V}_s| = V_{sd} \quad (4.57)$$

Here, \hat{V}_s is the peak value of the line-to-neutral voltage of the PCC and is assumed to be constant, as it is desirable to maintain the terminal voltage constant for the stable operation of distribution system. Therefore, from equations (4.55), (4.56) it is clear that the real and reactive powers are proportional to i_d and i_q , respectively.

Based on the desired real and reactive powers (P_{sref} and Q_{sref}), which are going to be delivered by the microsources, i_{dref} and i_{qref} are calculated from equations (4.55) and (4.56). These values are the reference inputs to the VSC current-control scheme as shown in Fig.4.15. Then, i_d and i_q track i_{dref} and i_{qref} . These i_{dref} and i_{qref} are based on P_{sref} and Q_{sref} .

The control block diagram of the current reference signal generator is shown in Fig.4.16.

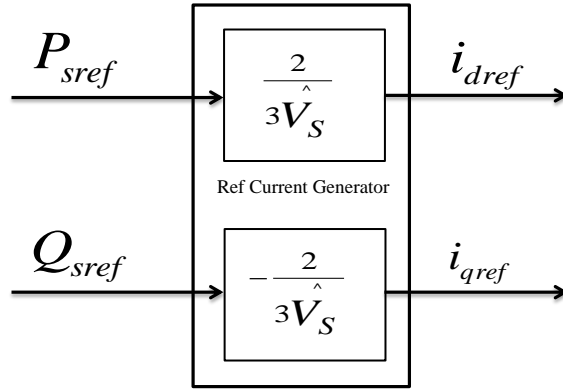


Figure 4.16: Control block diagram of the current reference signal generator

Now, from equations (4.27) and (4.28), it can be written,

$$P_s(t) = G_j(t)P_{sref}(t) \quad (4.58)$$

$$Q_s(t) = G_j(t)Q_{sref}(t) \quad (4.59)$$

where, $P_{sref} = (3/2)\widehat{V}_s i_{dref}$ and $Q_{sref} = -(3/2)\widehat{V}_s i_{qref}$

Therefore,

$$\frac{P_s(s)}{P_{sref}(s)} = \frac{Q_s(s)}{Q_{sref}(s)} = G_j(s) \quad (4.60)$$

That is, P_s and Q_s track their respective reference commands based on the transfer function $G_i(s)$, which is a first order transfer function with a time constant of τ_i .

Results : After design of controller for the real and reactive power flow, the reference values have been found for the VSC current controller.

b) Task : Design of VSC current controller based on dq-reference frame.

The design of VSC current controller is same as discussed in Section 4.1.1.a. Here, controller for real and reactive power flow generates the current reference values for current controller. This reference current is compared with the actual current and the error which is generated from this comparison is fed to current controller to change the value of the current and nullify the error by taking appropriate control action.

Results : From the current control analysis, the controller parameter values have been found. After doing modeling and analysis of single DER in grid connected mode, real and reactive powers delivered by the microsource to the grid are controlled by changing the P_{sref} and Q_{sref} values.

4.2.2 Modeling and control of multi DER units in grid-connected mode

A single line diagram of two DER units connected in grid is shown in Fig.4.17, and its schematic diagram of multi sources connected to a grid is shown in Fig.4.18

In grid connected mode of multi sources the control signals [P_{sref} and Q_{sref}] for each microsource have been given by central controller (CC). The function of the controller for real and reactive power flow and VSC current controller are same as discussed in the previous section. The results for real and reactive power delivered by the multisources are discussed in Chapter 5.

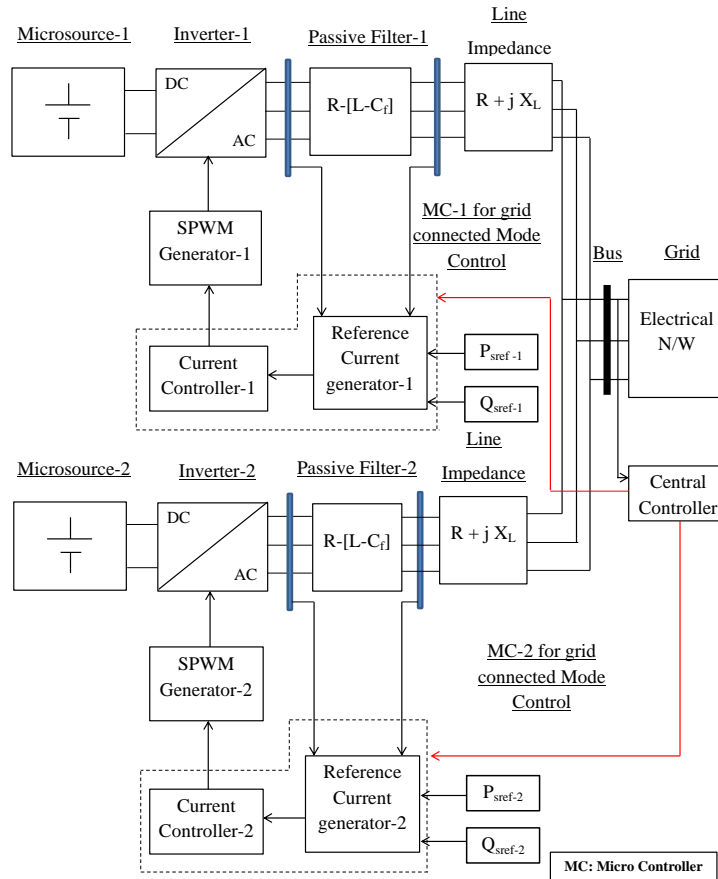


Figure 4.17: SLD of two DERs connected in grid connected mode

Results : By selecting proper reference values of the controller for real and reactive powers for each microsource, better performance of the distribution system in terms of stability, has been achieved.

4.2.3 Modeling and control of grid-connected microgrid

Based on the control strategies developed in Sections 4.1.1 and 4.1.2, in this section, design of grid connected microgrid has been discussed. The control strategy presented in grid connected mode takes advantage of suitable feed-forward compensation techniques to mitigate the impact of load dynamics, inherent inter-couplings, and nonlinearities of the control system. It consists of a seven bus system, among seven bus five are generator

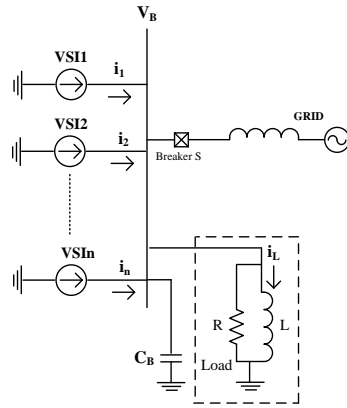


Figure 4.18: Schematic diagram of multi sources connected to a grid

bus and two are load buses as shown in Fig.4.12. In Fig.4.12 when $S=1$ it is in grid connected mode otherwise it is in islanded mode [38],[39].

It is clear from above discussion that during grid connected operation of a microgrid, the real and reactive powers share between grid and microsources have to be controlled to maintain the stability of a grid. As shown in Fig.4.12, the microsource-1 is connected to bus-1, microsources-2 and 6 are connected to bus-2, microsource-3 is connected to bus-3, microsources-4 and 7 are connected to bus-4, microsource-5 is connected to bus-5 and buses 6 and 7 are the load buses. A microgrid connects with the utility grid at PCC through a step down transformer. A static switch is also required for connecting or disconnecting of microgrid with utility grid.

Primary control tasks in grid-connected mode of a microgrid

As discussed previously, during grid connected operation the whole grid is connected to the utility grid and all microsources share the real and reactive power as per given reference value to each source. The control task of sharing real and reactive power with grid has to be full-filled by the controller for real and reactive power flow and VSC current controller, with the incursion of the feed forward and the ratio control. Here the primary condition is that the source which are going to feed current into the grid should not have

a THD grater than 5%. The simulation are carried out for the same and the results are discussed in Chapter 5.

After proper design of the controller for grid connected mode, the stability of the grid has to be maintained, in spite of occurrence of the faults, sudden change in large loads, unbalance loads, etc. So, by proper co-ordination and control of each microsource through its controller which is controlled by a central controller, a greater stability and proper load sharing have been achieved successfully. This is also observed in results discussed in Chapter 5.

4.3 Switching from Islanded to Grid-Connected Mode of the Entire Microgrid and Vice Versa

The importance and operation of microgrid in islanded as well as in grid connected mode has been discussed briefly in the previous part. The Fig.4.19 indicates the single line diagram of a microsource which may be connected in grid or islanded mode. As shown in Fig.4.19, if mode of operation is changed, then the control logic ought to be changed according to the mode of operation.

Based on the control strategies developed in above sections, a microgrid, consisting of seven buses and eight lines, has been designed for operation on both modes depending on the control signal given by central controller (CC). As shown in Fig.4.20., there is one master controller named as central controller (CC) and each source has two controllers: 1) Islanded Mode Controller (IMC) and, 2) Grid-connected Mode Controller (GMC). When islanded mode of operation has been desired, the central controller gives command to all islanded microsource controllers such that all microsourses are going to operate in islanded mode. if the grid connected mode operation is desired then CC gives command to all grid connected controller such that all microsourses are going to operate in grid connected mode. This idea is also very much clear from Fig.4.20. The MATLAB/SIMULINK circuit for a seven buses and eight lines microgrid is shown in Fig.4.21.

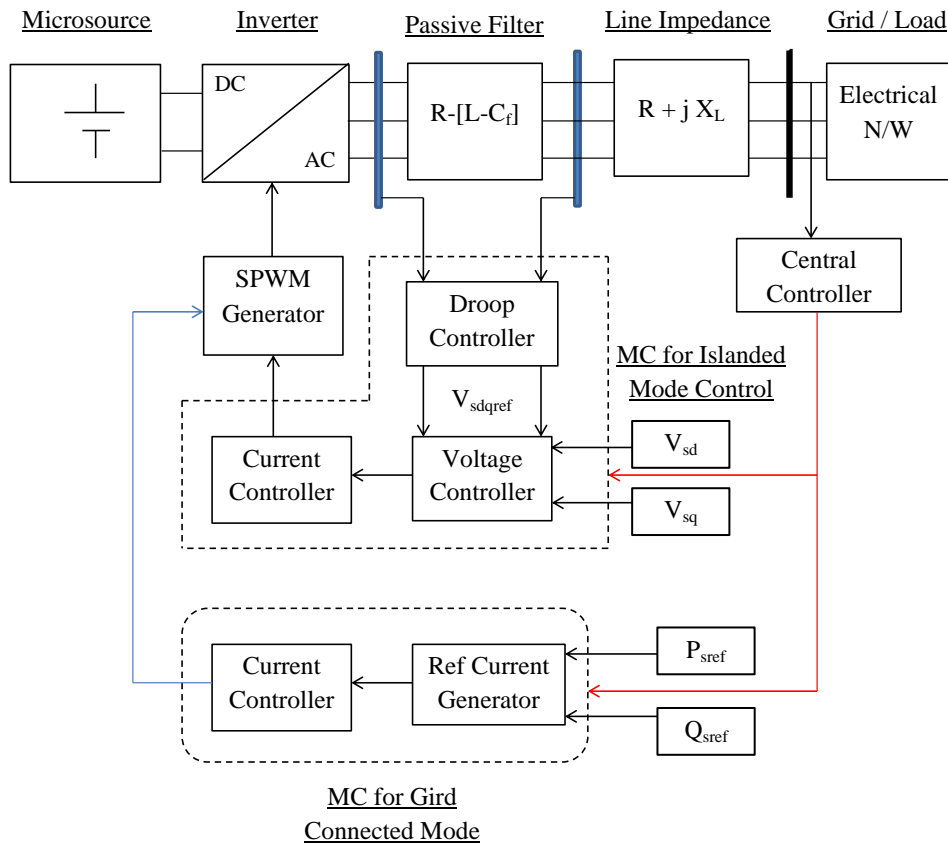


Figure 4.19: SLD of a microsource in grid connected/ islaned mode

For getting closed view of control task, its better to see the control logics for single microsource which may be connected in grid or islaned mode as per the system require- ment. The control logic for single source is shown in Fig.4.22.

Need for change of mode

Normally, microgrid is operates in grid connected mode. The advantage for grid con- nected mode is that, the deficit power can be taken from utility grid, so the loads are supplied without any power interruption. It also provides power to the utility grid when, there is a surplus amount of power generation in the microgrid. When there are some faults, stability problems or non-favorable circumstances in the utility grid, the microgrid

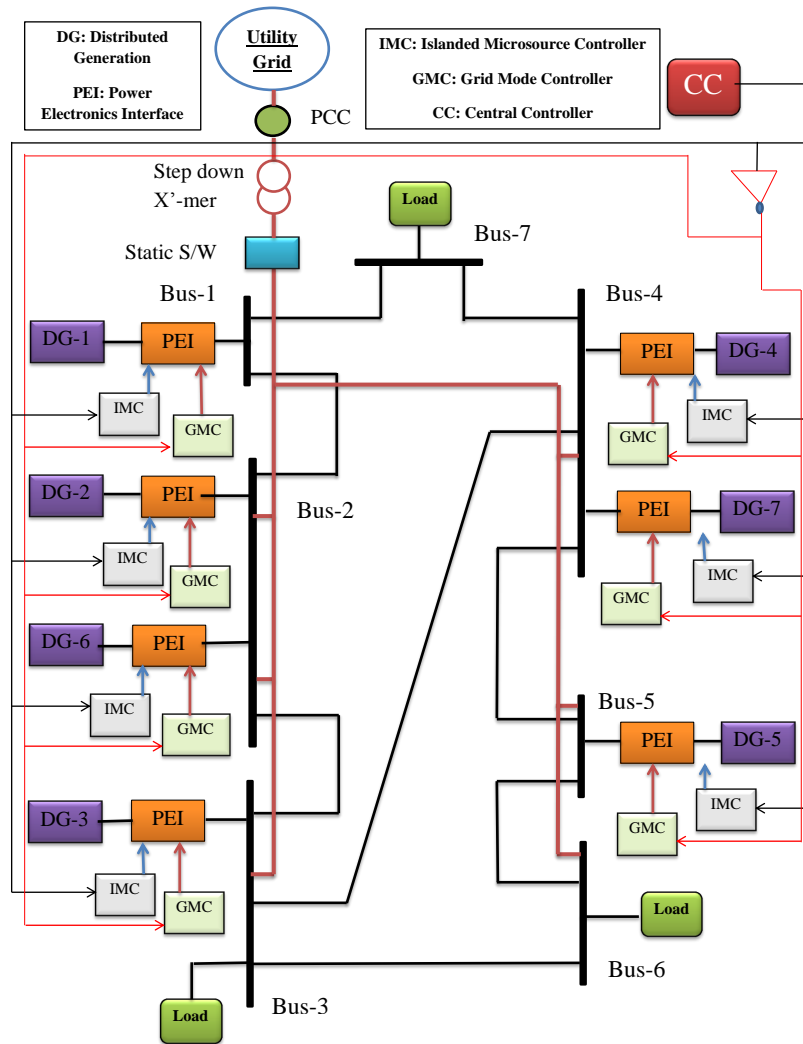


Figure 4.20: Seven bus microgrid network with all kinds of controllers

goes into islanded mode of operation. After clearance of such un-favorable conditions microgrid again goes back to grid connected mode. Thus, the control task has to be changed according to the change of mode, otherwise it will damage the microsources, PEIs or loads [40],[41].

Here, two separate control strategies have been developed for both modes of operation as shown in Fig.4.19. Hence, when microgrid is in islanded mode, the islanded mode control strategy has been adopted and when it is in grid connected mode, the grid connected mode control strategy has been used. The control strategy selection (task) has to be made by

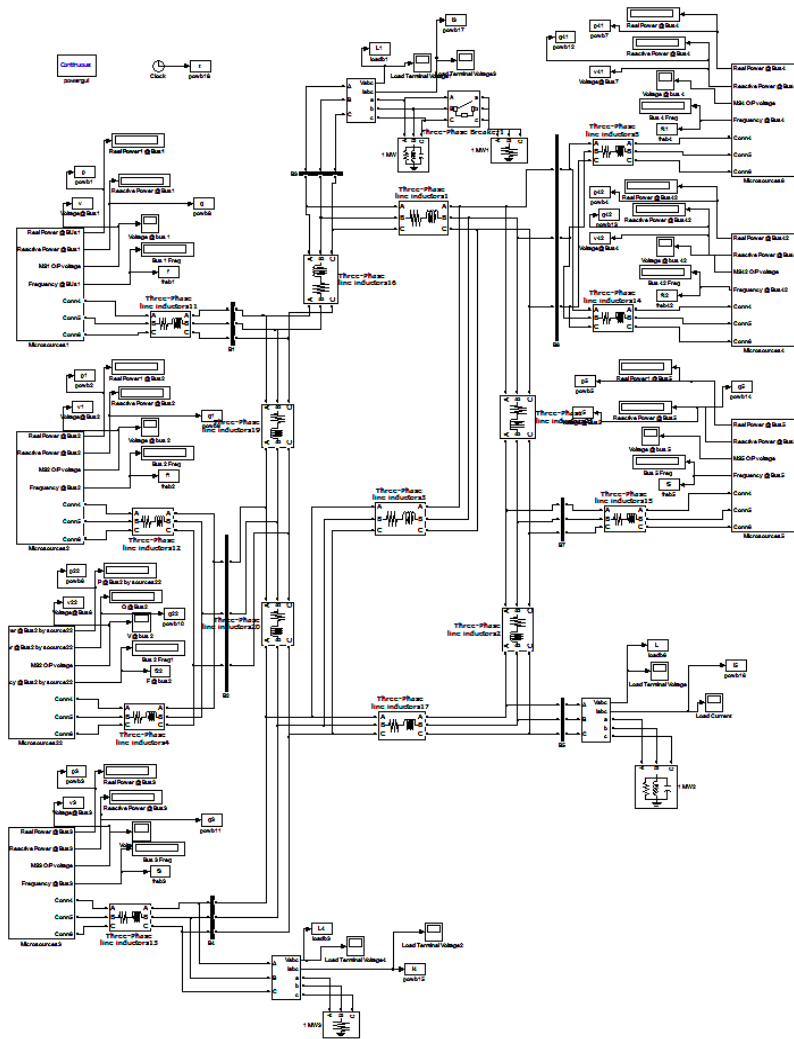


Figure 4.21: Matlab simulation circuit for seven bus microgrid network with all kinds of controllers

central controller (CC) and corresponding signal has to be sent to all local microsource controllers (MC).

The main challenge during change of operating mode is synchronization of microgrid with utility grid because there may be difference in frequency, amplitude or phase of voltage. Due to this problem there may be sharp transients produced during change of mode and it will damage the controllers, PEIs, critical loads and so on. Hence, the precaution has to be taken against this problem. There should be a proper match of voltage magnitude,

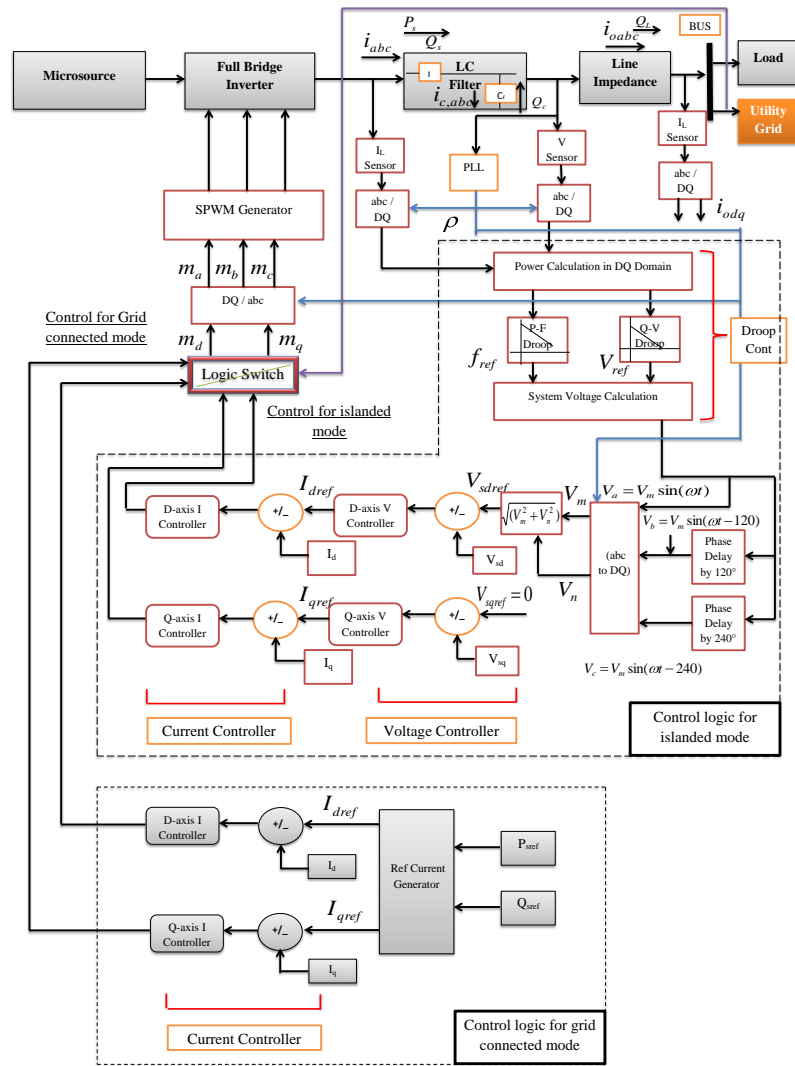


Figure 4.22: Control logic for single microsource in a microgrid

phase and frequency between utility grid and microgrid. The control strategy should be strong enough to mitigate such kinds of problems. In Chapter 5 the change of operating mode is simulated and its effect and simulation results are discussed in brief.

4.4 Summary

This chapter has discussed, the control of single DER unit, multi DER units and the entire microgrid in islanded and grid connected modes. Initially, the modeling and control of

single DER unit, multi DER units and the entire microgrid in islanded mode is discussed. The control strategy presented in islanded mode takes advantages of suitable feed-forward compensation technique to mitigate the impact of load dynamics, inherent inter-couplings and nonlinearities of the control system. Next, the VSI operates as a current controlled current source in grid connected mode is discussed. The design of controller for real and reactive power flow in conjunction with VSC current control method has been designed such that, it injects real and reactive powers according to set reference values into the grid. Finally, in this chapter operation and behavior of entire microgrid during change of operating mode is discussed.

Chapter 5

Results and Discussions

This chapter discusses the drawn simulation results, which were used to verify the design model of controllers for grid connected mode or islanded mode of microgrids. In this chapter firstly, closed loop dc-dc boost converter with PI controller has been simulated. Then, three phase current controlled VSI has been simulated for islanded and grid connected application. Further, single DER unit, multiple DER units and entire microgrid are simulated for both islanded and grid connected modes. Finally, at the end of this chapter, entire microgrid has been simulated during switching from one mode to other mode of operation. All simulation results are discussed based on the described theories and control algorithm from Chapter 2 to Chapter 4.

5.1 PI Controlled Close Loop DC-DC Converter

Simulation study is needed to verify the control structure presented in Chapter 2 for the designed close loop dc-dc converter and to show the proper working of the designed controller. Hence, to demonstrate the performance of PI controller, simulation study is carried out on Matlab/Simulink. The system parameters considered for the simulation are given in Table 5.1.

Fig.5.1 shows the behavior of the output voltages of the dc-dc boost converter without having any control on its duty ratio and Fig.5.2 shows the output voltage of the boost converter with PI controller. Fig.5.1 and Fig.5.2 represents the output voltage of the

Table 5.1: System Parameters which are Considered in a Boost Converter Simulation

Parameter	Value
Input voltage (V_1)	192 V
Output voltage (V_o)	814 V
Duty ratio D	0.76
Power rating	120 KW
Filter inductor (L)	0.14 H
Filter capacitor (C)	0.048 F
Load resistance (R)	5.52 Ω
Output voltage ripple (P-P)	0.25 V
Output current ripple (P-P)	0.1 A
Switching frequency f_s	10 KHz
Proportional gain of controller (K_p)	6.75×10^{-5}
Integral gain of controller (K_i)	1.36×10^{-4}

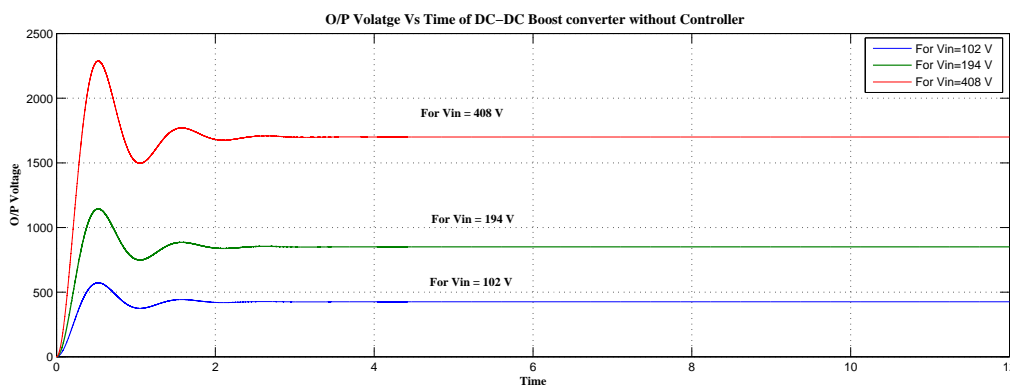


Figure 5.1: Output voltage of the boost converter without controller

boost converter against the variation in the input voltage. As we want to have constant dc bus voltage ($814 V_{dc}$) but from Fig.5.1 it can easily be observed that the output voltage gets changed as input voltage is changed. Fig.5.2 shows that the designed PI controller is working nicely and a good range of control in variation of the input voltage is achieved. The DC-DC boost converter with PI controller gives a controlled output of 814 V when the input voltage is 97 V and 388 V. This is a range for a designed controller gives a proper output voltage with an acceptable transient period. Here, D, L and C values are derived such that the hardware implementation based on these values is possible, and it also gives

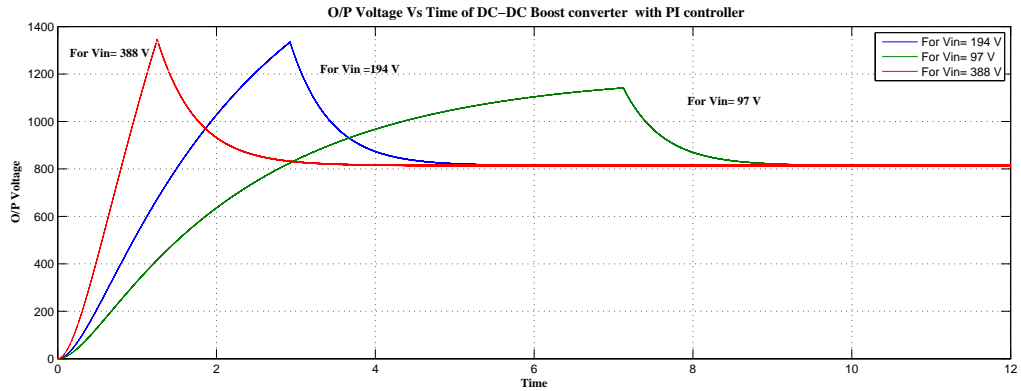


Figure 5.2: Output voltage of the boost converter with controller

the same results as shown in simulation. From the simulation results its clear that PI controller based DC-DC boost converter, which is explained in Chapter 2, is giving the desired performance.

5.2 Results of the Designed LC Filter

A power filter is used to meet the imposed utility distortion limits, to avoid parallel resonance and to improve the power quality. Moreover, Passive harmonic filters are often used to reduce voltage harmonics and current distortions in the distributed generation system. A series inductor (L) and a parallel capacitor (C_f) are used to attenuate any frequency above 50 Hz. The designing of this filter has been explained in Chapter 2.

As seen in the Fig.5.3, the inverter successfully converted the input DC voltage, which is supplied by a DG source, into an AC voltage. The inverter initially produces a PWM wave which develops due to the uni-polar switching of the IGBT-diodes of inverter. The pulse width modulator uses the carrier frequency which is very high compare to the modulating waveform. Therefore, it is very essential to attenuate such a high frequency especially when the voltage is being supplied to the load and utility grid. The utility grid having a frequency of 50 Hz, it is only feasible to allow signals with frequency up to 50

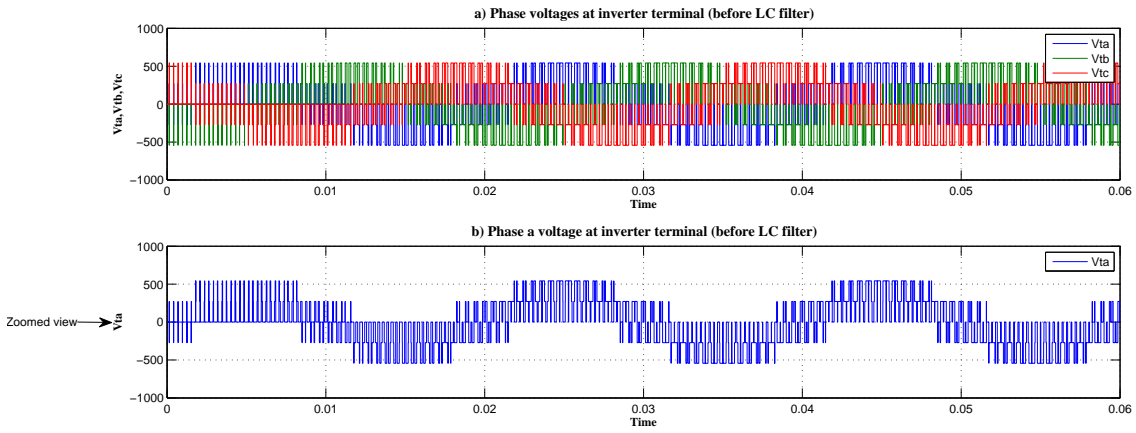


Figure 5.3: Inverter output voltages (3-phase) before filter and Zoomed view of inverter output voltages (1-phase) before filter

Hz and eliminate any higher order frequencies. From the sinusoidal wave, we can observe that the resultant waveform has been successfully tuned to 50 Hz.

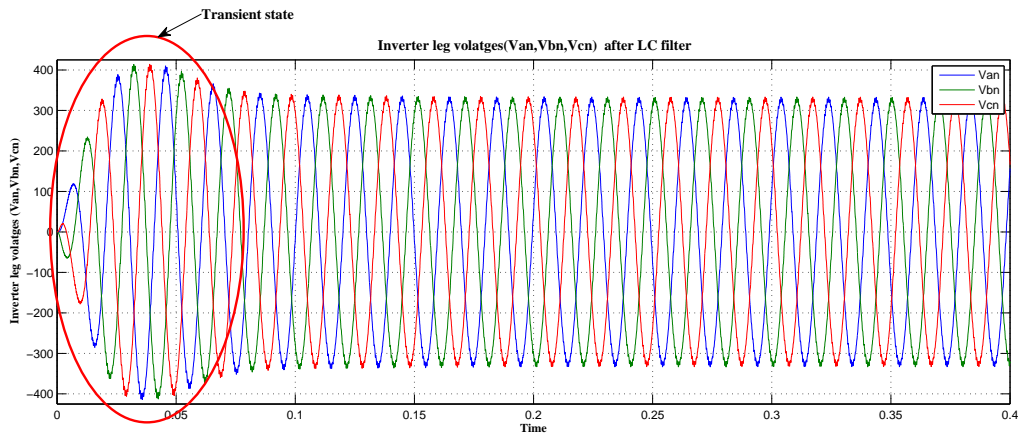


Figure 5.4: Inverter output voltages (3-phase) after filter

As explained in Chapter 2, the passive LC filter components have been designed such a way that it can eliminate all higher order harmonics having a frequency value equal to or greater than switching frequency. Practically, it is not possible to have a pure L and C_f values for physically implementation of a passive filter. So, to achieve more realistic simulation results, the non-ideality of L, C_f and IGBT switches are considered by inserting a resistance R in series with L. It is clearly observed from Fig.5.4 that the designed LC-

filter works nicely for a given values,

$$L= 0.1 \text{ mH}$$

$$C= 2.5 \text{ mF}$$

$$R= 1 \ \Omega$$

Using the derived equation (2.32) and (2.33) in Chapter 2, the transfer function for the LC -filter can be determined in such a way that it shows its stability.

$$G(S) = \frac{1}{2.5 \times 10^{-7}S^2 + 1 \times 10^{-4}S + 1} \rightarrow \text{For islanded mode}$$

$$G(S) = \frac{1}{0.1 \times 10^{-3}S + 1} \rightarrow \text{For gridconnected mode}$$

The second order two pole resonant LC filter characteristic of Fig.5.5 has a -40 dB/decade slope in gain magnitude above the corner (resonant) frequency and a total phase lag of 180 degrees. The gain characteristic has a peak which varies with the Q of the resonant circuit. This is of little importance unless the resonant frequency is close to the loop gain crossover frequency, when it could eliminate the gain margin and cause instability. As shown in Fig.5.5 it is easily observed that the higher order frequency components get attenuated very quickly. Fig.5.6 shows the root-locus plot of the LC filter, it proves that the designed filter is stable for all the values of gain. Fig.5.7 and Fig.5.8 show the bode plot and root-locus plot of the LC filter for grid connected mode of operation, they also proves that the designed filter is stable for all the values of gain.

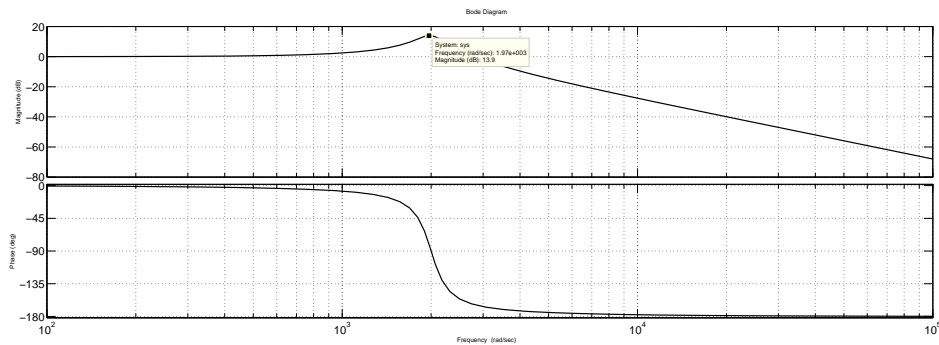
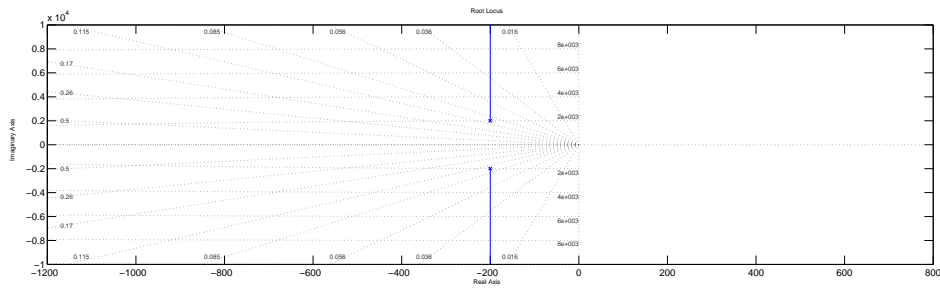


Figure 5.5: Bode plot of the designed LC filter for islanded mode



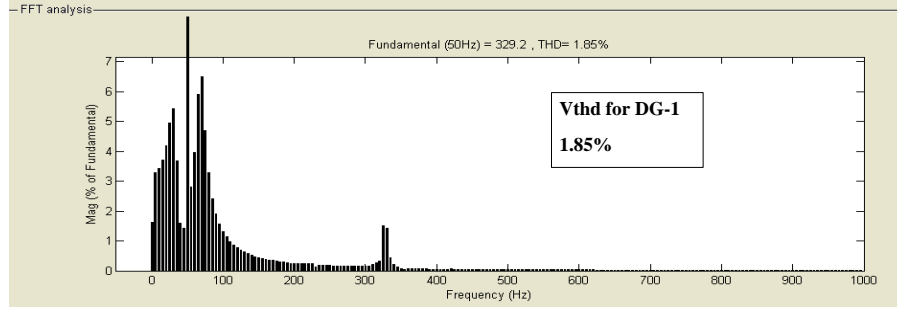


Figure 5.9: FFT analysis for THD of filter output voltage at no load

5.3 Control of Single DER Unit in Islanded Mode

The proposed control strategy for controlling of single DER unit in islanded mode is developed using MATLAB SIMULINK. As explained the control strategy in Chapter 4, based on that simulation results are carried out. Results and discussions on islanded DER unit are described in the following manner.

- based on load conditions;
 1. no load condition;
 2. balance load condition which is stepped up after few seconds;
 3. non-linear load condition;
 4. shared balance and non-linear load condition.
- based on fault condition.
- based on controller reference set point.
 1. changed in V_{sdref}

The DER unit parameters are $L= 0.1$ mH, $C_f= 2.5$ mF, $V_{DC}= 1200$ V, $V_{sdref}= 230$ V_{rms} [326 V_{P-P}], $v_{sqref}= 0$ V, $f= 50$ Hz. Using derived equation (4.16) in Chapter 4, the transfer functions of the current control compensators,

$$k_d(s) = k_q(s) = \frac{0.2s + 4.14}{s}$$

The parameters which are used to develop a whole control model are given in Table 5.2.

Table 5.2: System Parameters which are Considered in Islanded System

Parameter	Value
Nominal phase voltage at PCC	230 V_{rms}
Grid frequency	50 Hz
DC bus voltage	1200 V
Filter inductance	0.1 mH
Filter capacitance	2.5 mF
Filter resistor (R)	2.07 $m\Omega$
Switching frequency	1.8 KHz
PLL proportional gain (k_p)	180
PLL integral gain (k_i)	3200
PLL differential gain (k_d)	1
d-axis voltage loop controller ($K(s)$) proportional gain (K_p)	1.673
d-axis voltage loop controller ($K(s)$) integral gain (K_i)	374.752
q-axis voltage loop controller ($K(s)$) proportional gain (K_p)	1.673
q-axis voltage loop controller ($K(s)$) integral gain (K_i)	374.752
d-axis current loop controller ($K_d(s)$) proportional gain (K_p)	0.2
d-axis current loop controller ($K_d(s)$) integral gain (K_i)	4.14
q-axis current loop controller ($K_q(s)$) proportional gain (K_p)	0.2
q-axis current loop controller ($K_q(s)$) integral gain (K_i)	4.14

5.3.1 Based on the load condition

No load condition

According to the standards for distribution system, if the load changes from no load to full load condition, the terminal voltage of the DG source should not fall below 6% of its rated value. Generally when the inverter is not connected to the load, current flows out of the inverter will be zero. It means, it doesn't participate to supply any active or reactive powers but the output voltage has to be pure sinusoidal.

Fig.5.10 shows the output voltages measured after the filter for no load condition. The output voltages of the inverter are fed to the control loop as explained in Chapter

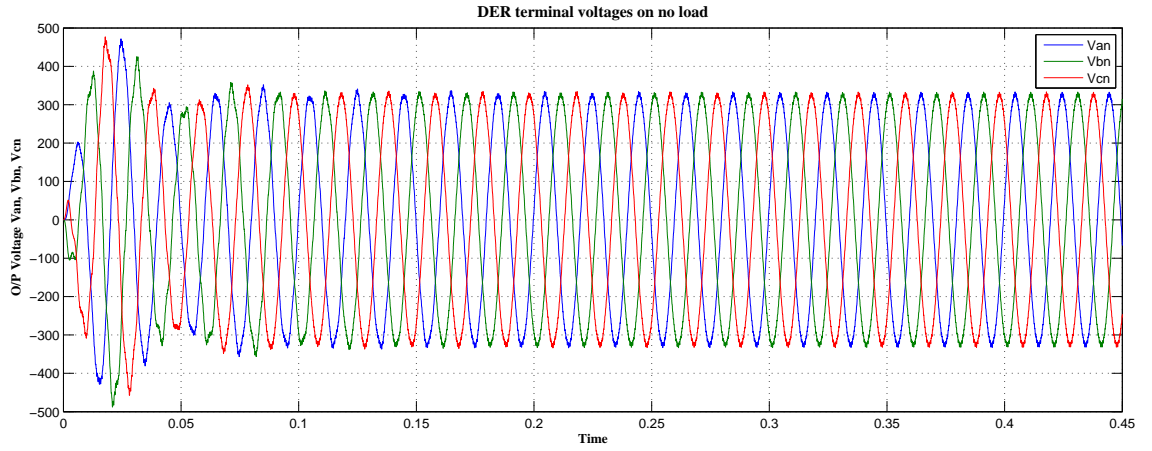


Figure 5.10: Inverter output voltage at no load condition

4. The waveform has a very small transient period which is acceptable. It indicates the capability of feed forward compensation and dynamically decoupling with the load. During the starting of VSI, there is an initial transient as the controllers act to establish the requested PCC voltages. The waveform has $230 V_{rms}$ and very lesser THD. Fig.5.11 is presented to show the output frequency at no load is maintained at 50 Hz.

Balanced load condition which stepped up after 0.5 seconds

Two types of passive loads were used to evaluate the system performance under different loading conditions.

Load 1: $P_{R1} = 200\text{KW}$, $P_{L1} = 0.5 \text{ KVAR}$, $P_{C1} = 0.1 \text{ KVAR}$

Load 2: $P_{R2} = 90\text{KW}$, $P_{L2} = 0.2 \text{ KVAR}$, $P_{C2} = 0 \text{ KVAR}$

Stepping the load during islanded mode of operation is investigated in this section. The working of the designed controller is shown in Fig.5.12. Initially the VSI supplies the balance load-1. It can be seen that as we stepped up the load by inserting the balance

load-2 in conjunction with the load-1, controller controls the inverter such that, it keeps supplying $230 V_{rms}$ at PCC. The load stepped up at 0.45 sec is clearly understood from Fig.5.12. The distortions in voltages occur at 0.45 second for a few milliseconds. Fig.5.13 shows the zoomed in graph of Fig.5.12 at 0.45 seconds. The load currents got changed from 400A to 600A at 0.45 second as load changed which is shown in Fig.5.12. Fig.5.13 shows the zoomed in graph for load currents at 0.45 second and it takes few milliseconds to get settle down. Load currents have initial transient period of less than 0.1 seconds which is acceptable according to the standards. Fig.5.14 got by doing the FFT analysis in MATLAB SIMULINK. As shown in Fig.5.14 the THDs for load voltages and load currents are approximately 1.27% and 1.33% respectively, which are less than 5% as per the standards for distribution system. As seen in Fig.5.12, it is investigated that as the

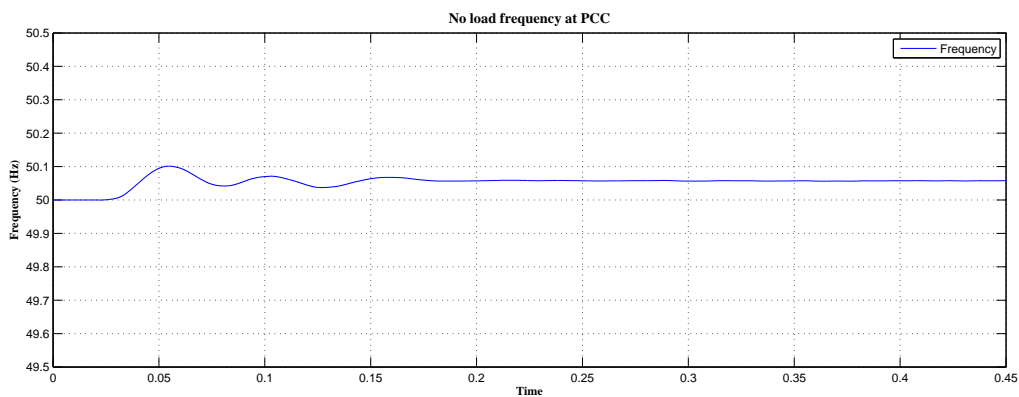


Figure 5.11: Inverter output frequency at no load condition

load steps up, the real power stepped up at 0.45 seconds and the frequency gets affected for a few seconds but it is within permissible limits of ± 0.5 Hz. In the islanded mode of operation we want our output voltage and frequency need to be stay within acceptable limits. Here, we can observe that the frequency and voltages are constant in spite of change in load. Therefore, the aim of voltage and current controller to maintain the PCC voltage and frequency at constant level during islanding mode is achieved successfully.

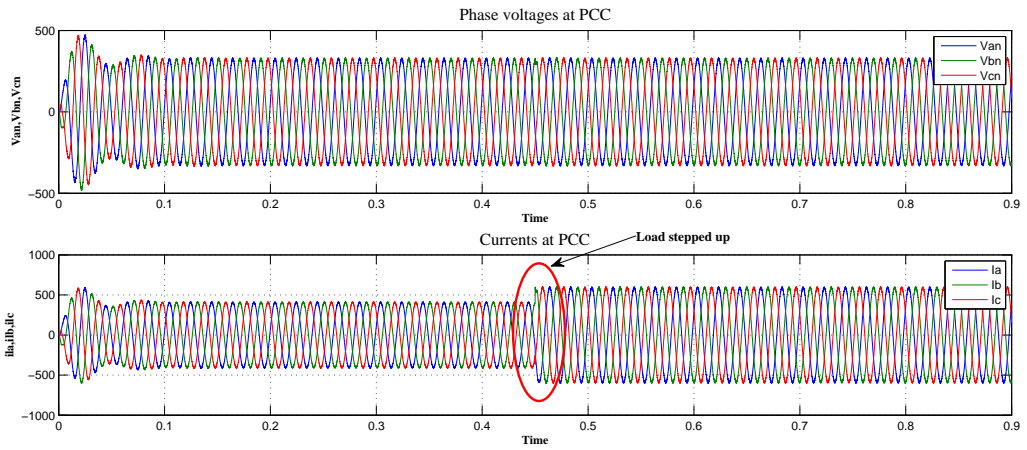


Figure 5.12: Phase voltages and currents at PCC for load stepping at 0.45 sec

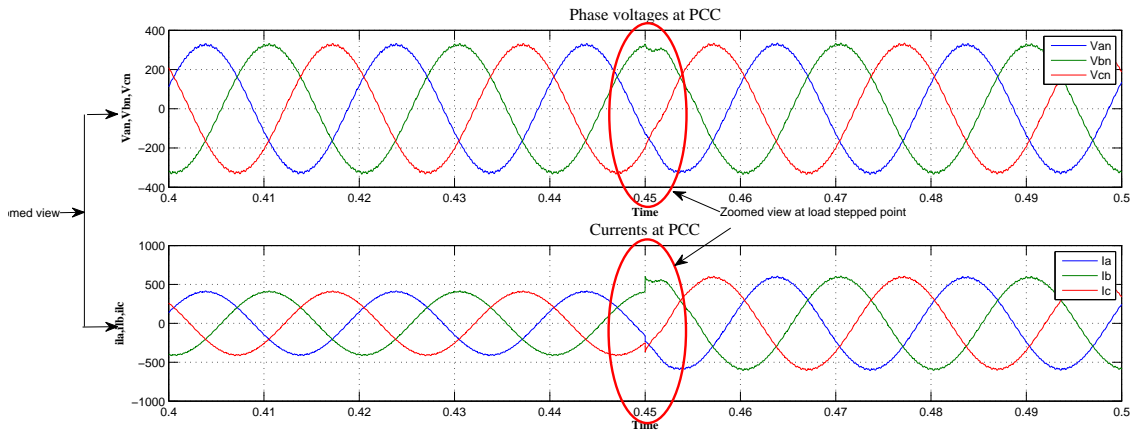


Figure 5.13: Zoomed view of phase voltages and currents at PCC for load stepping at 0.45 sec

Under non-linear load condition

As explained the control strategy in Chapter 4, we got the satisfied results for balanced load. Here we replaced the balance load with the nonlinear load, the output voltages without controller for this condition is shown in Fig.5.16. In the Fig.5.16 the peak of the voltages at PCC went to 500 V, which is not in our requirement. It may create problems to the load side. Moreover, from the Fig.5.16 it is also clear that due to nonlinearity of the loads, the voltage and current waveforms are distorted from its sinusoidal nature. To avoid this situation we provide feedback path to the inverter switching using designed

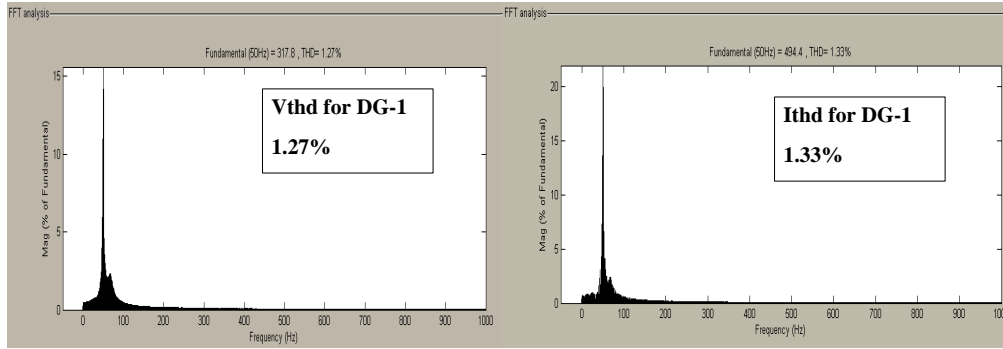


Figure 5.14: Voltage and current THDs at PCC

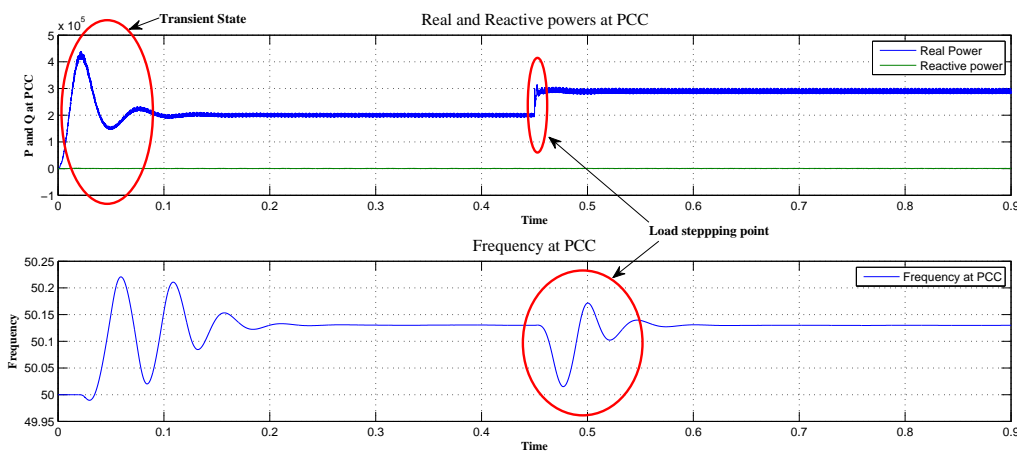


Figure 5.15: Real and reactive powers at PCC / Frequency at PCC for load stepping at 0.45 sec

controller such that peak comes down to 326 V and voltage waveform should maintain its sinusoidal nature within permissible time limits. The output voltages and currents at PCC using a controller is shown in Fig.5.17. From Fig.5.16 and Fig.5.17, it is obvious that the output load voltages, with controllers, are having a less THDs compare to the output voltages without controller.

The load currents don't get much affected by the controller. We have seen that for a non-linear load our designed controller is working properly. But as we know it is not necessary that it works properly for as non-linear load generates unbalancing in load currents which force neutral current to flow through the circuit. Hence, the current

strategy needs to be restructured as positive, negative and zero sequence components of the phase currents ought to be considered, so each phase have three controllers. This is not developed here.

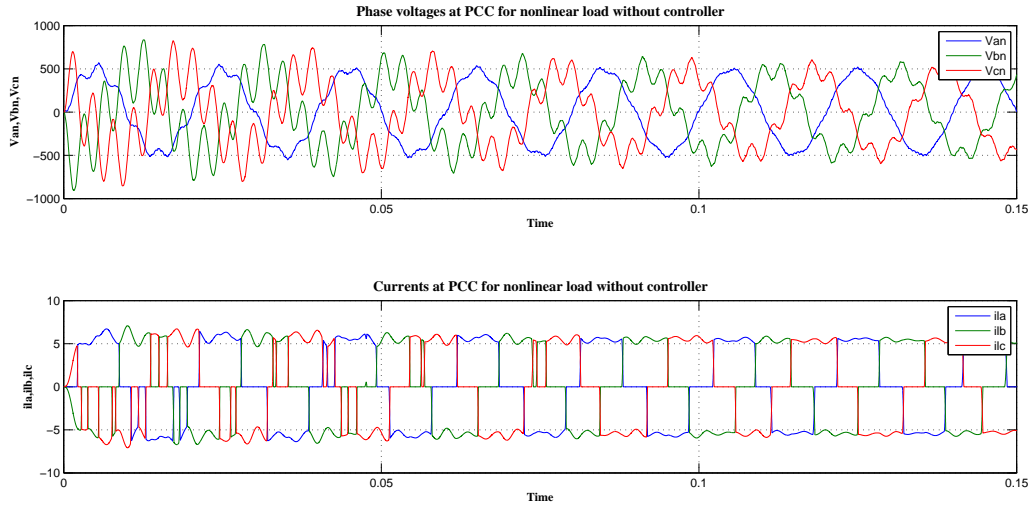


Figure 5.16: Phase voltages and currents at PCC without control for nonlinear load

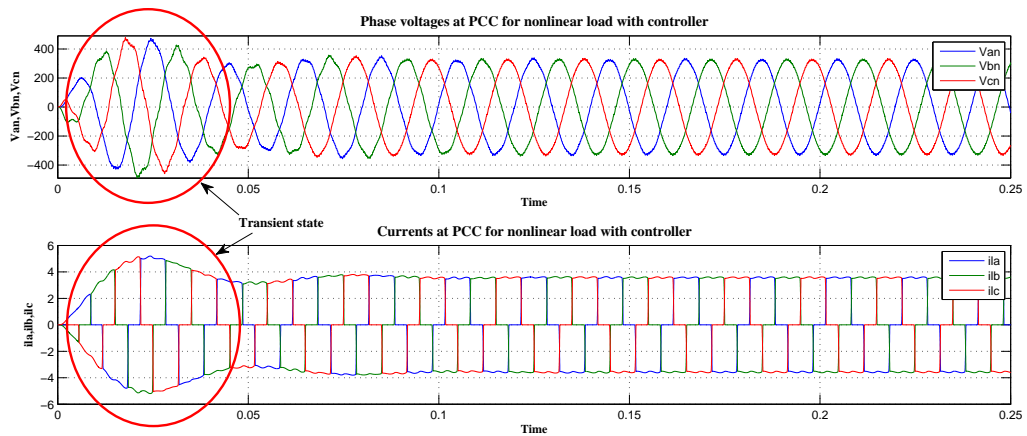


Figure 5.17: Phase voltages and currents at PCC with control for nonlinear load

Shared balanced and non-linear load condition

In this section, the VSI output is being shared with balance and non-linear load. The voltages and currents at PCC without controller and with controller are shown in Fig.5.18 and Fig.5.19 respectively. The voltage amplitude at PCC remains to peak of 326 V in the case of VSI with controller, while in the case of VSI without controller the voltage amplitude at PCC went to peak of 500 V and it is not the desired value, according to the required value of voltage at PCC. It shows that designed controller is working properly. Fig.5.18 shows the voltages and currents at PCC without using controller. The waveforms are deteriorating from their sinusoidal wave shape. It is also visible from Fig.5.18 and Fig.5.19 that the waveforms with controller having a less THDs compare to the waveforms without controller.

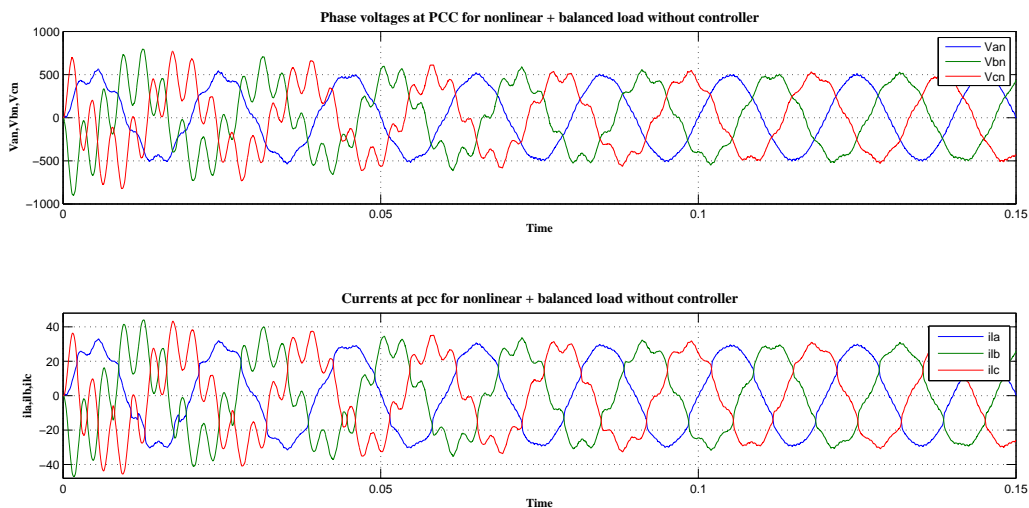


Figure 5.18: Phase voltages and currents at PCC without control while sharing balanced and non linear load

Due to the presence of nonlinear load circuit, power factor becomes poor so, it will draw more current from the source, as a result there would be a more losses in the system. Having considering this point, to reduce the reactive power requirements of the system we have taken $V_{sqref} = 0$. Consequently, the reactive power requirements of the system has been reduced hence the circuit power factor gets improved and it will draw less current

from the source, thus system losses will be reduced. Here from Fig.5.18 and Fig.5.19, it is clear that with controller the load current requirement gets reduced than without controller. Thus, the system efficiency would be improved.

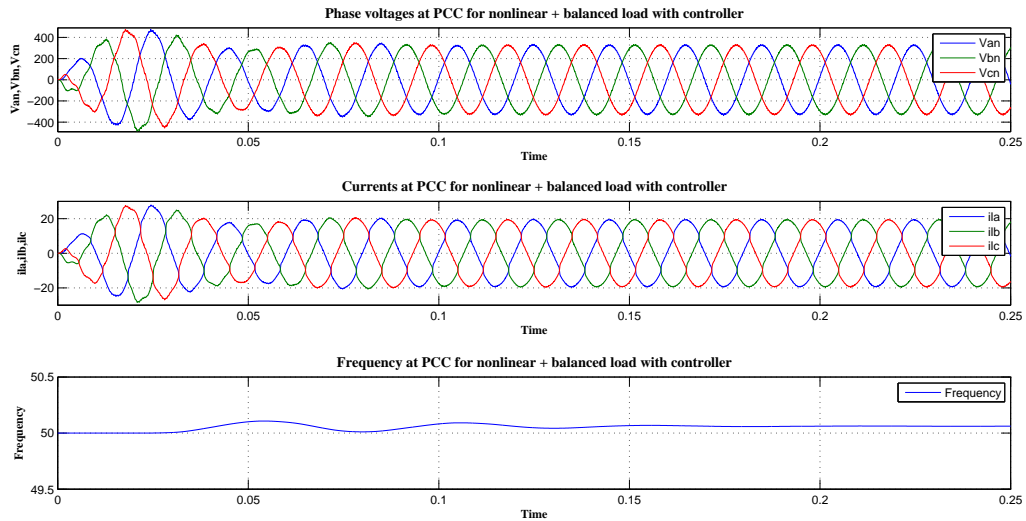


Figure 5.19: Phase voltages, currents and frequency at PCC with control while sharing balanced and non linear load

5.3.2 Fault condition

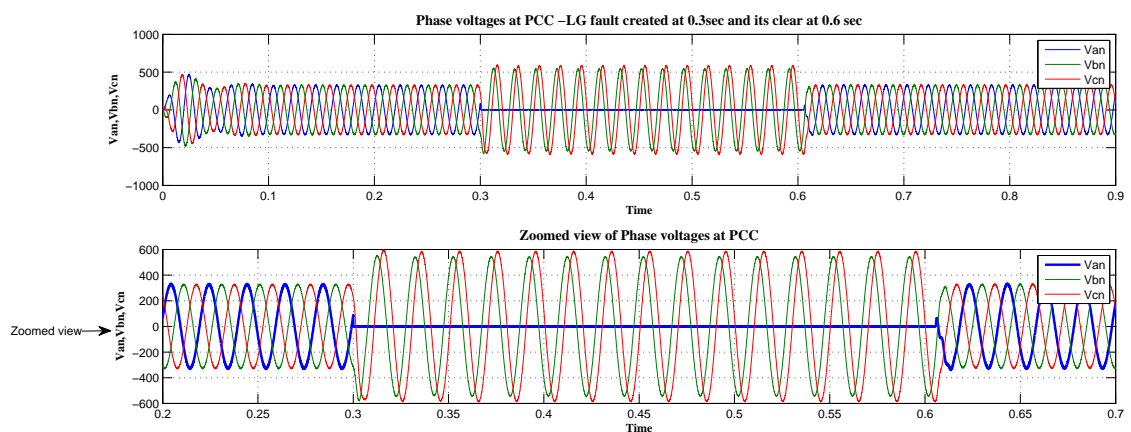


Figure 5.20: Phase voltages and its zoomed view at PCC for LG fault created at 0.3 sec and cleared at 0.6 sec

For showing the rigidity of the designed controller; an LG fault has been created on R- phase at 0.3 sec and it was cleared at 0.6 sec. Fig.5.20 shows the phase voltages at PCC and its zoomed view. It is observed that the controller could maintain the PCC voltage at peak of 326 V before and after experienced of an unbalanced condition, while the system without controller may lose its stability after having an experience of such an uncertain circumstances.

5.3.3 Based on the controller reference set point

Change in the reference voltage set point of a controller (V_{sdref})

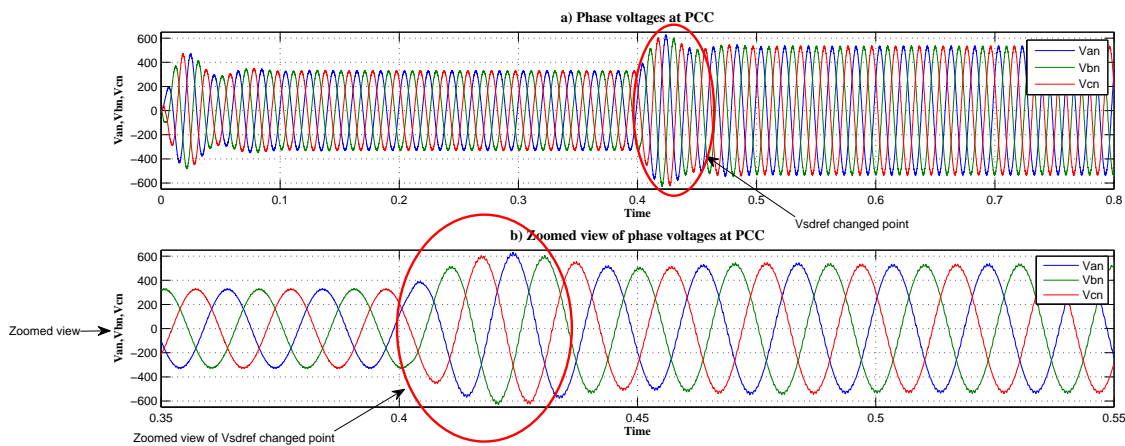


Figure 5.21: Phase voltages and its zoomed view at PCC for a changed in V_{sdref} to a peak of 525 V

Fig.5.21 is presented to show the beauty of a designed controller. As we change the set point of the controller, i.e. (V_{sdref}), the output voltages at PCC should be changed and the peak of PCC voltages should reach to the changed reference value within permissible time limits. This is shown in Fig.5.21, as V_{sdref} changed to a peak of 525 V, the output voltages of the DER at PCC reached to a peak value of 525 V within approximately 0.06 sec. It indicates that the designed controller is working efficiently.

Fig.5.22 shows that, as V_{sdref} has been changed from a peak of 326 V to a peak of 525 V at 0.4 sec, the actual V_{sd} also changed to a new peak of 525 V, i.e., it exactly tracked

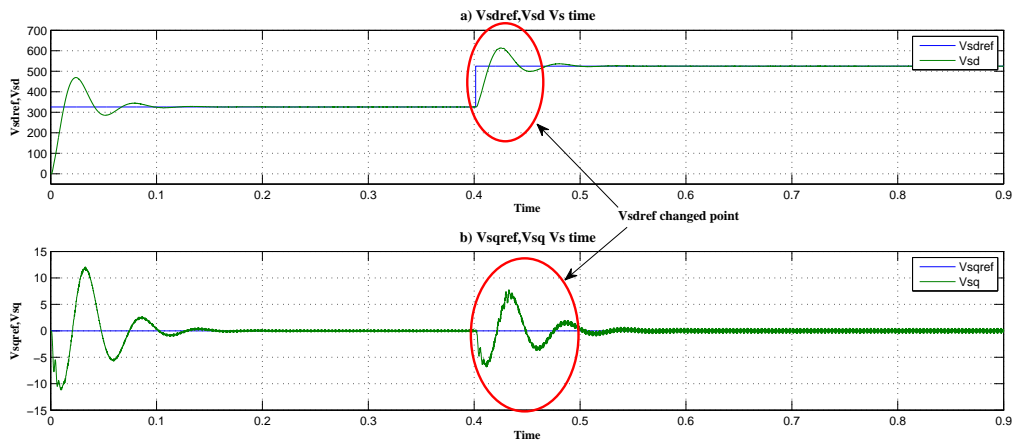


Figure 5.22: [V_{sdref} and actual V_{sd}] and [V_{sqrref} and actual V_{sqr}]

the reference signal (V_{sdref}). The frequency plot shown in Fig.5.23 also indicates that as V_{sdref} changed, there is some disturbance in frequency but it is within tolerable limits of ± 0.5 Hz.

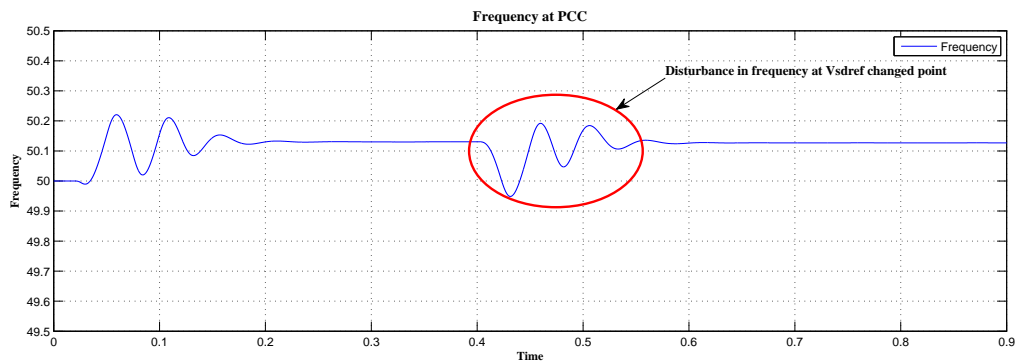


Figure 5.23: Frequency response for a changed V_{sdref}

Above all cases prove that the designed controller for single DER unit in islanded mode works satisfactory for all the conditions.

5.4 Control of parallel connected two DER units in islanded mode

The proposed control strategy for controlling of parallel connected DER units in islanded mode is developed using MATLAB SIMULINK. As explained the control strategies in Chapter 3, based on that the simulation results are carried out. The comments and discussion on the output results are explained briefly. Results and discussions for the parallel connected two DERs in islanded mode are described in the following manner:

1. based on the reactance values met between the feeding point (i.e. PCC) and the load terminal point;
2. based on the droop coefficient values

For the sake of simplicity, the parameters of the DER unit-1 and 2 are taken same as in above section. The extra parameters which are used to develop an entire control model are given in Table 5.3. The compensators of the current control scheme have the transfer function,

$$k_d(s) = k_q(s) = \frac{0.2s + 4.14}{s}$$

Table 5.3: System Parameters which are Considered for Two DERs Connected in Islanded System

Parameter	Value
Feeder impedance between PCC-1 to Load bus	$(0.5 + j0.314) \Omega$
Feeder impedance between PCC-2 to Load bus	$(1.0 + j0.628) \Omega$
Feeder impedance between Load bus to Load terminal	$(1.2 + j0.8999) \Omega$
Frequency Droop (P-f droop co-efficient (m)) for DER-1	0.0005 rad/sec/KW
Voltage Droop (Q-V droop co-efficient (n)) for DER-1	0.11225 V/KVAR
Frequency Droop (P-f droop co-efficient (m)) for DER-2	0.0005 rad/sec/KW
Voltage Droop (Q-V droop co-efficient (n)) for DER-2	0.11225 V/KVAR
P_{ref} for DER-1 and DER-2 in P-f droop	1000 KW
Q_{ref} for DER-1 and DER-2 in Q-V droop	9 KVAR
f_{ref} for DER-1 and DER-2 in P-f droop	50 Hz
V_{ref} for DER-1 and DER-2 in Q-V droop	230 V_{rms}

Two types of passive loads were used to evaluate the system performance under different loading conditions.

Load 1: $P_{R1} = 40\text{KW}$, $P_{L1} = 0.5 \text{ KVAR}$, $P_{C1} = 10 \text{ KVAR}$

Load 2: $P_{R2} = 30\text{KW}$, $P_{L1} = 0 \text{ KVAR}$, $P_{C1} = 0 \text{ KVAR}$

5.4.1 Based on the reactance values met between the feeding point (i.e. PCC) and the load terminal point

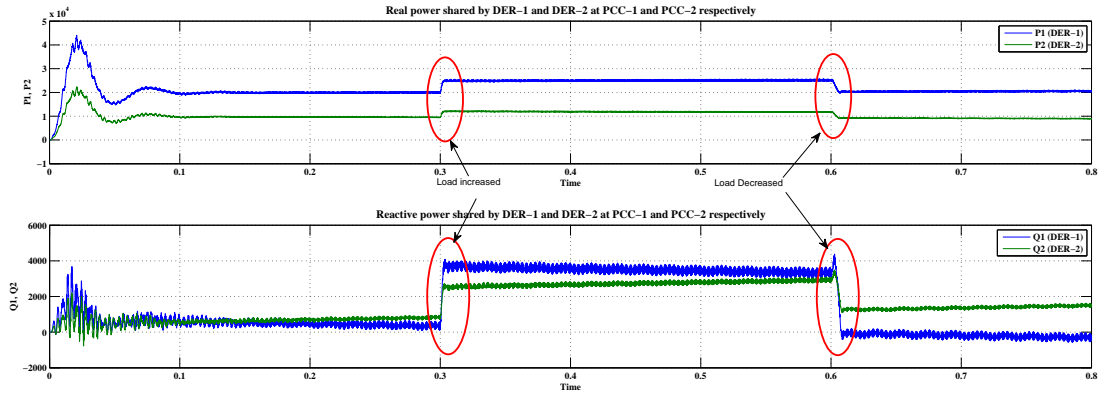


Figure 5.24: Real and Reactive power shared by DER-1 and DER-2

Suppose, DER-1 and DER-2 are connected with PCC-1 and PCC-2 respectively and they are feeding loads through a load bus-1. Here the droop coefficients are taken same for both the DERs to get the clear idea about the dependency of the sources on the reactance value, which faces between the feeding point and the load point, for sharing of the powers.

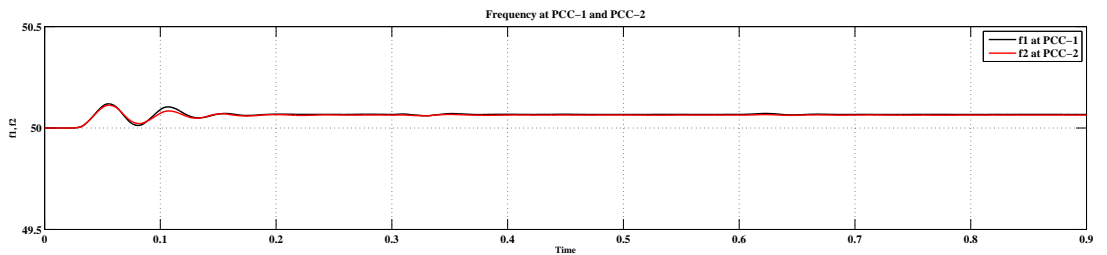


Figure 5.25: Frequency at PCC-1 and PCC-2

As we know, $\frac{P_1}{P_2} = \frac{X_2}{X_1}$. From Fig.5.24 it is clear that the power sharing by the two DERs depend on the reactance presents between the source and the load. Here DER-1

shares more power compare to the DER-2, as it is clear from Table 5.3 that the reactance having a more value between DER-2 and load terminals compare to the reactance value between DER-1 and load terminals. Fig.5.24 shows that, the real power delivered by the DER-1 is approximately double than DER-2, as the reactance between the DER-1 and load terminal having a half value compares to the reactance between the DER-2 and load terminal. Further to show the proper co-ordination of the droop controller, we have stepped up the load-1 at 0.3 sec by the amount of load-2. It is clear from the Fig.5.24 is that the stepped up in real power delivered by the DER-1 is approximately double than DER-2. In other words Fig.5.24 also reveals that as load increased the real and reactive power shared by the DERs are also got changed according to the reactance value seen between the DER terminals to the load terminals. Hence, we may say the designed droop controller work effectively. Fig.5.25 presented to show the frequency response of the DER-1 and DER-2 at PCC-1 and PCC-2 respectively and it also reveals that both DERs generate the same frequency. At start, because of transient state there is a little disturbance in frequency but it is within acceptable limits. Above discussed points indicate the beauty of the droop controller to share the powers among parallel connected DERs such that they should maintain the system stability. Therefore, the designed droop controller which is explained in Chapter 3 is giving desired performance.

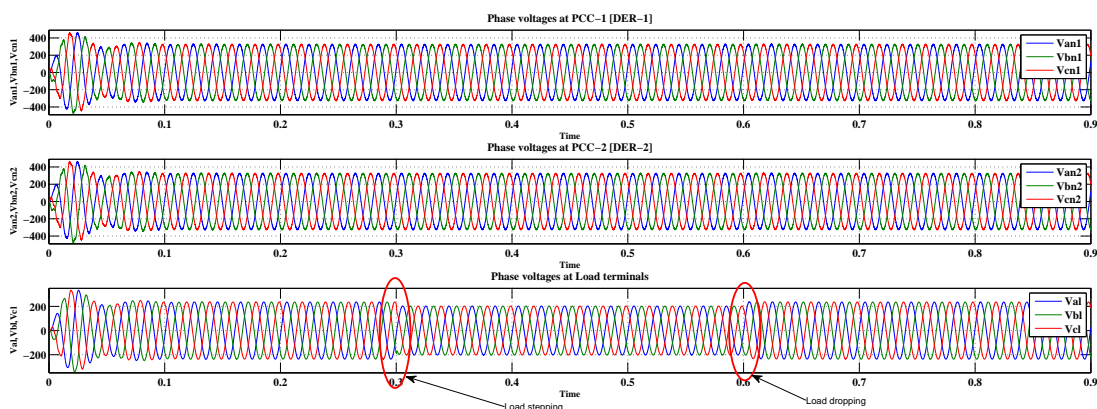


Figure 5.26: Phase voltages at PCC-1, PCC-2 and Load terminals

The accuracy of voltage and current controllers confirm from the Fig.5.26 and for

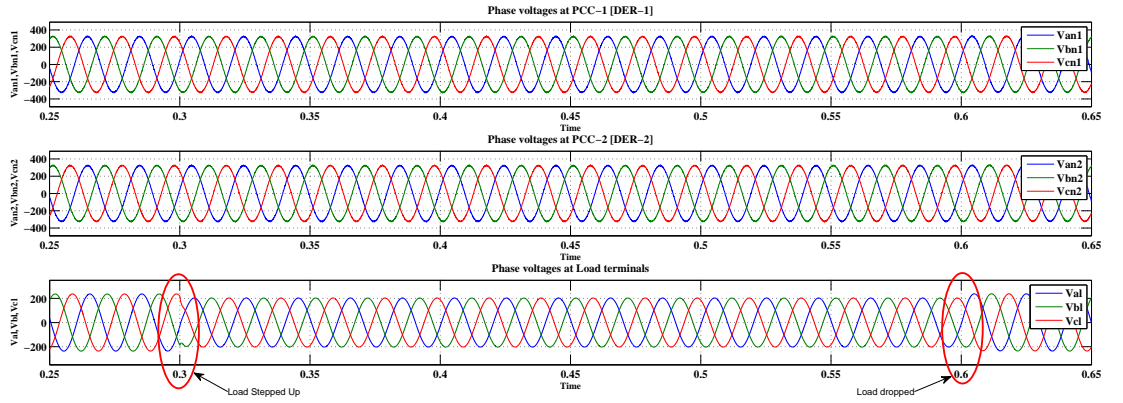


Figure 5.27: Zoomed view of phase voltages at PCC-1, PCC-2 and Load terminals

getting more clarity, its zoomed version is shown in Fig.5.27. It indicates the voltages at PCC-1 and PCC-2 are at constant peak of 326 V. To check the ability of the designed controllers for maintaining the constant voltages at PCC, the load is stepped up by adding load-2 along with load-1 at 0.4 sec. Fig.5.26 indicates, as load stepped up the load terminal voltages got reduced but the PCC voltages are maintained at peak value of 326 V. In all, shows that the designed droop controller, inner current loop controller and outer voltage loop controller are working effectively and efficiently.

5.4.2 Based on droop coefficient values

The extra parameters rather than taken in Section 1 are given in Table 5.4.

As we know, $\frac{P_1}{P_2} = \frac{m_2}{m_1}$. It is obvious from this equation, the DER having a large value of the droop coefficient, it will share less amount of power compared to the others. Here DER-2 has a larger value of droop coefficient compared to the DER-1. Therefore DER-2 will share less amount of power compared to the DER-1, which is also clear from the Fig.5.28. From Fig.5.28 it is also clear that as load is stepped up at 0.3 seconds, the real power shared by each DER also increases in proportion to their droop values. In addition of this, as load dropped at 0.6 seconds, the power shared by DERs are also reduced in same proportion to their droop values. Here at 0.3 seconds load-2 were added to load-1

Table 5.4: System Parameters which are considered for Two DERs Connected in Islanded System- Based on Droop Coefficient Values

Parameter	Value
Feeder impedance between PCC-1 to Load bus	$(0.5 + j0.314) \Omega$
Feeder impedance between PCC-2 to Load bus	$(0.5 + j0.314) \Omega$
Feeder impedance between Load bus to Load terminal	$(1.2 + j0.8999) \Omega$
Frequency Droop (P-f droop co-efficient (m_1)) for DER-1	0.00012 rad/sec/KW
Voltage Droop (Q-V droop co-efficient (n_1)) for DER-1	0.11225 V/KVAR
Frequency Droop (P-f droop co-efficient (m_2)) for DER-2	0.0002 rad/sec/KW
Voltage Droop (Q-V droop co-efficient (n_2)) for DER-2	2.1 V/KVAR
P_{ref} for DER-1 in P-f droop	820 KW
P_{ref} for DER-2 in P-f droop	500 KW
Q_{ref} for DER-1 in Q-V droop	9 KVAR
Q_{ref} for DER-2 in Q-V droop	1.6 KVAR
f_{ref} for DER-1 and DER-2 in P-f droop	50 Hz
V_{ref} for DER-1 and DER-2 in Q-V droop	230 V_{rms}

and at 0.6 seconds again load-2 was removed to show the droop controllers effectiveness. Fig.5.29 is presented to show the frequency are also maintained at same level. Here at 0.3 and 0.6 seconds, where loads are getting changed, the frequency are slightly disturbed but it is within its permissible zones of ± 0.5 Hz.

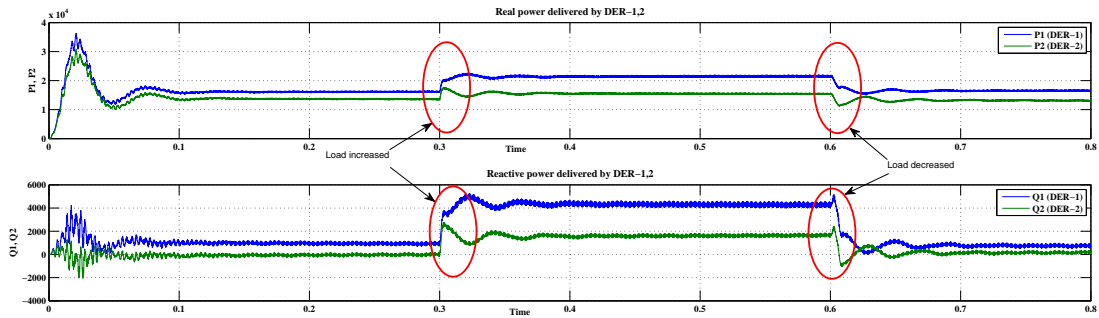


Figure 5.28: Real and Reactive power shared by DER-1 and DER-2 depends on droop setting

Fig.5.30 indicates the accuracy of inner current loop controller and outer voltage loop controller, in spite of the load changes at 0.3 sec, the PCC-1 and PCC-2 voltages are maintained at their constant level while the terminal voltages at load terminals get reduced. This indicates that our designed controllers are working properly.

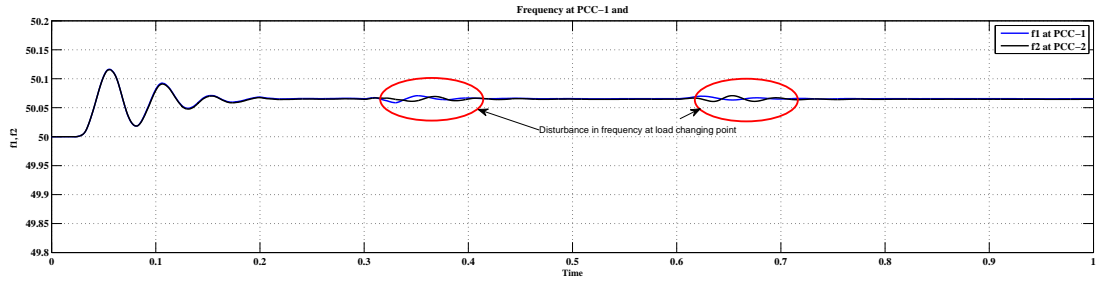


Figure 5.29: Frequency at PCC-1 and PCC-2

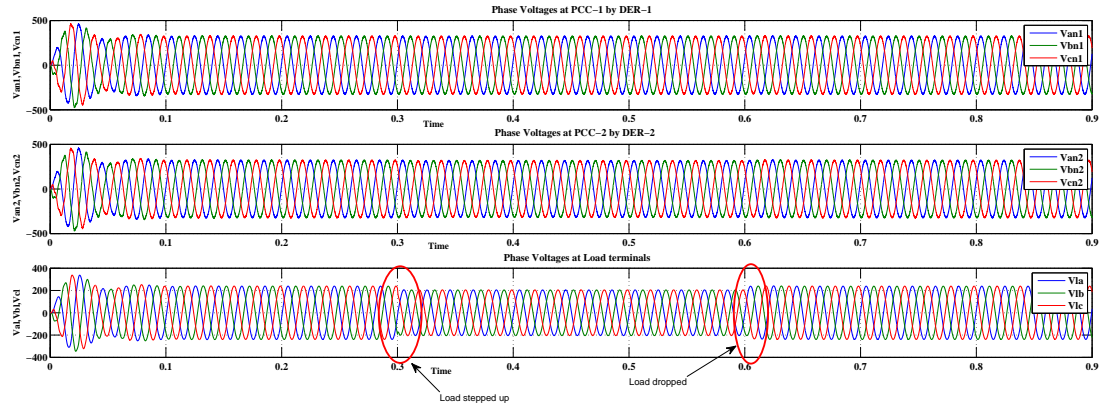


Figure 5.30: Phase voltages at PCC-1, 2 and load terminals for different droop setting

Above discussion with necessary simulation results proves that the designed controllers are working properly.

5.5 Islanded Mode of the Entire Grid

To verify the stability of the presented seven buses, eight lines microgrid as in Chapter 3, simulation study is carried out on MATLAB SIMULINK. Here, for simplicity we have assumed that all the DERs having an output voltages of $1200 V_{dc}$. Moreover if the DERs do not able to generate output voltages of $1200 V_{dc}$, the designed DC-DC closed loop boost converter with PI controller would maintain it. The system parameters considered for the entire microgrid network are mentioned in the Table 5.5.

At this point, observation of the stability for the entire network of the microgrid is

Table 5.5: System Parameters which are Considered for the Entire Microgrid in Islanded Mode

Parameter	Value
Line impedance between DG-1 and Bus-1	$(0.5 + j0.314) \Omega$
Line impedance between DG-2 and Bus-2	$(0.5 + j0.314) \Omega$
Line impedance between DG-6 and Bus-2	$(1.0 + j0.628) \Omega$
Line impedance between DG-3 and Bus-3	$(0.5 + j0.314) \Omega$
Line impedance between DG-4 and Bus-4	$(0.5 + j0.314) \Omega$
Line impedance between DG-7 and Bus-4	$(0.5 + j0.314) \Omega$
Line impedance between DG-5 and Bus-5	$(0.25 + j0.157) \Omega$
Feeder impedance between Bus-1 and Bus-2	$(1.0 + j0.5997) \Omega$
Feeder impedance between Bus-2 and Bus-3	$(1.2 + j0.8999) \Omega$
Feeder impedance between Bus-3 and Bus-6	$(1.8 + j1.1999) \Omega$
Feeder impedance between Bus-5 and Bus-6	$(1.0 + j0.5999) \Omega$
Feeder impedance between Bus-4 and Bus-5	$(1.2 + j0.9313) \Omega$
Feeder impedance between Bus-4 and Bus-7	$(1.5 + j0.9999) \Omega$
Feeder impedance between Bus-1 and Bus-7	$(1.5 + j0.9999) \Omega$
Feeder impedance between Bus-3 and Bus-4	$(3.6 + j2.3979) \Omega$
Load at Bus-3	$P_R = 20 \text{ KW}$
Load at Bus-6	$P_R = 30 \text{ KW}, P_L = 0.1 \text{ KVAR},$ $P_C = 10 \text{ KVAR}$
Load-1 and Load-2 at Bus-7	$P_{R1} = 40 \text{ KW}, P_{L1} = 0.5 \text{ KVAR},$ $P_{C1} = 10 \text{ KVAR}$ and $P_{R2} = 30 \text{ KW}$
P-f droop co-efficient (m) for all DERs	$0.0005 \text{ rad/sec/KW}$
Q-V droop co-efficient (n) for all DERs	0.11225 V/KVAR
P_{ref} for all DERs in P-f droop	1000 KW
Q_{ref} for all DERs in Q-V droop	9 KVAR
f_{ref} for all DERs in P-f droop	50 Hz
V_{ref} for all DERs in Q-V droop	$230 V_{rms}$

the main concern. Here stability means plug and play operation is possible without any kind of disturbances in the system, i.e., after removing or introducing a certain amount of loads or microsources, system should not get collapsed. For the sake of simplicity, the droop coefficient values are taken same for all the DERs as we did in above section. Practically, the droop settings are different for each source but here we are considering the power sharing by the each source depends on the reactance seen between its terminals to the feeding point. Thus, for the sake of convenience if we take the droop coefficient values same for all the sources as discussed in above section, it does not create much

difference with the system performance, so our consideration is also valid to study the islanded mode of the entire microgrid.

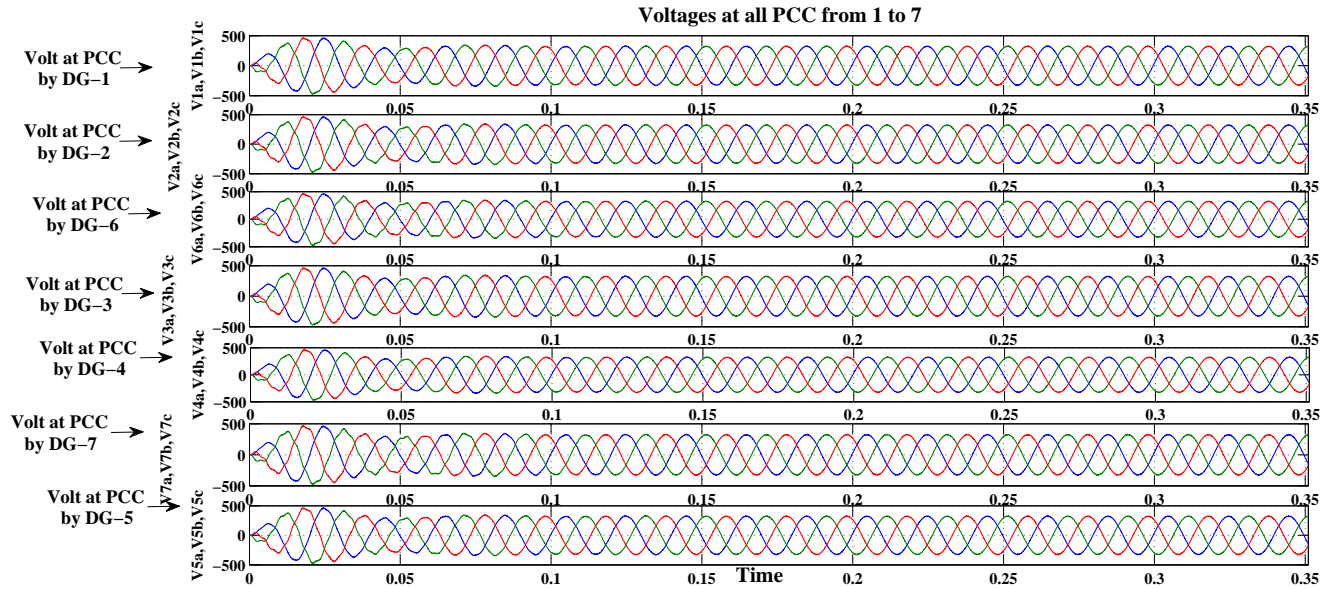


Figure 5.31: Phase voltages at terminals of DG-1 to DG-7 in the islanded microgrid network

To maintain the stability of the system, the terminal voltage and frequency values of each source should be retained at constant value. Fig.5.31 indicates the terminal voltages of all DERs at their respective PCCs are maintained at their reference values, which are given by the droop controllers. From Fig.5.33 it is clear that the frequency at each PCC are also preserved at constant value. So stability of the system may be well-maintained and system is not going to be collapsed even by sudden application or removal of large loads. This statement also proves from the drawn simulation results as shown in Fig.5.31 and Fig.5.32, as at 0.3 sec 30 KW loads are applied at bus-7, so voltages at load buses are changed but the PCC voltages are sustained at their constant value. As shown in Fig.4.20 of Chapter 4, DG-2 and DG-6 are connected in parallel at bus-2 and DG-4 and DG-7 are also connected in parallel at bus-4. From the drawn simulation results as shown in Fig.5.31, it is clear that the voltage waveforms at bus-2 and bus-4 are purely sinusoidal having a magnitude of $230 V_{rms}$ and 50 Hz frequency. It indicates that the system had maintained its stability and parallel operation of multi sources at one bus is also possible.

This shows the beauty of the designed voltage- current controller for islanded mode of operation of the entire microgrid.

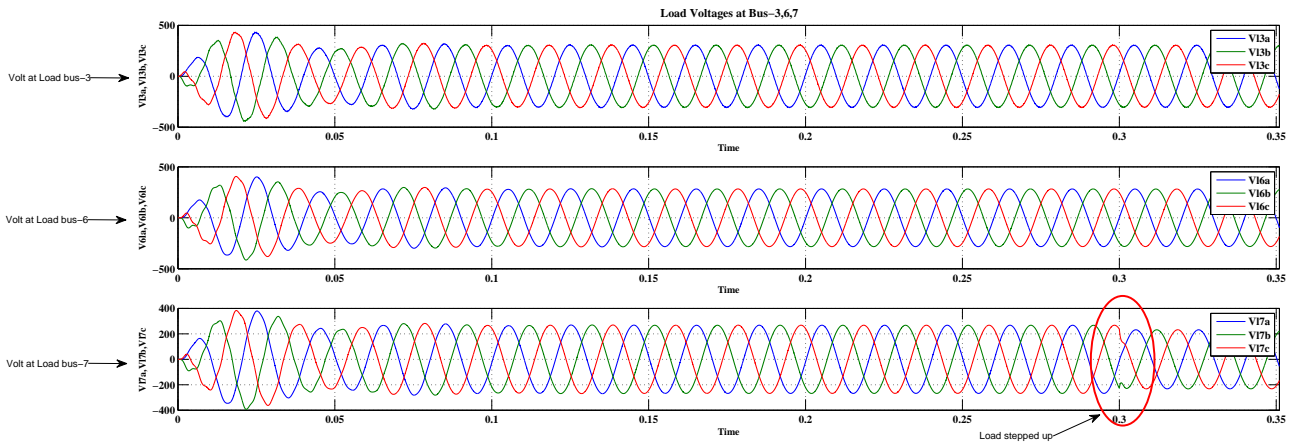


Figure 5.32: Load voltages at Bus-3, Bus-6 and Bus-7 in the islanded microgrid network

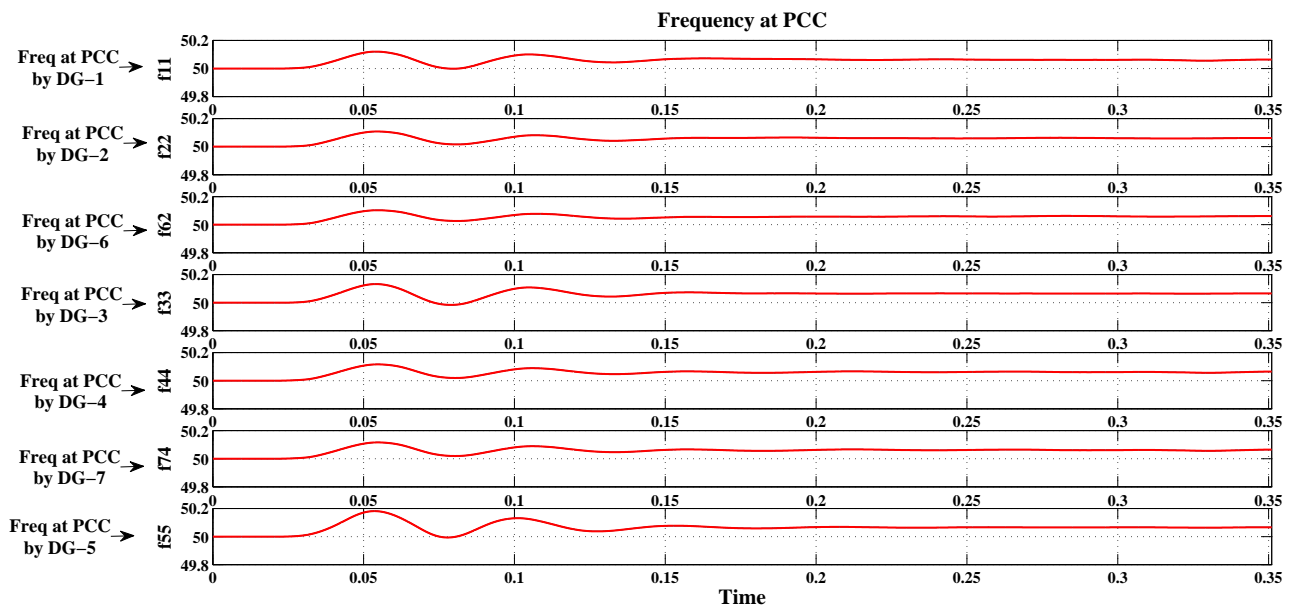


Figure 5.33: Frequency at terminals of DG-1 to DG-7 in the microgrid network

Fig.5.34 are presented to show the ability of the sources to share the real powers according to their ratings. Fig.5.34 shows that the load sharing by all the DERs were very efficiently, hence system would maintain its stability. For maintaining the grid stability

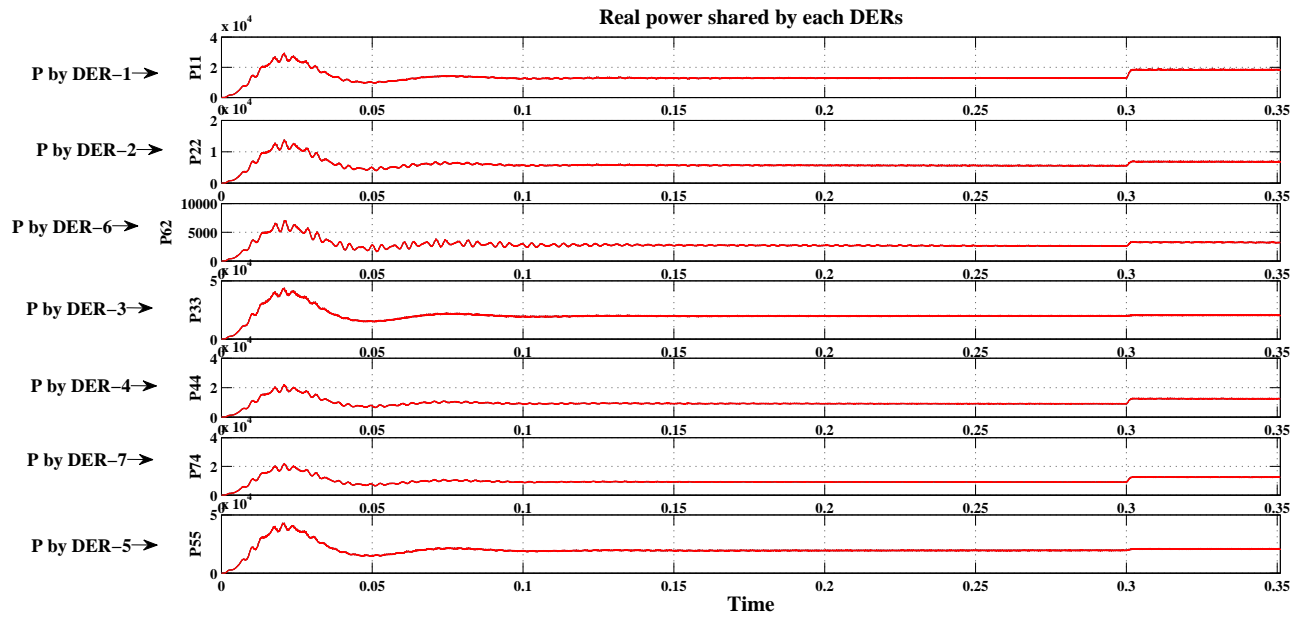


Figure 5.34: Real power dispatched by all DGs in the microgrid network

in islanded microgrid, the primary goal of the controllers is that, each microsource should maintain their terminal voltages and frequency at constant level and all the local loads need to be supplied without exceeding source ratings. Fig.5.35 is presented to show the THDs level of all DGs and all are within permissible limits according to the standards. From the drawn simulation results it is clear that the designed droop controllers, VSI based voltage and current controllers are working very effectively and efficiently. Hence, the system well- preserved its stability.

5.6 Control of Single DER Unit in Grid-Connected Mode

The proposed control strategy for control of single DER unit in grid connected mode is developed using MATLAB SIMULINK. As explained the control strategy in Chapter 4, based on that simulation results are carried out. The comments and discussions on the output results are explained in brief. The system parameters considered for simulation are given in Table 6 below.

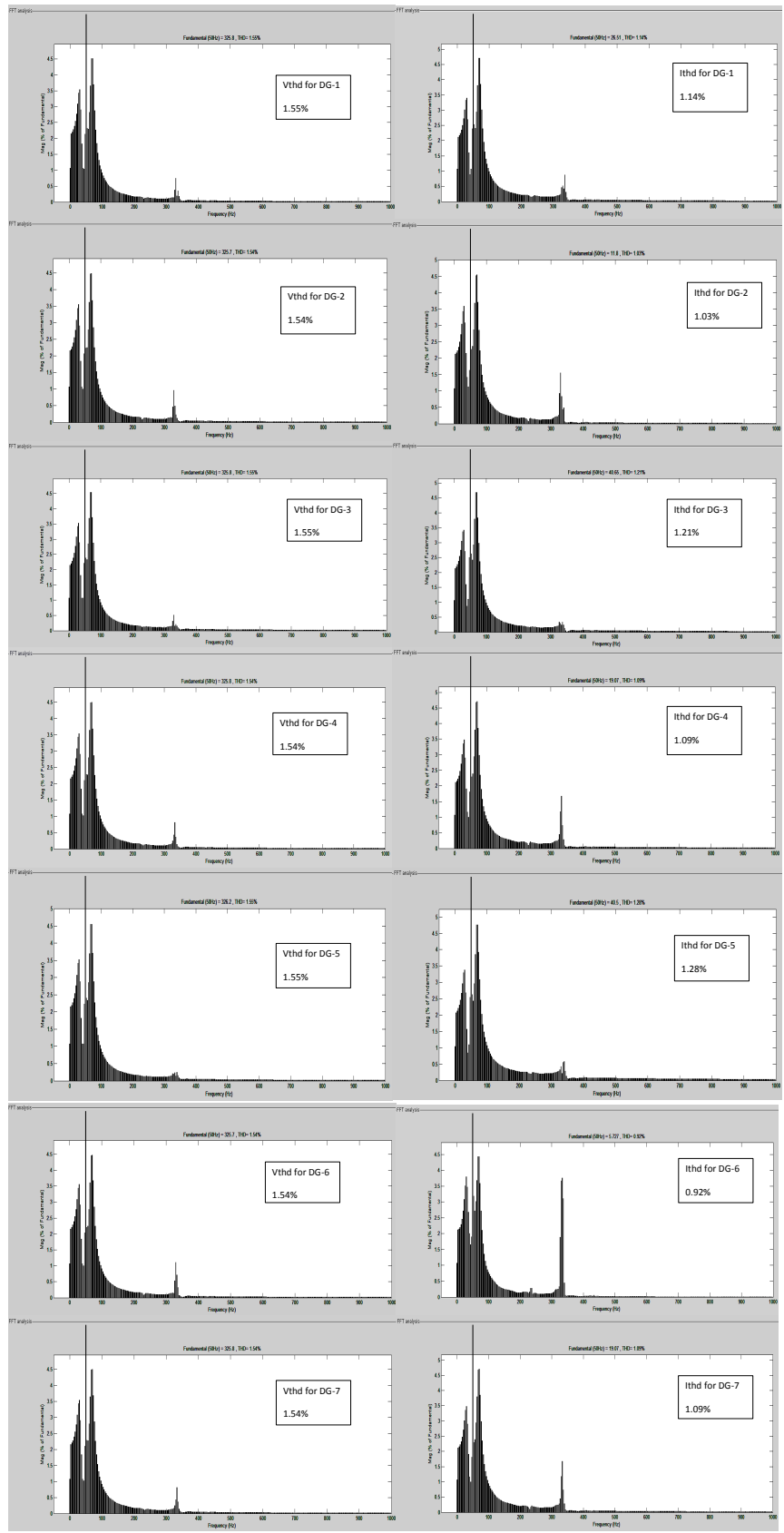


Figure 5.35: FFT analysis for THDs of all DGs in the islanded microgrid network

Table 5.6: System Parameters which are Considered for Single DER Unit in Grid-Connected Mode

Parameter	Value
Nominal Grid voltage	400 V_{rms}
Grid frequency	50 Hz
Coupling impedance	$(0.01 + j0.0)\Omega$
DC bus voltage	1200 V
Filter Inductor (L)	0.1 mH
Filter capacitor (C)	2.5 mF
Filter Resistor (R)	2.07 $m\Omega$
Switching Frequency	1.8 KHZ
d-axis current loop controller ($K_d(s)$) proportional gain (K_p)	0.2
d-axis current loop controller ($K_d(s)$) integral gain (K_i)	4.14
q-axis current loop controller ($K_q(s)$) proportional gain (K_p)	0.2
q-axis current loop controller ($K_q(s)$) integral gain (K_i)	4.14

Results and discussions on the grid connected system are described in the following manner.

- Control of active power and reactive power for a given fixed reference value.
- Sharing of active and reactive power for a different reference values.

5.6.1 Control of active and reactive powers for a given fixed reference value

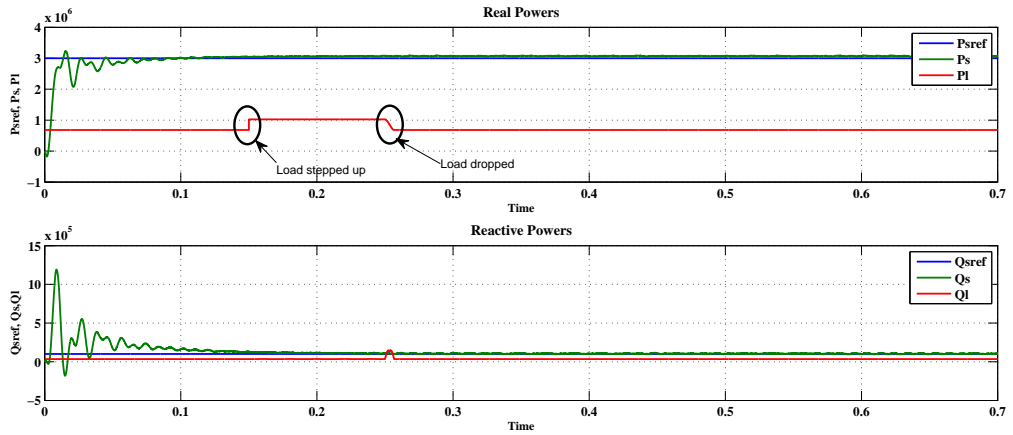


Figure 5.36: Control of active and reactive powers for a given fixed reference value

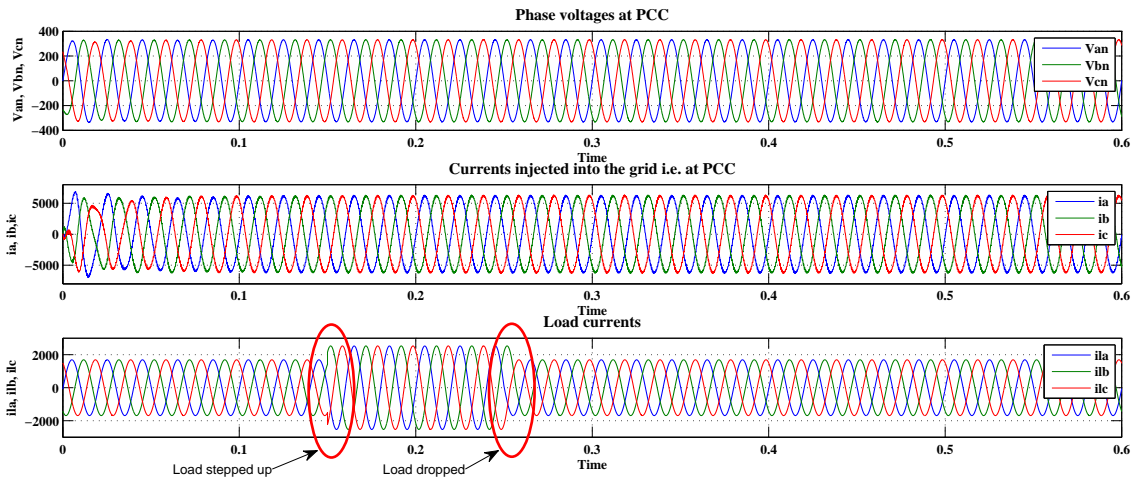


Figure 5.37: Load voltages, grid injected current and load currents as load Stepped up at 0.15 second and again step down at 0.25 second

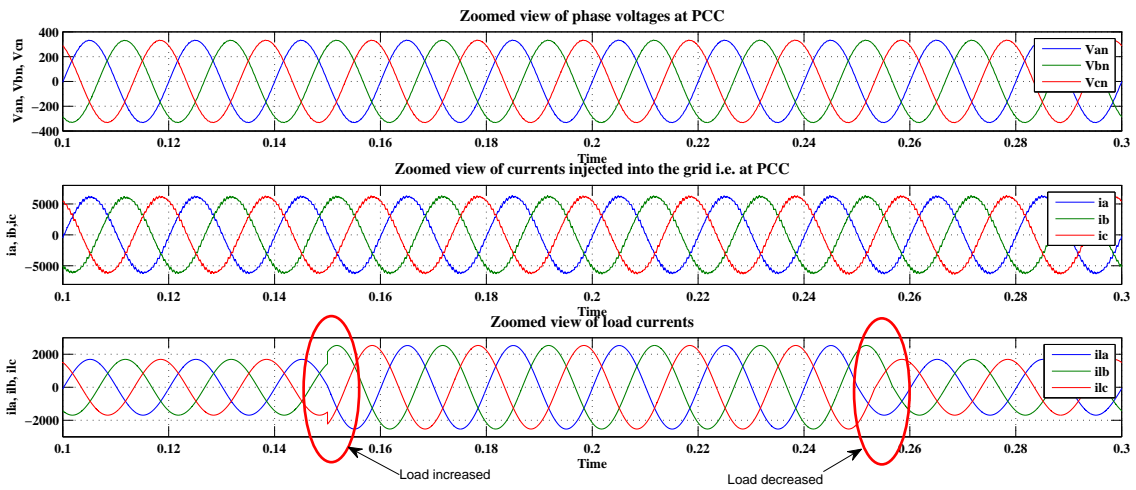


Figure 5.38: Zoomed view of load voltages, grid injected current, load currents as load stepped up at 0.15 second and again step down at 0.25 second

Fig.5.36 shows the sharing of active and reactive powers between the inverter and the grid according to the specified values of the controller. The fixed load gets switched to another higher value but the injection of active and reactive are same as the reference values to the controllers. As shown in Fig.5.36 P_{sref} is set to supply 3000 KW and Q_{sref} is set to supply 100 KVAR, so it is clearly visible that inverter supply the same amount of power to the grid, even if, after 0.15 seconds load is stepped up and again after 0.25

seconds load is dropped but inverter keeps on supplying the same amount of power.

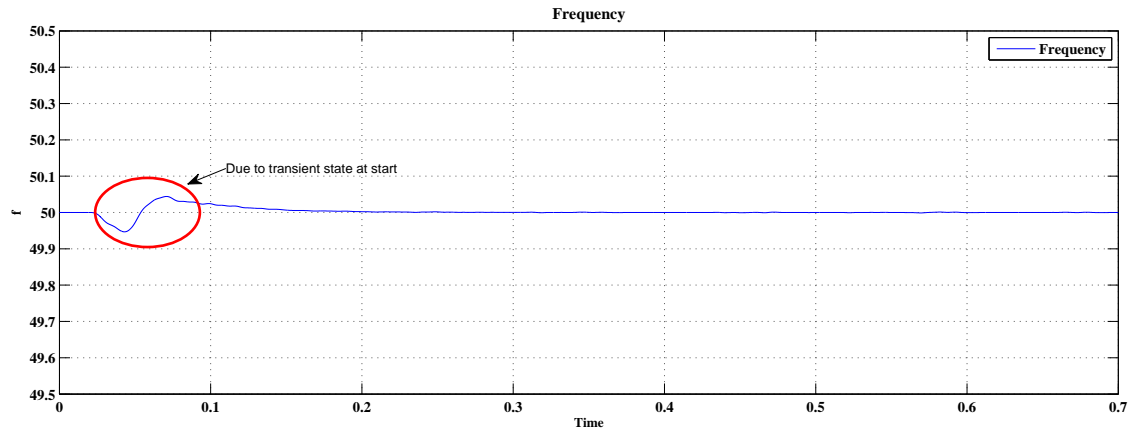


Figure 5.39: Frequency at PCC as load stepped up at 0.15 second and again step down at 0.25 second

As per Fig.5.37 and Fig.5.39 we can observe that, as VSI is connected to the utility grid, the voltages, frequency and the current injected by the DERs at PCC are not affected by the change in the load. So, they remain at constant values but the load currents go up as load changed to the higher values. Graphs are shown for the values $P_1= 1000$ KW and $Q_1= 50$ KVAR stepped up to $P_2= 1500$ KW and $Q_2= 51$ KVAR. For getting more clarity of the above said zoomed view of Fig.37 is shown in Fig.5.38.

5.6.2 Sharing of active and reactive powers for a different reference values

Fig.5.40 shows the injected active and reactive powers from the source to the utility grid according to the specified values to the controller. The main aim of the grid connected controller is to share proper amount of the active and reactive powers to the utility grid. As we have seen in the previous section, the values of the load is predefined so that we can fix our reference values for the active and reactive powers to the controllers, which is not there in practical case. The active power controller reference (P_{sref}) is set to 3000 KW and reactive power controller value (Q_{sref}) is set to 100 KVAR up to 0.2 seconds after 0.2 seconds, the value of (P_{sref}) got changed to 4000 KW up to 0.4 sec, finally after 0.4

sec, the value of (P_{sref}) got changed to 6000 KW. The results are shown in Fig.5.40. It shows that controllers are working properly for the given reference values of the active and reactive powers. In other words, the outputs of the inverter, P_s and Q_s , are exactly track the controller reference inputs P_{sref} and Q_{sref} . Fig.5.41 indicates as the (P_{sref}) changes there is a little distortion in a frequency but it is within permissible range of $\pm 0.5Hz$. Finally, Fig.42 shows that the THD level for voltages at PCC and currents injected by the DG into the utility grid. It shows that both are within acceptable limits. These types of controllers have some limitations such as forecasting of network load is important for proper load sharing among the sources and the utility grid. As a result, the stability of the system should be maintained, which has already been explained in Chapter 3.

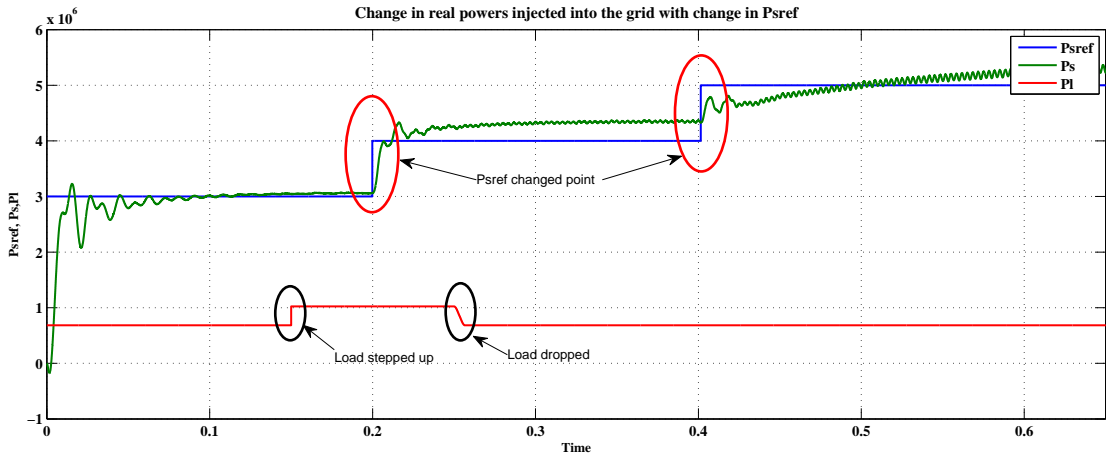


Figure 5.40: Reference active power switched at 0.2 and 0.4 seconds

5.6.3 Control of two DER units in grid-connected mode

As we know, the parallel operation of the DERs enhances the system performance, stability and so on. Here, parallel operation of the DERs is not as much important as in islanded mode, because the DER can inject only that much amount of power which is given to its controller as a reference set points for real and reactive power flow. So, for this mode of operation the main concern is whether the parallel connected DERs would be able to maintain the system stability or not, by proper sharing of the real and reactive

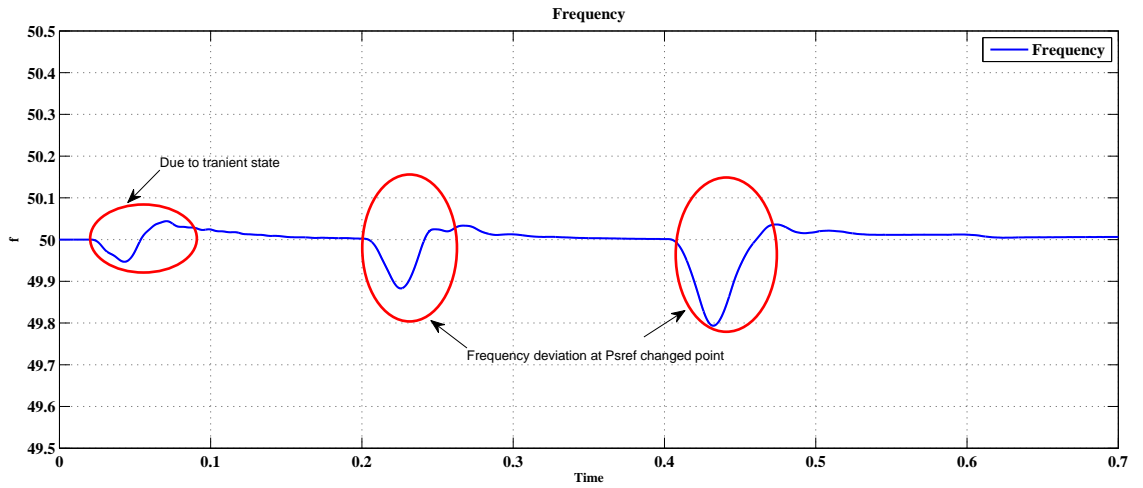


Figure 5.41: Frequency plot for change in reference active power

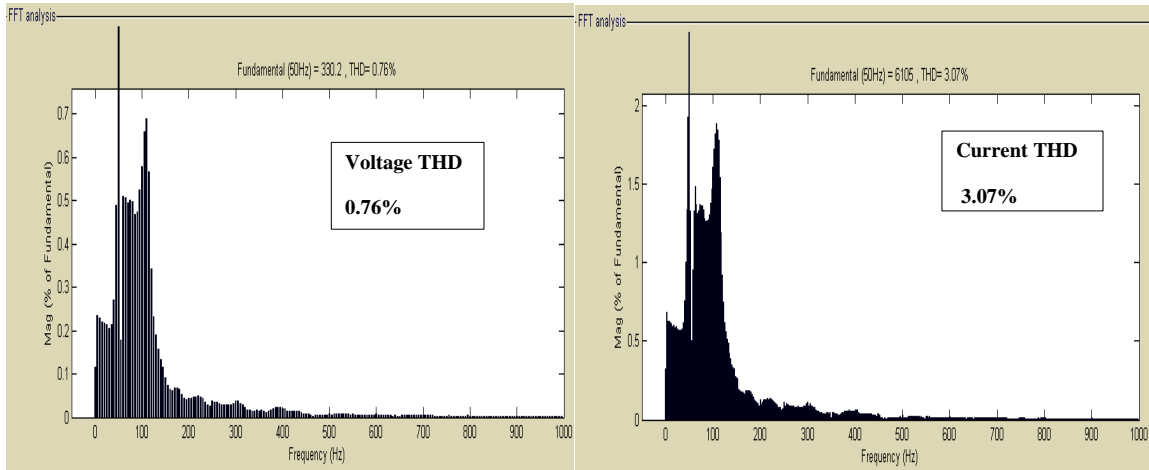


Figure 5.42: Voltage and current THDs for single grid connected DER unit

powers. In grid connected mode no need for bothering about the amount of power sharing by each DER, because the amount of power sharing is decided by the set reference point to the controller. The simulation results are drawn and shown in Fig.5.43. It shows that system maintaining its stability for multisource connected in parallel and feeding to the grid.

Here, DER-1 is set to generate $P_{sref1} = 4.5$ MW and $Q_{sref1} = 100$ KVAR and DER-2 is set to generate $P_{sref2} = 3$ MW and $Q_{sref2} = 300$ KVAR. As shown in Fig.5.45, the real power reference set points for both the DERs are changed at 0.35 seconds. The reference

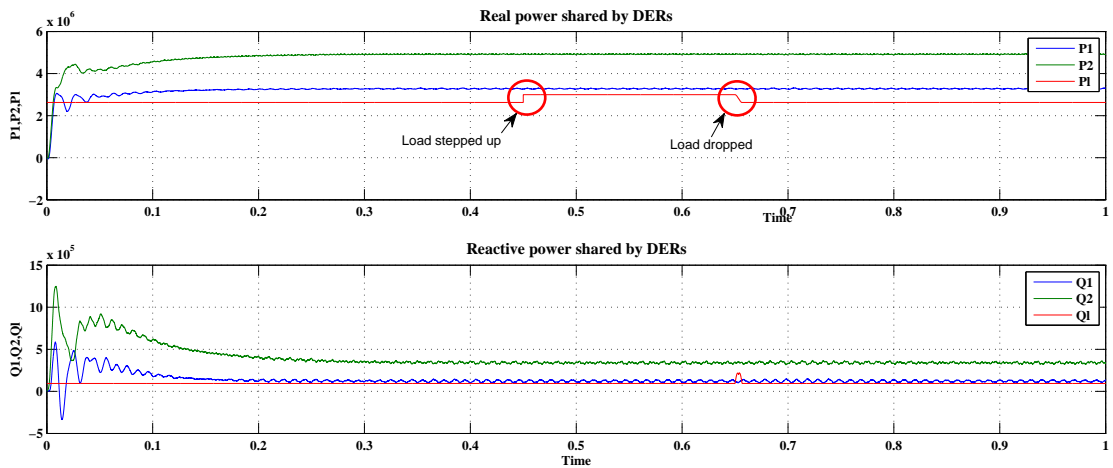


Figure 5.43: Real power shared by two DERs in grid connected mode

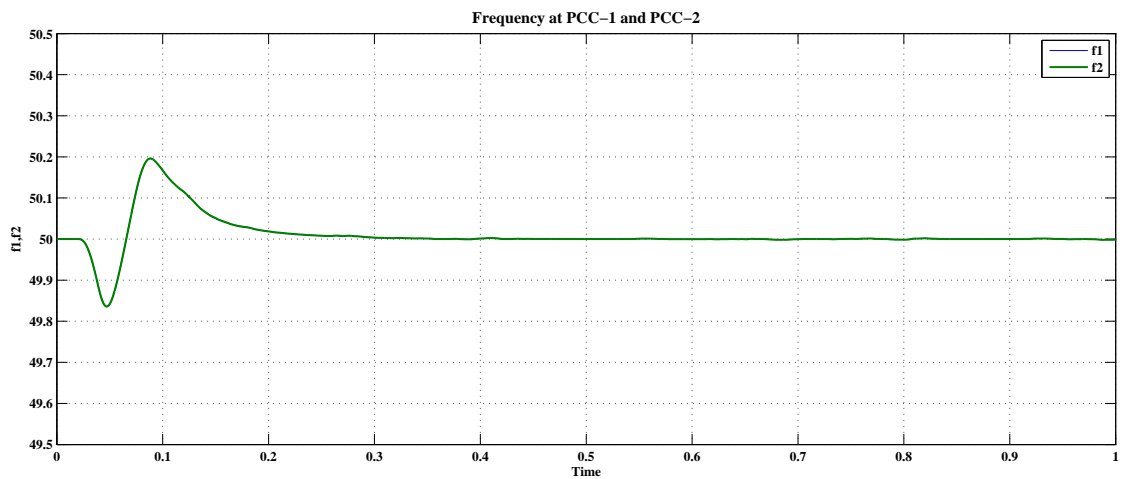


Figure 5.44: Frequency plot for two DERs in grid connected mode

set point for the DER-1 is change to $P_{sref} = 3$ MW and for DER-2 is changed to $P_{sref} = 4.5$ MW. The drawn simulation result shows that the designed controller works correctly as an actual output of the DER is exactly track to the reference set point. It is also clear from the Fig.5.45 is that the load of $P_1 = 6$ MW and $Q_1 = 250$ KVAR is changed to a load of $P_2 = 7$ MW and $Q_2 = 750$ KVAR at 0.35 seconds. Although the load changes at 0.35 and 0.45 seconds, P_{sref1} and P_{sref2} are not changed, it shows the beauty of the designed controller.

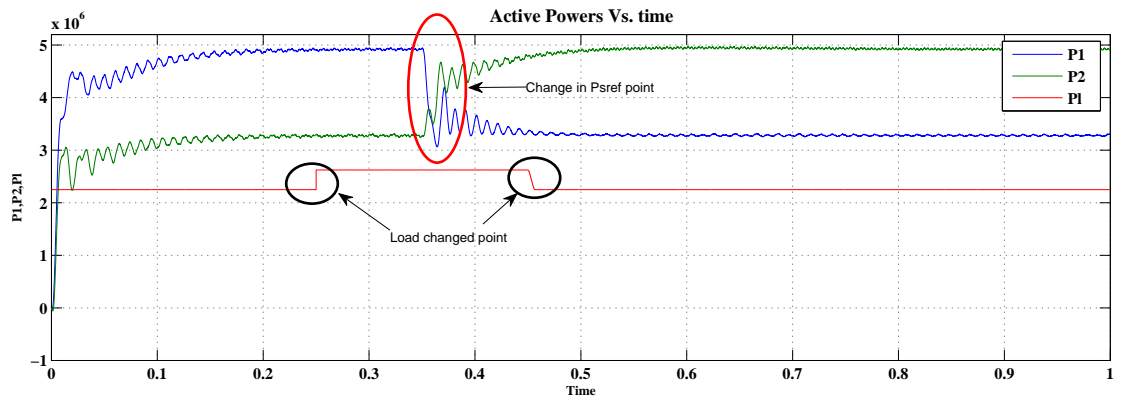


Figure 5.45: Real power shared by two DERs for changing in reference active power at 0.35 seconds

5.6.4 Control of grid-connected microgrid

To verify the stability of the presented seven buses, eight lines grid connected microgrid as in Chapter 3, simulation study is carried out on MATLAB SIMULINK. The system parameters such as line impedances, DC bus voltages, switching frequency, filter parameters, load values and so on, are taken same as in islanded grid and the value for current controller are taken same as mentioned in Table 6. The remaining parameters are given in Table 7.

In grid connected mode of operation the primary condition for the stability of the grid network is, the proper sharing of the real and reactive powers between the utility grid and microgrid. So, the central controller has to give the correct reference power set points to all microsources. Hence, for doing this task, proper forecasting of the load is required. To follow this, real power reference is given to each microsource as shown in Table 7. Fig.5.46 proves that, the real power dispatched by all DGs are according to their reference set points to the respective controller of DGs.

Fig.5.47 and Fig.5.48 show that the PCC voltages and frequencies are tightly regulated

Table 5.7: System Parameters which are Considered in Grid-Connected System

Parameter	Value
P_{sref} for DG-1	3.0 MW
Q_{sref} for DG-1	100 KVAR
P_{sref} for DG-2	2.0 MW
Q_{sref} for DG-2	200 KVAR
P_{sref} for DG-3	1.0 MW
Q_{sref} for DG-3	50 KVAR
P_{sref} for DG-4	6.0 MW
Q_{sref} for DG-4	400 KVAR
P_{sref} for DG-5	2.5 MW
Q_{sref} for DG-5	150 KVAR
P_{sref} for DG-6	4 MW
Q_{sref} for DG-6	300 KVAR
P_{sref} for DG-7	5 MW
Q_{sref} for DG-7	400 KVAR

by the utility grid and all voltage waveforms having a shape of sinusoidal nature with a 50 Hz frequency. It also proves that the system maintains its stability, i.e., it does not get collapsed. Fig.5.49 is presented to show the THDs level of all DGs and all are within permissible limits according to the standards [except DG-7, but it is not difficult to reduce it within allowable range]. The above discussion and drawn simulation results prove that the designed controllers for real and reactive power flow, VSI based current controller works efficiently and maintain the stability of the entire microgrid in the grid connected mode of operation.

5.7 Switching from Islanded to Grid-Connected Mode and Vice Versa

As we have discussed in Section 4.3 of Chapter 4, according to the system requirement central controller (CC) gives command to the islanded mode controllers (IMC) or to the grid-connected mode controllers (GMC) to operate microgrid in islanded mode or grid connected mode respectively.

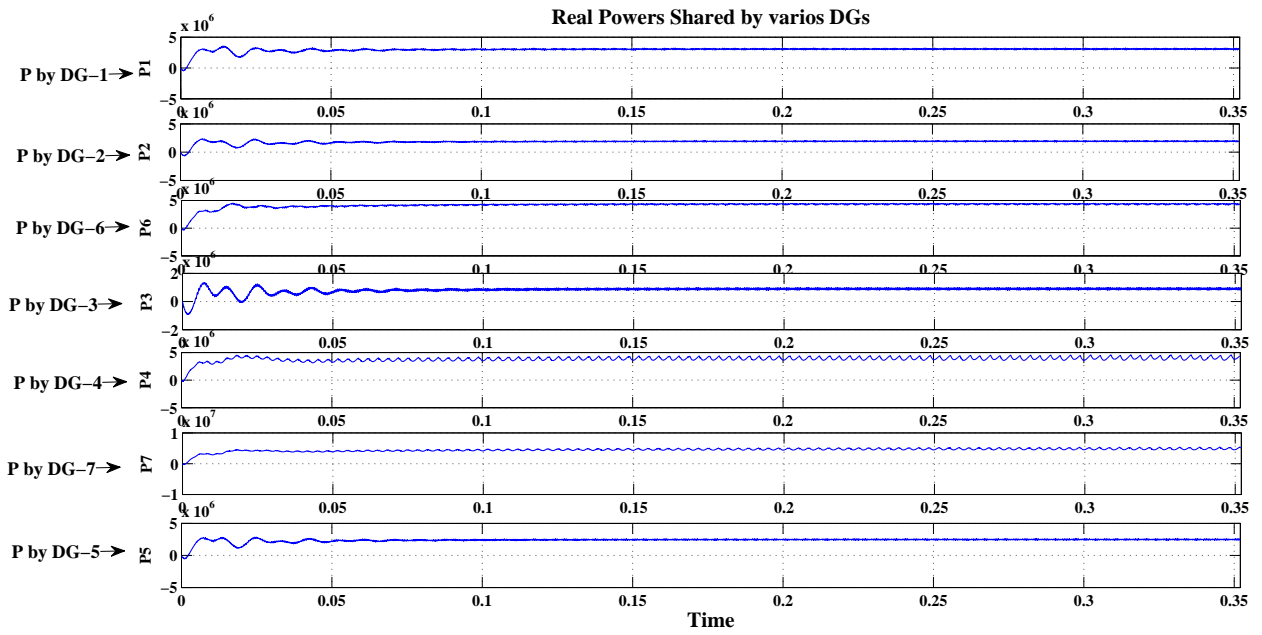


Figure 5.46: Real power shared by all DGs connected in grid connected mode of the entire microgrid

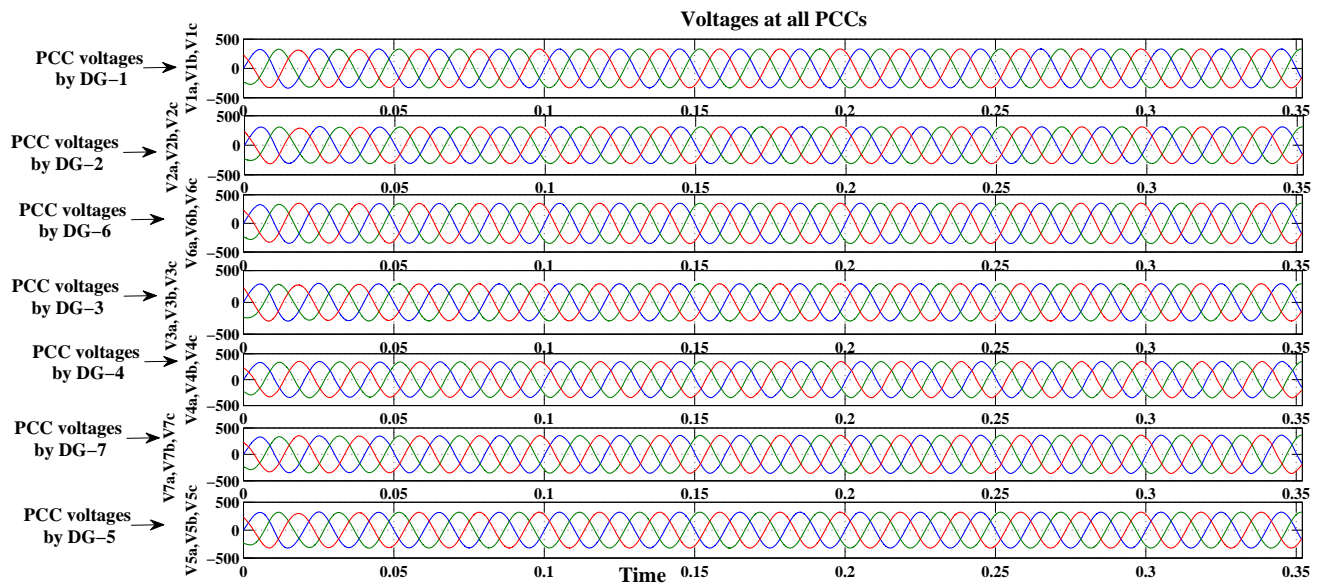


Figure 5.47: Phase voltages at terminals of all DGs in grid connected mode of the entire microgrid

The most challenging task in microgrid is to switch it from one operating mode to other operating mode. The entire seven buses and eight lines microgrid network is simu-

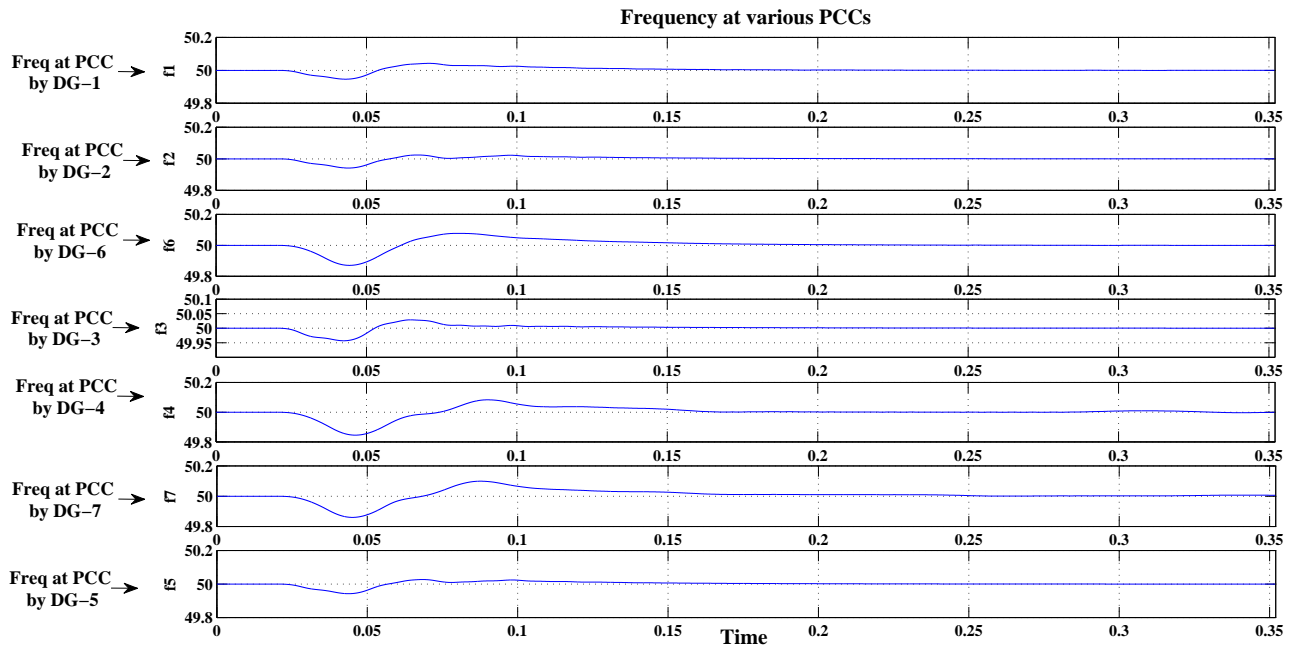


Figure 5.48: Frequency at each PCC in grid connected mode of the entire microgrid

lated on MATLAB/SIMULINK and results are drawn. All the parameter values are same as taken in islanded and grid connected networks.

Fig.5.50 indicates when the microgrid is switched from the islanded to grid connected mode at 0.2 sec, there was a small disturbance occurred for a duration of less than few milliseconds. To get more clarity in the waveforms at switching instant its zoomed view at switching instant of 0.2 seconds is presented in Fig.5.51. Fig.5.52 shows the zoomed view of DG-1 terminal voltages at switching instant of 0.2 seconds. So based on this context, we may say that the switching from islanded to grid connected mode is achieved without any kind of disturbances. Fig.5.53 shows the frequencies are well- within acceptable limits at all PCCs and Fig.5.54 shows the real power dispatched by all microsources. Simulation results proves that the designed controllers are working satisfactory for islanded to grid connected mode of operation of the entire microgrid network.

Fig.5.55 indicates when the microgrid is switched from the grid connected to islanded mode, a sharp impulsive transient has occurred. Its zoomed view is shown in Fig.5.56. It

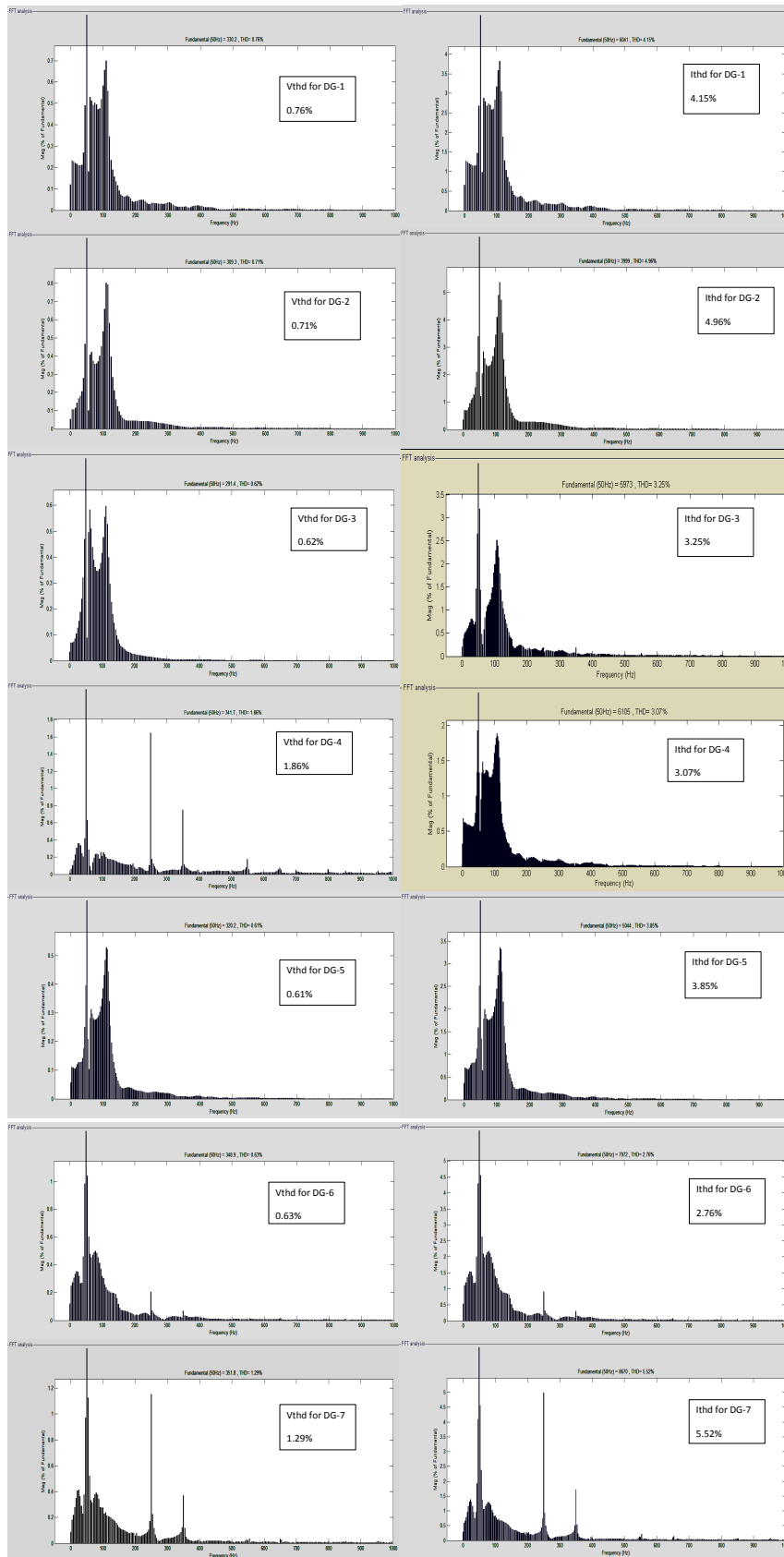


Figure 5.49: FFT analysis for THDs of all DGs in the grid connected mode of microgrid network

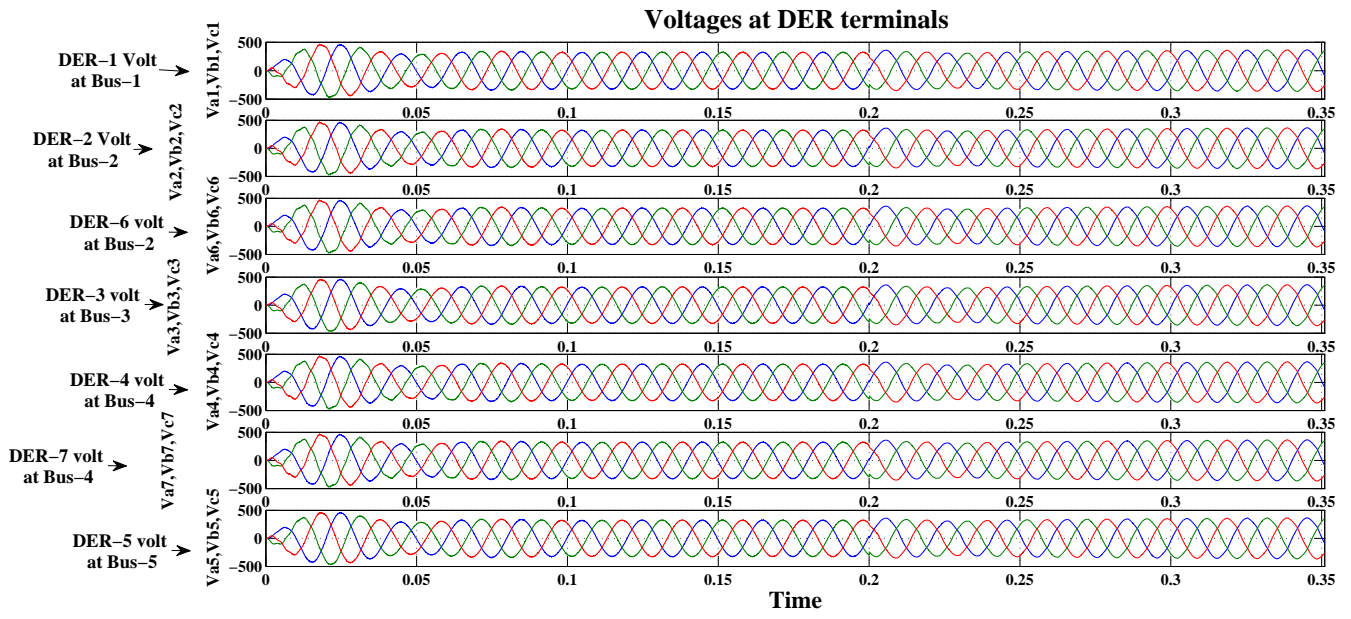


Figure 5.50: Phase voltages at PCCs while switching from islanded to grid connected mode of microgrid at 0.2 seconds

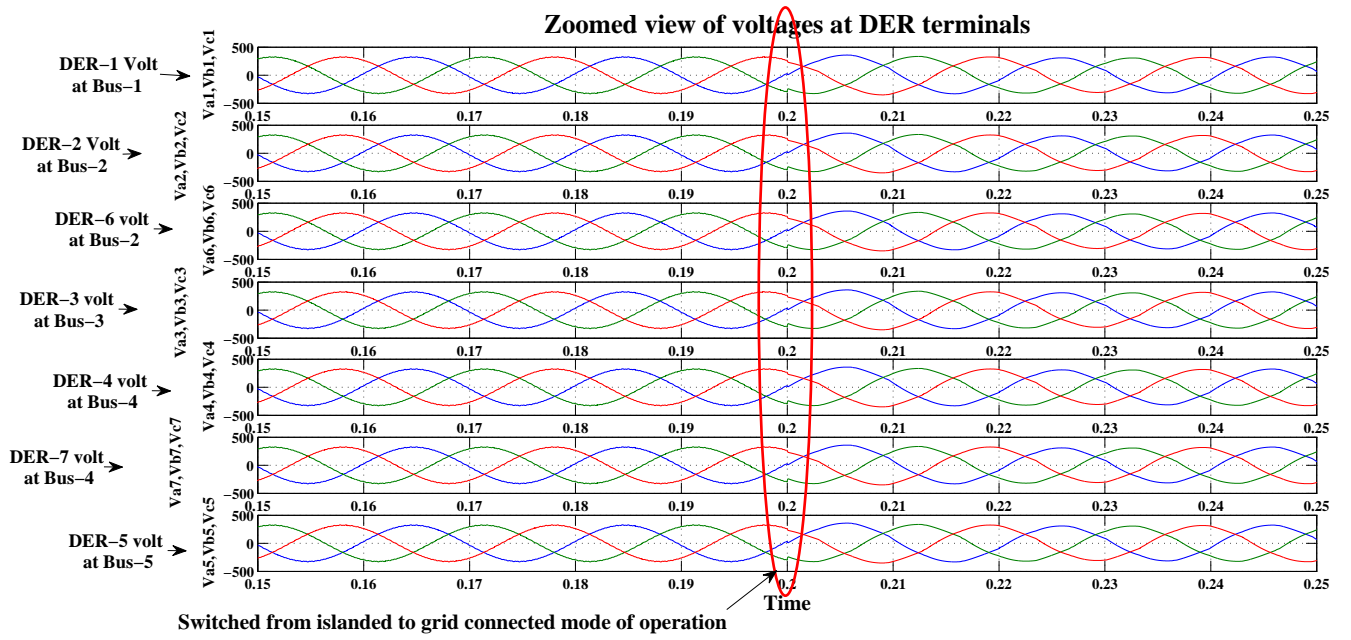


Figure 5.51: Zoomed view of phase voltages at PCCs while switching from islanded to grid connected mode of microgrid at 0.2 seconds

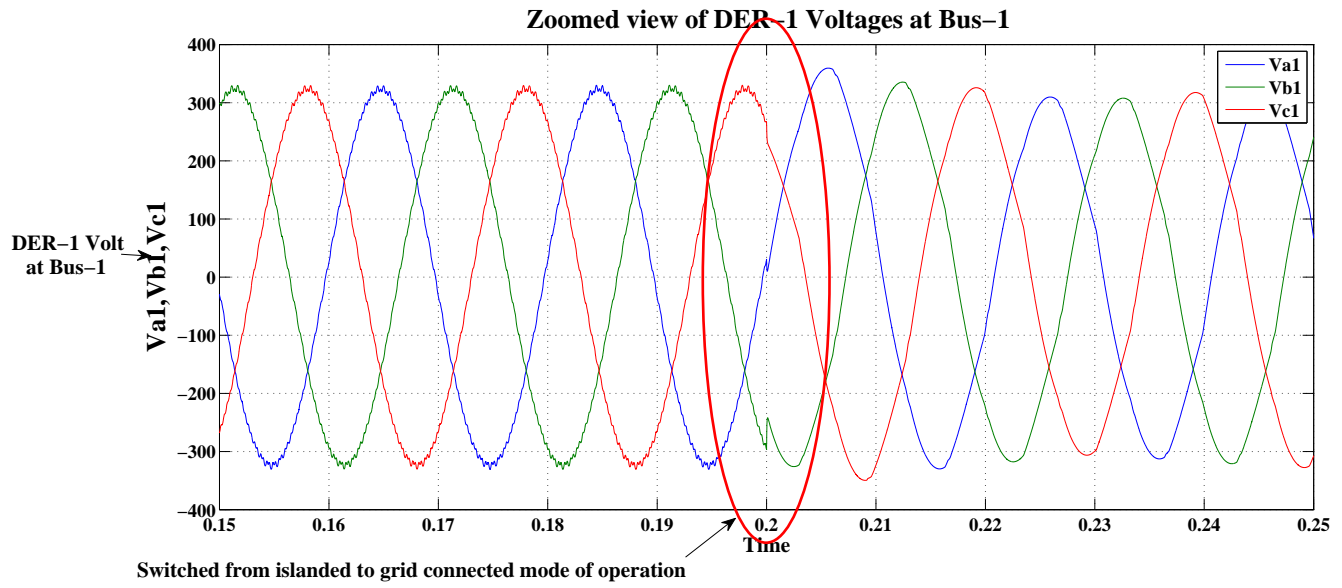


Figure 5.52: Zoomed view of phase voltages of DG-1 terminals during switching from islanded to grid connected mode at 0.2 seconds

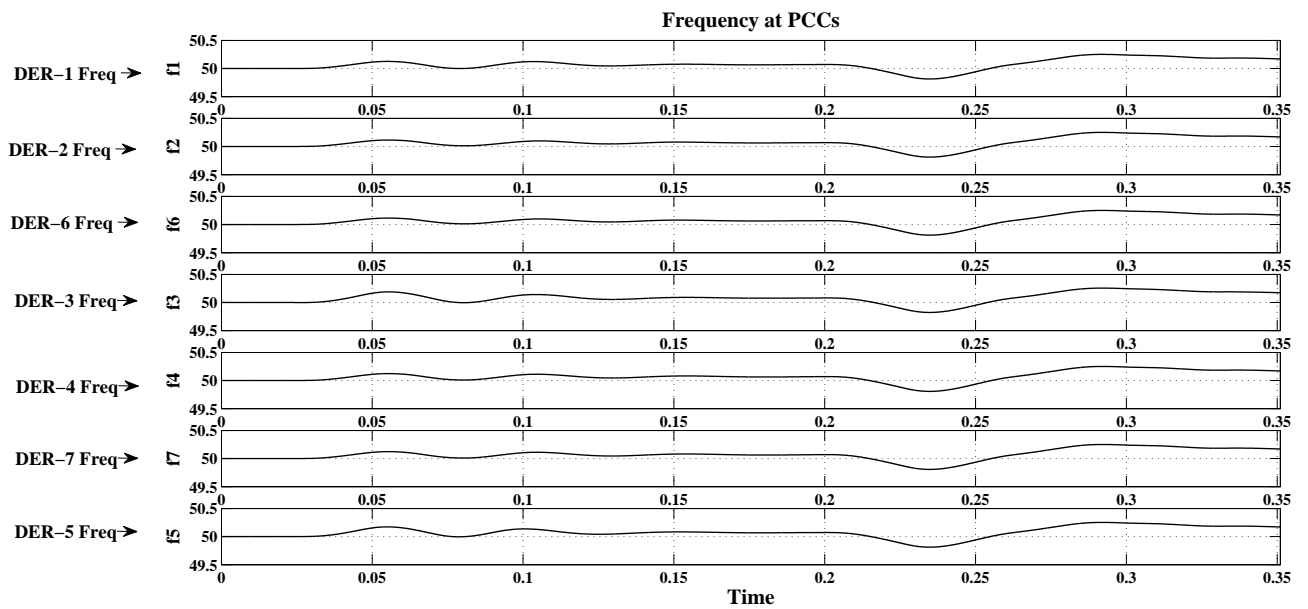


Figure 5.53: Frequencies of all DGs

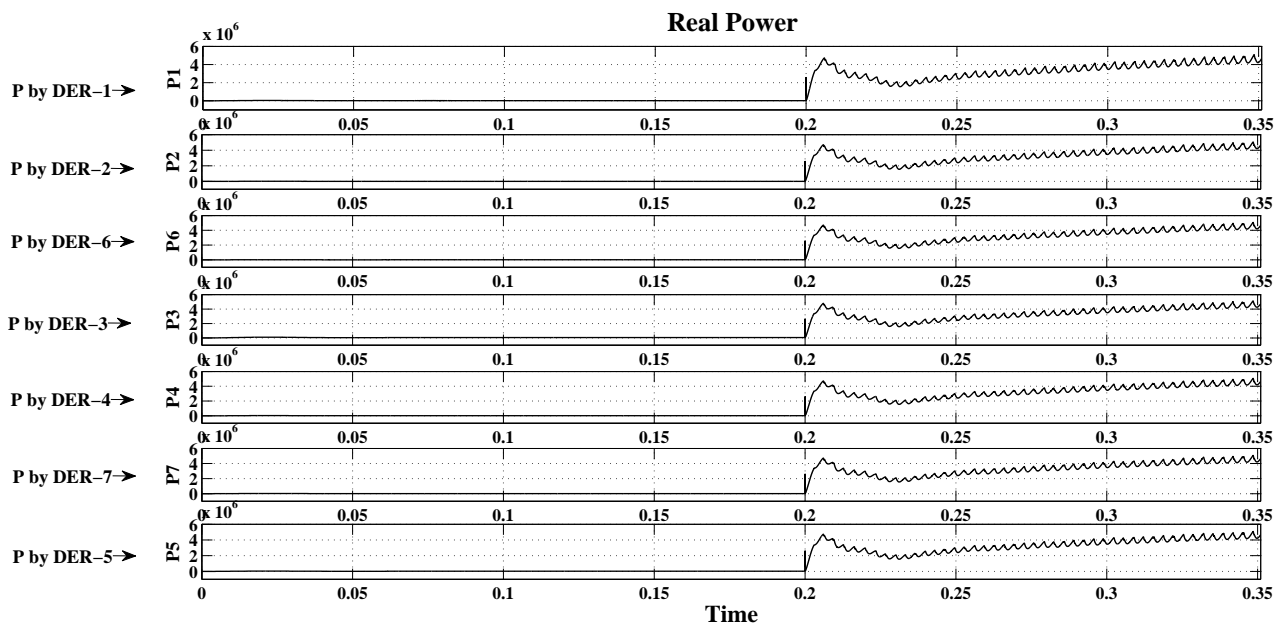


Figure 5.54: Real power dispatched by all DGs during mode changing from islanded to grid connected mode

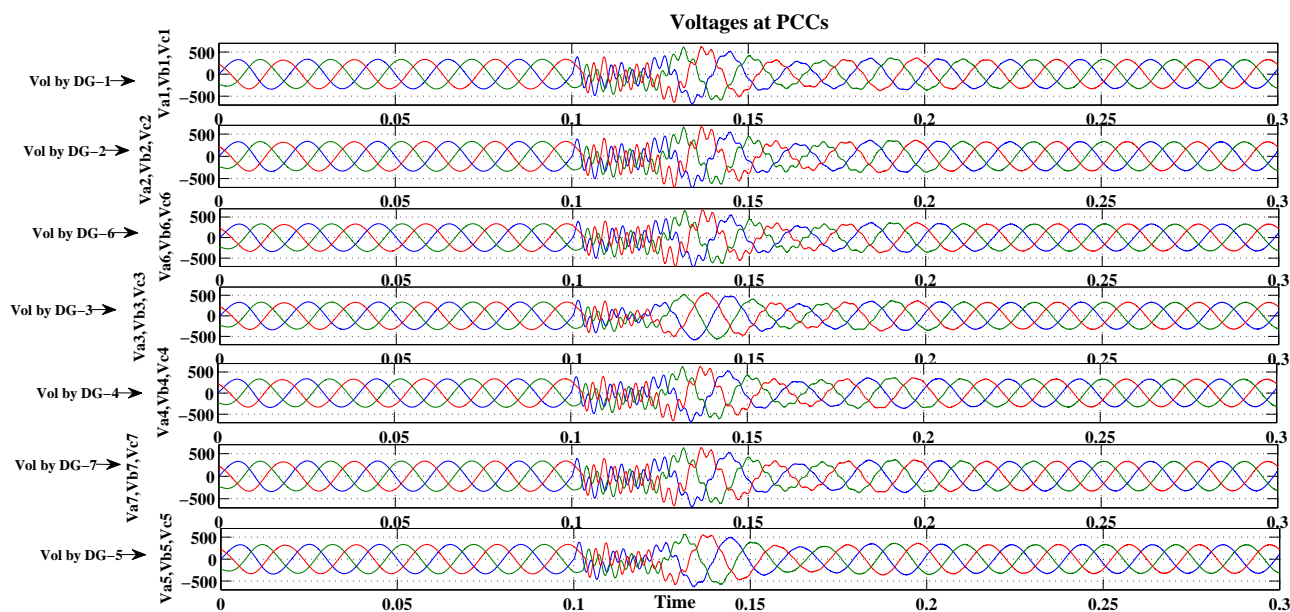


Figure 5.55: Phase voltages at PCCs while switching from grid connected to islanded mode of microgrid at 0.1 seconds

may damage the PEIs, controllers and sensitive loads. So, we need to take care against this problem. During switching instant, the waveforms are distorted but the time duration

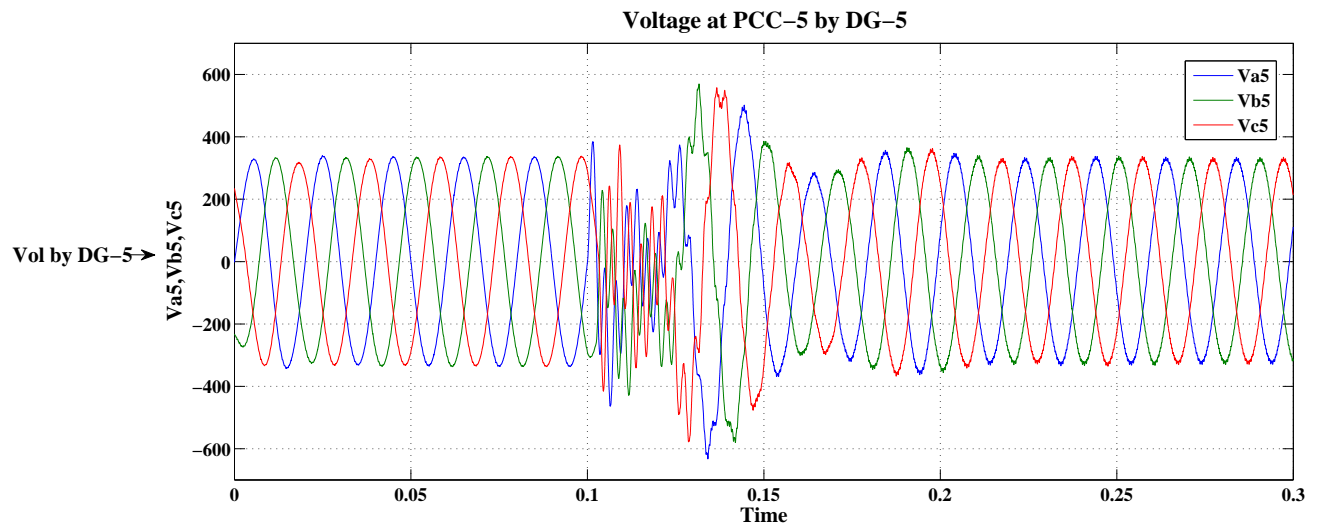


Figure 5.56: Zoomed view of phase voltages of DG-5 terminals during switching of islanded to grid connected mode at 0.1 seconds

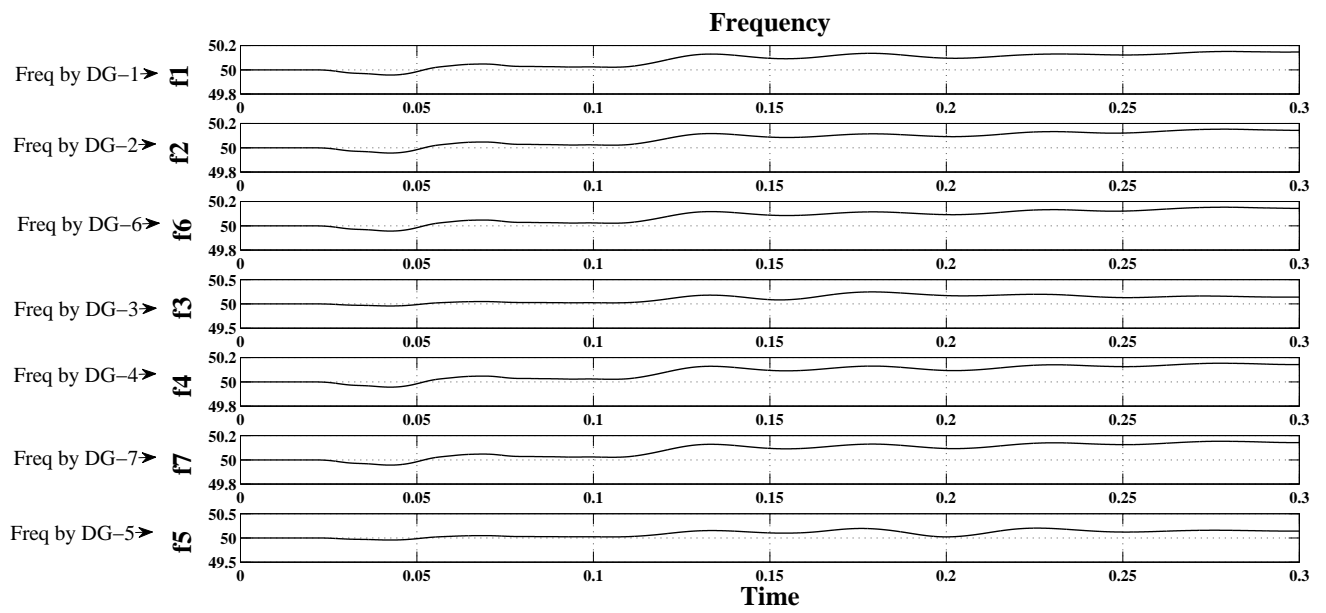


Figure 5.57: Frequencies of all DGs

of distortion are less than 0.06 seconds, hence according to standards if time duration less than 3 cycles, loads are not going to be affected by it. Therefore we may say our designed

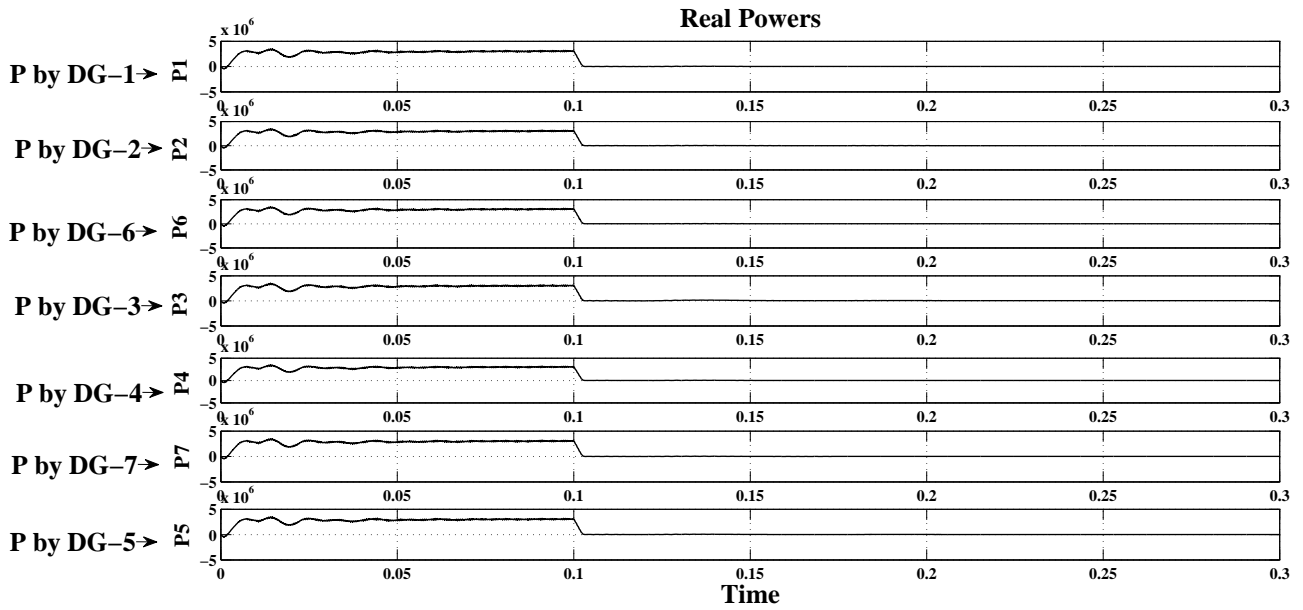


Figure 5.58: Real power dispatched by all DGs during mode changing from grid connected to islanded mode

controller achieved good task. To mitigate a sharp impulsive transients at switching instant, a proper control scheme need to be developed for synchronization of the microgrid with the utility grid.

Fig.5.58 shows the frequencies are well- within acceptable limits at all PCCs and Fig.5.59 indicates the real power dispatched by all DGs.

5.8 Summary

Drawn simulation results for closed loop DC-DC converter with PI controller, shows that it full-fills our requirements in all conditions. Further, our designed LC filter works nicely and reduced harmonics in output voltages much within IEEE specifications for harmonic order. Simulation results of microgrid in islanded or grid connected mode of operation shows the designed controller for single, multi DER units and entire microgrid are working well-effectively and efficiently.

Chapter 6

Conclusions and Future Scope of Research

In this chapter, the general conclusion of the thesis is drawn and the further scope of research is discussed. The conclusions are based on the work carried out and reported in the earlier chapters.

6.1 Conclusions:

The present thesis attempts to investigate the issues involved in the renewable driven microgrids. A microgrid can be operated either in islanded or in grid-connected mode. The primary concern with required to the islanded-mode operation of a microgrid is the implementation of proper control strategy which will regulate voltage and frequency and keep these values within acceptable limits. The line frequency and voltage fluctuations depend on the frequency of occurrence and magnitude of load fluctuations. The load fluctuation will cause voltage and frequency fluctuation and sometimes it may throw them beyond their permissible ranges. Similarly, in the grid-connected mode of operation, the main aim is to implement the proper control strategy which will regulate the active and reactive power exchange with the utility grid. It is necessary to develop suitable methods for controlling active and reactive power flows so as to ensure stable microgrid operation in the grid-connected mode. For all above mentioned reasons, this study was intended

in the development of the control strategies for both the modes of operation of a microgrid.

The thesis presents modeling and control strategies for islanded and grid connected single unit of DER, multi units of DER and the entire microgrid. In this context, dq- reference frame based droop controller along with VSI based voltage and current controller are designed. Moreover, integration of feed forward and ratio control techniques with feedback loop control could potentially contribute to the improvements in the control tasks. The focal control task in islanded mode of operation is that the voltage and frequency values at PCC should stay within permissible limits. However, in the grid connected mode of operation, there would be a good control over the sharing of active and reactive powers to the utility grid is the main concern. Apart from that, for a grid connected VSI, the voltages and frequency are controlled by the utility grid. So, the challenge is that the grid-injected currents should not be distorted while sharing the real and reactive powers as per the given reference set points to the controller. In other words, DERs should not inject the current having THDs greater than 5 % and the current and voltage waveforms should be sinusoidal with 50 Hz frequency at PCC. It is clear from the results obtained that the designed controller works effectively and efficiently for both modes of operation. A detailed analysis shows that this approach has a superior behavior compared to existing ABC- reference frame based control. Further, it is observed that, while switching from islanded mode to grid-connected of single DER unit, the swell phenomenon is produced for the time duration of 0.4 seconds, but it is within the acceptable limits as suggested in the IEEE 519 standard. Finally, it is investigated that, while switching from islanded mode to grid-connected mode for the entire microgrid, a small disturbance is produced for a few milliseconds, but it is much within acceptable limits according to the IEEE 519 standard.

6.2 Future Scope of Research:

In the present work, unbalance and harmonics effects have not been considered. If unbalance and harmonics effects are taken into consideration then we have to redesign the

control structure and filter components. In the unbalanced system, neutral current can not be assumed to be zero. Hence, we have to follow the symmetrical components approach for the analysis of an unbalanced system, which leads us to design three controllers (+ve, -ve and zero sequence) per phase. Moreover, in order to set the active and reactive power references of the controllers in the grid-connected mode of operation, it is required to schedule base-case operation of the microgrid, which is still to be addressed. Apart from that, it is also clear that, during switching from grid connected to islanded mode of operation, a sharp impulsive transient dose occur, which may damage the sensitive loads, controllers or PEIs. As such a proper control scheme for synchronization of the microgrid with the utility grid is to be developed to mitigate the particular problem.

Bibliography

- [1] Paolo Piagi and Robert H. Lasseter, "Autonomous Control of Microgrids," in *Proceeding of IEEE/PES General Meeting*, June 2006.
- [2] R. H. Lasseter, "Microgrid and Distributed Generation," *Journal of Energy Engineering, American Society of Civil Engineers*, September 2007.
- [3] S. Chowdhury, S. P. Chowdhury, and P. Crossley, *Microgrids and Active Distribution Networks*. London, United Kingdom: IET, 2009.
- [4] R. H. Lasseter, "Microgrids," in *Proceedings of IEEE/PES Winter Meeting*, vol. 1, pp. 305-308, August 2002.
- [5] L. Philipson, "Distributed and Dispersed Generation: Addressing the Spectrum of Consumer Needs," in *Proceedings of IEEE/PES Summer Meeting*, vol. 3, pp. 1663-1665, July 2000.
- [6] John L. D. Monaco and P. E., "The Role of Distributed Generation in the Critical Electrical Power Infrastructure," in *Proceedings of IEEE/PES Winter Meeting*, vol. 1, pp. 144-145, January 2001.
- [7] K. A. Nigim and Wei- Jen Lee, "MicroGrid Integration Opportunities and Challenges," in *Proceedings of IEEE/PES General Meeting*, pp. 1-6, June 24-28, 2007.
- [8] A. A. Salam, A. Mohamed, and M. A. Hannan, "Technical Challenges on Microgrids," *ARPJ Journal of Engineering and Applied Sciences*, vol. 3, no. 6, pp. 64-69, December 2008.

- [9] Marian K. Kazimierczuk, *Pulse-width Modulated DC-DC Power Converters*. London, United Kingdom: John Wiley and Sons, 2008.
- [10] Y. Ye, M. Kazerani, and V. H. Quintana, "Modeling, Control and Implementation of Three-Phase PWM Converters," *IEEE Transactions on Power Electronics*, vol. 18, no. 3, pp. 857-864, May 2003.
- [11] E. Acha, V. G. Agelidis, O. Anaya-Lara, and T. J. E. Miller, *Power Electronics Control in Electrical Systems*. India: Planta Tree, 2002.
- [12] S. Debnath, "Maximizing the Power Obtained from Solar Panel Inter-Connections," M.Tech. thesis, EE Dept., IIT M., Chennai, Madras, 2010.
- [13] A. Yazdani and R. Iravani, *Voltage-Sourced Converters in Power System- Modeling, Control, and Applications*. New Jersey: John Wiley and Sons, 2010.
- [14] P. b. c. and V. John, "Higher Order Output Filter Design for Grid Connected Power Converters," in *Proceeding of Fifteenth National Power Systems Conference (NPSC)*, Powai, Maharashtra, December 16-18, 2008.
- [15] Katsuhiko Ogata, *Modern Control Engineering*. New Jersey: Prentice Hall, 2010.
- [16] Paul C. Krause, *Analysis of Electric Machinery and Drive Systems*. U.S.A.: John Wiley and Sons, 2002.
- [17] V. Blasko and V. Kaura, "A New Mathematical Model and Control of a Three-Phase AC-DC Voltage Source Converter," *IEEE Transactions on Power Electronics*, vol. 12, no. 1, pp. 116-122, January 1997.
- [18] F. Katiraei, R. Iravani, N. Hatziargyriou, and A. Dimeas, "Microgrids Management-Controls and Operation Aspects of Microgrids," *Power and Energy Magazine, IEEE*, pp. 54-64, May-June 2008.
- [19] S. Ruihua, Z. Chao, L. Ruomei, and Z. Xiaoxin, "VSCs based HVDC and its control strategy," in *Proceeding of IEEE/PES Transmission and Distribution Conference and Exhibition*, pp. 1-6, December 05, 2005.

- [20] Y. Hu, Z. CHEN, and H. McKenzie, "Voltage source converters in distributed generation systems," in *Proceeding of Third International Conference on, Electric Utility Deregulation and Restructuring and Power Technologies*, pp. 2775-2780, April 6-9, 2008.
- [21] N. Kroutikova, C. A. Hernandez-Aramburo, and T. C. Green, "State-space model of grid-connected inverters under current control mode," in *Proceeding of IEEE Applied Power Electronics Conference and Exposition (APEC)*, vol. 1, no. 3, pp. 329-338, May 2007.
- [22] I. Vechiu, A. Llaria, and H. Camblong, "Control of Power Converters for Microgrids," *Journal of Ecological Vehicles-Renewable Energies*, March 26-29, 2009.
- [23] W. Leonhard *Control of Electrical Drives*. New York: Springer-Verlag, 2001.
- [24] V. Kaura and V. Blasko, "Operation of a phase locked loop system under distorted utility conditions," *IEEE Transactions on Industry Applications*, vol. 33, no. 1, pp. 58-63, January/February 1997.
- [25] M. B. Delghavi and A. Yazdani, "A Control Strategy for Islanded Operation of a Distributed Resource (DR) Unit," *IEEE Transactions on Power Electronics*, vol. 978, no. 1, pp. 4241-4244, May 2009.
- [26] J. A. Pecas Lopes, C. L. Moreira, and A. G. Madureira, "Defining control strategies for analysing microgrids islanded operation," in *Proceeding of IEEE Power Tech, 2005*, vol. 18, no. 2, pp. 1-7, June 27-30, 2005.
- [27] Q. Zeng, L. Chang, and P. Song, "SVPWM based current controlled with grid harmonic compensator," in *Proceeding of Annual Power Electronics Specialists Conference*, pp. 2495-2500, 2004.
- [28] T. Kawabata and S. Higashino, "Parallel operation of voltage source inverters," *IEEE Transactions on Industrial Application*, vol. IA-24, pp. 281-287, 1988.

- [29] S. Golestan, F. Adabi, H. Rastergar, and A. Roshan, "Load Sharing Between Parallel Inverters Using Effective Design of Output Impedance," in *Proceeding of Australasian Universities Power Engineering Conference (AUPEC' 08)*, pp. 1-4, 2008.
- [30] A. Mohd, E. Ortjohann, D. Morton, and O. Omari, "Review of control techniques for inverters parallel operation," *Electric Power Systems Research*, vol. 80, pp. 1477-1487, June 2010.
- [31] A. Tuladhar, H. Jin, T. Unger, and K. Mauch, "Control of Parallel Inverters in Distributed AC Power Systems with Consideration of Line Impedance Effect," *IEEE Transactions on Industrial Applications*, vol. 36, no. 1, pp. 131-138, January/ February 2000.
- [32] A. M. Salamah, S. J. Finney, and B. W. Williams, "Autonomous controller for improved dynamic performance of AC grid, parallel-connected, single phase inverters," in *Proceeding of IET Generation, Transmission and Distribution*, vol. 2, pp. 209-218, 2008.
- [33] P. Kundur *Power System Stability and Control*. New York: Marcell Dekker, 2001.
- [34] Y. Mohamed and E. El-Saadany, "Adaptive Decentralized Droop controller to preserve power sharing of paralleled Inverters in Distributed Generation Microgrids," *IEEE Transaction on Power Electronics*, vol. 23, no. 6, pp. 2806-2816, November 2008.
- [35] K. De Brabandere, B. Bolsens, J. V. Keybus, A. Woyte, J. Driesen, and R. Belmans, "A Voltage and Frequency Droop Control Method for Parallel Inverters," *IEEE Transactions on Power Electronics*, vol. 22, no. 4, pp. 1107-1115, July 2007.
- [36] H. Matthias and S. Helmut, "Control of a Three Phase Inverter Feeding an Unbalanced Load and Operating in Parallel with Other Power Sources," *EPE-PEMC 2002 Dubrovnik and Cavtat*, pp. P1-P10, 2002.

- [37] Y. Xuel, J. Deng, and Shuangbao Ma, "Power Flow Control of a Distributed Generation Unit in Micro-grid," in *Proceeding of Power Electronics and Motion Control Conference-IPEMS*, pp. 291-296, April 06-09, 2008.
- [38] H. Kakigano, Y. Miura, and T. ISE, "Configuration and Control of a DC Microgrid for Residential Houses," in *Proceeding of Transmission and Distribution Conference and Exposition: Asia and Pacific*, pp. 1-4, October 26-30, 2009.
- [39] Y. Li, D. M. Vilathgamuwa, and P. C. Loh, "Design, analysis, and real time testing of a controller for multibus microgrid system," *IEEE Transactions on Power Systems*, vol. 19, no. 5, pp. 1195-1204, September 2004.
- [40] F. Blaabjerg, R. Teodorescu, M. Liserre, and A. V. Timbus, " Overview of Control and Grid Synchronizaation for Distributed Power Generation Systems," *IEEE Transactions on Industrial Electronics*, vol. 53, no. 5, pp. 1398-1407, October 2006.
- [41] R. Majumder, A. Ghosh, G. Ledwich, and F. Zare, "Control of Parallel Converters for Load Sharing with Seamless Transfer between Grid Connected and Islanded Modes," *IEEE Transactions on Power Systems*, July 20-24, 2008.

